Transactions of the 15th International Conference on
Structural Mechanics in Reactor Technology (SMIRT-15)
Seoul, Korea, August 15-20, 1999

Current Research and Development of Damping and Seismic Isolation Technology in Japan

Kohei Suzuki

Tokyo Metropolitan University, Japan

ABSTRACT: This paper summarizes recent research and development of damping and vibration control technology in Japan. As a chairman of the JSME Research Subcommittee of Damping which was founded in 1992, the author introduces current activities in the area of passive vibration control techniques, new damping materials, damping devices and the practical application to seismic design enforcement.
Seismic isolation systems and devices achieved significant anti-earthquake performances to various structures during the Southern Hyogo Prefectural Earthquake (Kobe Earthquake) on January, 1995. Thus, specific interests of this paper are also focused on the technical scope of the seismic isolation problems.

1 INTRODUCTION

The research and development related to the damping materials, damping devices and passive vibration control technologies in Japan have been significantly advanced in the past decade. As a typical example, the application of damping materials such as laminated damping steel sheet (LDSS) to the motor vehicle body and electrical home appliance have been highly progressed in Japanese industries. Also, in the field of earthquake engineering, various types of passive dampers having the capacity of high seismic energy absorption have been proposed for utility.

In 1989, the author and his colleagues from different universities and industries formed a Sub-committee of Damping Technologies in the Dynamics, Control and Measurement Division of JSME (Suzuki;1993). The particular attention of this committee is focused on the following topics.

(1) Damping characteristics of metal and nonmetal materials such as viscoelastic material (VEM), super plastic alloy (SPA), shape memory alloy (SMA) and laminated damping steel sheet (LDSS).

(2) Study and development on the applicability of newly proposed passive dampers and energy absorbers to the seismic and nonseismic structural design procedure.

(3) Vibration test and measurement methodology by which design-based damping value can be identified and evaluated.

Due to the stringent regulations by the Japanese Government to reduce environment pollution such as noise of motor vehicles, the research and development on damping materials have been rapidly spread among various Japanese vehicle industries. This trend

has been further enhanced by the industries' understanding of the noise and vibration reduction in products can enhance the value in the market. With regard to the research and development of the damping technology, activities have been carried out among the committees. For example, Society of Damping Technology (SDT) was established to develop damping materials and demonstrate their application to the industrial sectors for the purpose of vibration and noise reduction

In the Damping '91 Conference at San Diego, the activities of SDT with current trend of the damping materials related technology in Japan were reported (Tokita et al.;1991). The report introduced some typical trends around damping materials technology. According to the report, appropriate damping effects were achieved either by addition of the damping materials such as free-layer bonding or by replacement such as LDSS. Figure 1 shows pie chart showing percentage use of yearly produced LDSS for various industrial products in Japan. Major users are the motor vehicle and electric appliance industries. Recently, the application to building structures and general machineries is also being increased.

In 1997, JSME held a symposium "New Damping Technology towards 21st Century" as one of the events for celebrating the centennial anniversary of the foundation. About 100 topics were presented from the academic sectors as well as from the industries.

This paper overviews the above mentioned current activities on this area by demonstrating several typical examples to nuclear technology as well as non-nuclear one.

2 DAMPING MATERIALS

Damping materials can be generally classified into following 4 categories.

(1) Viscoelastic materials such as rubbers, polymer compounds, silicone gels and many polymeric and glassy materials.

(2) High damping alloys which are developed for getting high damping capacity to practical construction purposes.

(3) Composite materials which are manufactured as a combination of two or more materials. Examples of such systems include metal matrix composites, nonmetal matrix composites and sandwiched or surface-treated materials such as LDSS.

(4) Damping functional materials. Characteristics of these material can be functionally controlled depending on temperature and excited frequency.

Many research and development works regarding these materials have been carried out and presented during past years. Here, study on characterization of viscoelastic materials and application of LDSS are overviewed.

2.1 Characterization of viscoelastic materials' behavior

Characteristics of viscoelastic materials is strongly influenced by temperature and frequency change. Viscosity of the materials decreases with increasing temperature, while it increases with rising frequency of excitation. Therefore, these polymeric materials are expected to possess a wide variety of high damping, thermal stability and strength. Figure 2 illustrates typical damping and strength behavior in accordance with temperature. Feasible damping effect can be achieved at certain "transition " temperature region between glassy and rubber states.

In order to characterize the damping behavior of these materials, mathematical modeling of the state equation is particularly important. Standard models of the equation hitherto utilized are generalized Maxwell model and Voigt model which are represented by eqs.(1) and (2),

respectively.

$$\sigma = E\varepsilon + \mu \frac{d\sigma}{dt} \quad (1)$$

$$\frac{d\varepsilon}{dt} = \frac{1}{E}\frac{d\sigma}{dt} + \frac{\sigma}{\mu} \quad (2)$$

where σ, ε, E and μ mean stress, strain, modulus of elasticity and coefficient of viscosity. However, these modelings have the limitation for practical use since the variation of E and μ with frequency is much more rapid than is usually observed in real materials.

Recently, new model was proposed to represent viscoelastic behavior (Bagley, R.L. et al.1983). By applying this model, the state equation of stress-strain relation can be expressed by

$$\sigma(t) = E_0 \varepsilon(t) + \mu D^q[\varepsilon(t)] \quad (3)$$

In this equation, $D^q[\varepsilon(t)]$ means "fractional integral" which is determined by

$$D^q[\varepsilon(t)] = \frac{1}{\Gamma(1-q)} D\left[\int_0^t \frac{\varepsilon(\xi)}{(t-\xi)^q} d\xi\right] \quad (4)$$

where $\Gamma(\cdot)$ is Gamma function and q is fraction such as 1/2, 2/3, 2/5 etc. and D means operator of differentiation. Shimizu applied this model to silicone gel materials (Shimizu, N., 1997) and Sunakoda utilized it to characterize viscoelastic damper for the plant structures.

2.2 Application of LDSS

Generally, LDSS can be divided into two types; (1) constrained layer type and (2) unconstrained layer type. In the former type, resin layer having high viscous damping is sandwiched between two steel sheets and in the later type resin layer is bonded on single sheet as shown in Fig. 3. Although both of two types can provide high damping ability to the panel-like structures by utilizing viscosity of resin materials, their damping mechanism is completely different. In the constrained type, high damping can be achieved by shear deformation of the resin layer, while in the unconstrained type, vibration energy can be absorbed by expansion and contraction of the resin layer.

Nippon Steel Corporation experimentally investigated and clarified the characteristics of LDSS as follows (Kadowaki;1996).

(1)Three layered constrained LDSS has higher damping capacity than the unconstrained type, but the weight is about half of unconstrained type.

(2)Vibration response level of LDSS panel is remarkably suppressed at higher frequency range and no appreciable reduction at low frequency range.

(3)Spotwelding given to the nodal of LDSS panel affects the damping.

In view of the practical application, a vibration test was conducted on vehicle oilsump using LDSS. From the results, a remarkable damping effect was observed when comparing to the conventional steel oilsump. Figure 4 shows a bar chart which compares the response of oilsump with or without LDSS.

3 SEISMIC ISOLATORS AND DAMPERS

3.1 Seismic isolator

On January 17, 1995, the huge Southern Hyogo Prefectural Earthquake (Kobe Earthquake) occurred at Hyogo Prefecture, Awaji island and Osaka Prefecture. The total number of damaged houses and buildings were about 400,000 including about 100,000 completely collapsed buildings. The most severe damages were observed on large number of buildings along the seismicity VII (by Japanese Meteorological scale) zone in Kobe City. However, two big buildings constructed on the seismic base isolators near the region were not damaged. On the contrary, the maximum response was reduced to less than 30% by the way of seismic isolator systems.Figure 5 demonstrates the configurations of "high damped laminated rubber"(HDLR) and "laminated rubber with lead plug"(LRLP). According to the recent technical information through the Building Center of Japan (BCJ), the number of proposals for obtaining the authorization to construct isolated buildings have remarkably increased after the Kobe Earthquake. During the fiscal year 1995, more than 80 isolated buildings were approved by the BCJ for construction on base isolators.

The base isolator systems to the building floor on which important or expensive structures and equipments such as central work stations to be installed have also been developed in Japan. Figure 6 shows an example of the base isolator proposed by Kajima Corporation (Harada et al.;1989). This ball bearing base isolator (BBBI) consists of a large main ball bearing, several small sub-ball bearings and a bowl-shaped base. At the time of the Kobe Earthquake, this base isolator system has worked quite effectively in the computer room of the existing bank building in Osaka City.

Many types of floor isolators have been developed by the industries and construction companies.

3.2 New types of dampers and absorbers

In order to maintain high performance of structures, machineries, equipments and piping systems, many types of damping devices such as elasto-plastic damper, adaptive damper, electro-rheological damper, viscoelastic damper, granular damper have been proposed. Some of them were developed by the Japanese industries such as Hitachi, IHI, Mitsubishi and others and several dampers were developed by the joint projects among the governmental, the academic and the industrial sectors.

A typical example of the corporative works for developing damping devices is a national project monitored by NUPEC (Nuclear Power-plant Engineering Commission) under the sponsorship of MITI. In this project, two stages of seismic proving tests were carried out for the nuclear piping with damper systems by using two-dimensional large size shaking table at Tadotsu, Kagawa Prefecture. In the first stage, test was carried out on the piping system having conventional supports; hydraulic dampers and mechanical snubbers. While in the second stage, testing was made on the piping systems with supports which were developed by the industries as seismic energy absorbers. The energy absorbers such as elasto-plastic absorber (EAB) developed by Hitachi and lead excursion damper (LED) developed by Mitsubishi were used. Figure 7 shows the configurations of the EAB (Namita;1995).

Through this project, it was confirmed that nuclear pipings having conventional supports could maintain enough strength against the most severe design seismic excitations. It was also recognized that newly developed energy absorbers such as EAB and LED could be introduced in place of conventional supports for plants in the near future. The number of the conventional snubbers can be tremendously reduced since individual EAB or LED can absorb much more seismic energy.

Magnetic dampers can be recognized having many advantages such as good linearity, thermal stability and good reliability over conventional mechanical dampers. Toshiba's

group recently proposed a new type of vibration absorber based on a magnetic spring and damper system (Aida et al.;1995). In this damper, a pair of double cylindrical magnets face with each other across a certain gap. One magnet fixed to the target structure and another to the moving mass of the dynamic absorber. Figure 8 describes an outline of this damper, and Fig. 9 shows an example of application of the magnetic damper to rotation machineries.

Electro-rheological fluid (ER fluid) is known as a class of highly functional fluid whose apparent viscosity can be varied in response to the applied electric field. ER fluid has attractive characteristics since the viscosity can vary over a wide range and its response is as rapid as in several milliseconds. It is known that the ER fluid is utilized in mechanical damping components such as a shock absorber system, a squeeze film damper bearing, a dynamic damper and an engine mount (Morishita et al.;1995). Figure 10 shows an example of the ER damper.

4 FUTURE SCOPE OF DAMPING TECHNOLOGY

Future scope of damping technology in Japan will be to develop higher capacity damping materials and devices which can be applied to the structures and mechanical systems. New materials which will be hopefully applied as damping materials could be invented by both of academic and industrial sectors based on the eager desire in the area of the 21st century's technologies such as space engineering and bio-technology.

4.1 Adaptive damping materials

Any vibration damped material which could be effective over a wide frequency range will be one of the hopeful materials. If the damping characteristics of the specific material can be controlled depending on the excitation level, the material can be applied for the anti-vibro structure design.

From this viewpoint, thixotropic materials are note worthy substances because they can liquefy when they are stirred or shaken and can return to original state after being left it free. By utilizing this specific characteristics, it is possible to make the damping device whose capacity can be controlled with respect to the vibration intensity. A passive adaptive damping device using the thixotropic material was designed by the scientists of Hitachi Co.Ltd. (Matsuda et al.;1995). The configuration of the damper is illustrated in Fig. 11. Figure 12 shows an example of the test results of this damper. In this figure, change of dynamic characteristics of the damper such as natural frequency and damping ratio to the base excitation is presented.

4.2 Multi-functional adaptive damper

Towards the 21st century's, multi-functional adaptive technologies are expected to be required in various engineering fields. The "multi-functional damper" can adaptively select active, passive or hybrid operation control mode according to the specific demand.

The author and his colleagues proposed a kind of this adaptive damper, i.e.,the "mechatro damper" shown in Fig. 13 (Sunakoda et al.;1995). It consists of a "mechanical" ball screw and nut element and an "electrical" D.C. servo motor with a gear amplifier. This damper can control damping forces by applying SMC (slide mode control) algorithm for the use of VSS (variable structure system). Figure 14 shows the frequency response characteristics for the hybrid mode system in which apparent advantage compared to the conventional passive systems can be recognized.

5 CONCLUSION

A brief survey and overview to the progress of damping researches and technologies in Japan was presented, particularly, focused on seismic and nuclear structure engineering. It should be carefully noticed that similar works and more developed investigations are carried out in overseas such as United States and European countries. Mutual exchange of the informations related to the damping technology still has to be put forward and cooperative works including international conference on the damping problems should be promoted.

Reference

1. Suzuki, K., "A brief survey of research works about vibration damping", *Trans. JSME, Ser.C*, 59-566, 1993, pp. 2908-2914.
2. Tokita, Y. & H. Okamura, "The society of damping technology in Japan and its activities", *Proceed. of Damping '91 Conf.*, 1, 1991, pp.1-16.
3. Bagley, R.L., "On the fractional calculus model of viscoelastic behavior", *J. Rheology*, 30-1, 1986, pp.133-155.
4. Shimizu, N., "Dynamic characteristics of viscoelastic vibration system", *Trans. JSME, Ser.C*, 61-583, 1995, pp.166-170.
5. Kadowaki, N., "The recent study on properties of vibration damping steel sheets and its applications", *Trans. of Annual Conf. on Vehicle Dynamics, JSME*, 1996, pp.76-81.
6. Harada, M. et al., "Base isolation system for earthquake protection of precision machinery system", *PVP-Vol. 182, ASME 1989*, 1989, pp.142-155.
7. Namita, Y. et al., "Development of seismic design method for piping system supported by elasto-plastic damper", *Trans. JSME, Ser.C*, 60-590, 1995, pp.3874-3880.
8. Aida, Y. et al., "Dynamic vibration absorber using magnetic spring and damper", *PVP-Vol.312, ASME 1995*, 1995, pp.439-445.
9. Morishita, S. & Y.K. An, "On dynamic characteristics of ER fluid squeeze film damper", *Trans. JSME, Ser.C*, 61-591, 1995, pp.4245-4250.
10. Matsuda, H. et al., "A study on passive adaptive vibration control elements by using thixotropic materials", *Trans. JSME, Ser.C*, 61-588, 1995, pp.3217-3221.
11. Sunakoda, et al., "Semiactive seismic isolation system by using mechatro damper", *Proceed. of 2nd Inter. Conf. on MOVIC*, pp.41-46, July 1994.

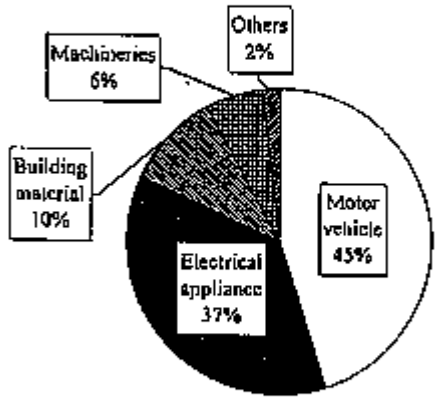

Figure 1 Percentage of produced LDSS application

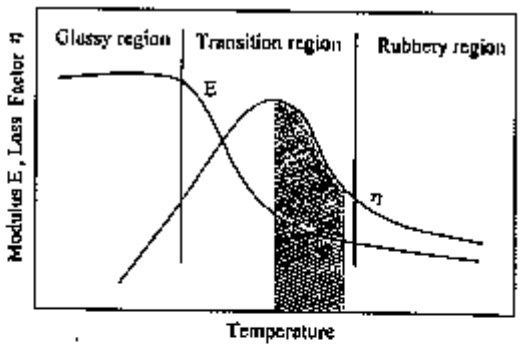

Figure 2 Damping and strength behavior of viscoelastic material

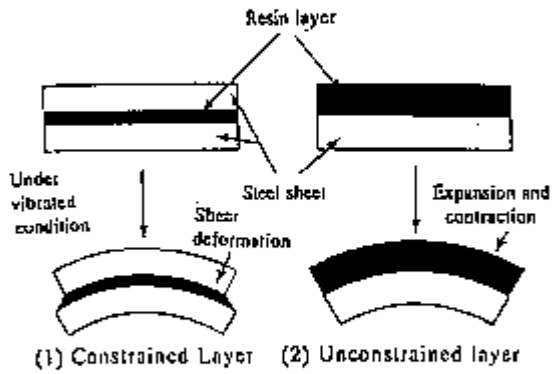

Figure 3 Schematic configurations of LDSS

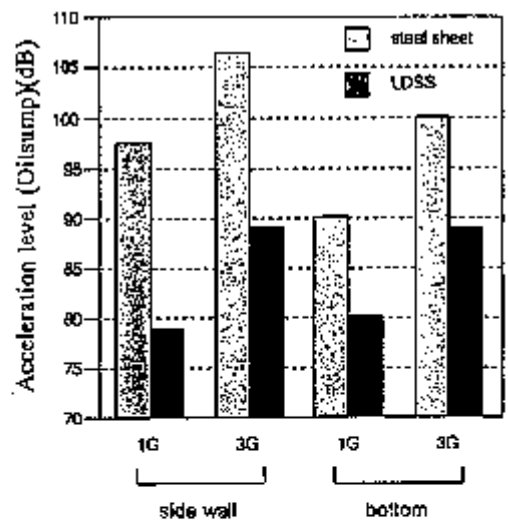

Figure 4 Response of vehicle oilsump with / without LDSS

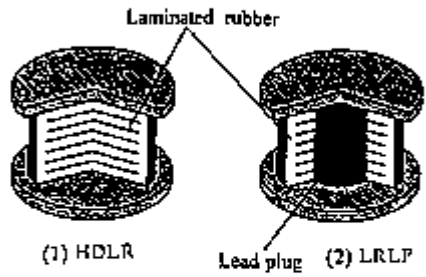

Figure 5 Schematic views of HDLR and LRLP isolators

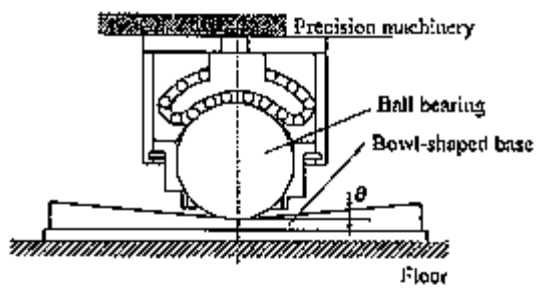

Figure 6 Ball bearing base isolator (BBBI)

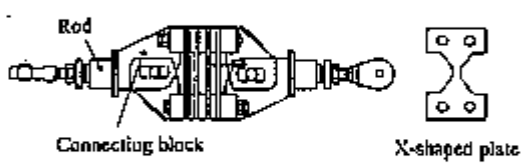

Figure 7 Configuration of EAB

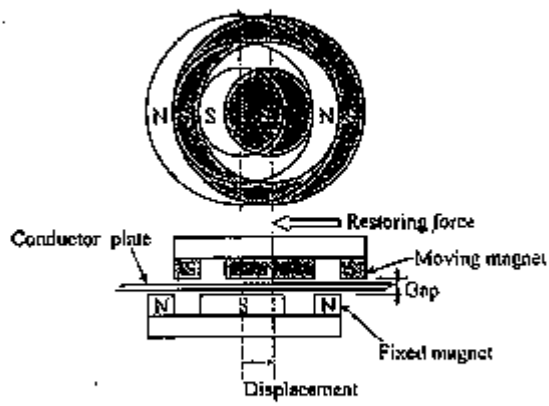

Figure 8 Magnetic damper system

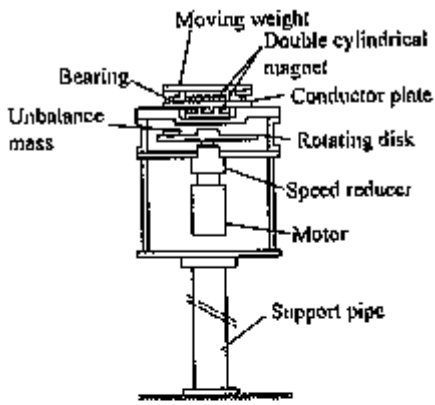

Figure 9 Magnetic damper mounted on rotating machinery

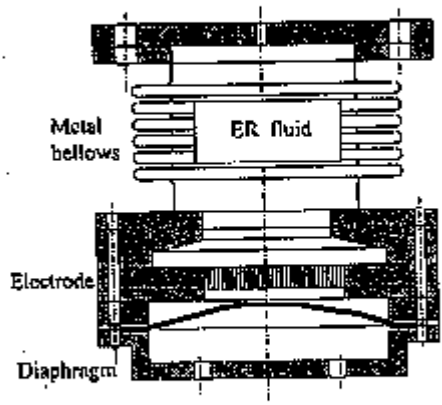

Figure 10 Electro rheological fluid damper
("ER damper")

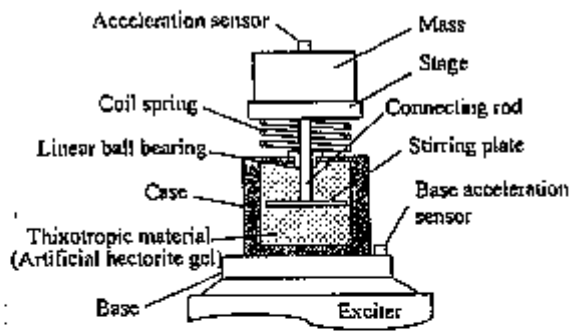

Figure 11 Passive adaptive damper
("thixotropic damper")

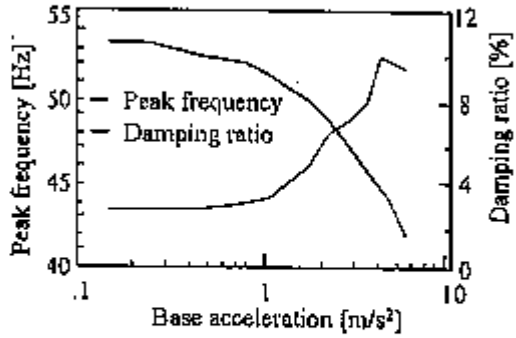

Figure 12 Vibration characteristics of "thixotropic damper"

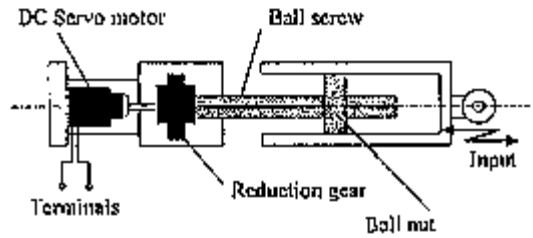

Figure 13 Multi-functional adaptive damper ("mechatro damper")

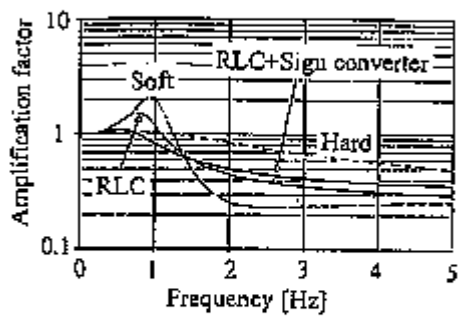

Figure 14 Frequency response characteristics of the "mechatro damper"

Transactions of the 15th International Conference on
Structural Mechanics in Reactor Technology (SMiRT-15)
Seoul, Korea, August 15-20, 1999

A Primary Study of Base-Isolation Technology in NPP

Sun Lei and Gu Fangyu

Nuclear Power Institute of China, China

ABSTRACT Earthquake is one of the damage factors to nuclear plant Safety. This paper was about the research of Base-Isolation Method of NPP in China, financed by Nuclear Industry Science Funds of China. In the subject, Φ440Lead-Rubber Bearing was manufactured, its mechanical characteristics was tested and the quasi-static force-displacement curves were obtained. On the other hand, the effect of the containment base-isolated was analyzed and compared the seismic responses of containment with that non-isolated, the advantage of using base-isolation technology was qualitative presented.

1. BACKGROUND

Base-Isolation System was developed as one of remarkable technology to reduce the seismic load of building and equipment in recent year. For example, in Japan, only 80 base-isolated buildings had been constructed for about 10 years -from 1986 to 1994, but after the Great Hanshin earthquake in 1995, the number including under-construction is increasing to over 400 until now, It was applied widely in computer center, office building and residential building.

Isolation system consisted of isolators and energy dissipaters. It was located between foundation and superstructure, having two main functions: the first, to reduce the first natural frequency of building for avoiding in resonance with main energy frequency of earthquake wave; the second , to absorb the earthquake energy.

Today, there were two nuclear power plants (PWR) applied the Base -Isolation System , One was CRUAS in France, another was KOEBERG in South Africa .In Japan ,a series studies about base-isolation technology had been done ,the range including Light Water Reactor, Fast Breeder Reactor and International Thermo-Nuclear Experimental Reactor.

This subject had been subsidized by Nuclear Industry Science Foundation of China .It was the first time in China to study how to apply the Base-Isolation Technology in NPP. In the subject, special rubber material to manufacture bearing was developed and three Φ440 Lead-Rubber bearing specimens were produced and tested. Then, adopting this system's characteristics, a seismic response analysis of containment of Daya Bay NPP was carried out to investigate the effect of this technology. The test and analysis results were introduced in this paper.

2. PROPERTY TEST OF LEAD -RUBBER BEARING

In this test, the quasi-static characteristics of three bearing specimens (A, B, C, Φ440mm) were

determined. The specimen size is indicated in Fig.1, diameter: 440mm(including 6mm thickness rubber Protection around); design thickness of rubber sheet: 6mm, 16 layers (actual total thickness of rubber was 97.9mm); steel sheet thickness: 2mm, 15 layers; Lead core diameter: 50mm; design load: 1000N/cm^2; design shear deformation: larger than 400%.

The contents and results of test:

a. Vertical loading test

In non-bias vertical loading condition, the relationship of vertical load and vertical deformation was measured. Force- Displacement curves were recorded (refer to Fig.2).

b. Pressuring- shearing test

In non-bias vertical loading condition (1000KN), loading circulation force in horizontal direction with 50 sec/circle speed, the relationship of horizontal shear force and shear deformation was measured, and the hysteresis curves were plotted (refer to Fig.3).

From Fig.2 and Fig.3, it could be seen that the characteristics of specimen A and C were identical with full hysteresis curve, better than specimen B. The cause was that specimen B was over- vulcanized during manufacture. For the limited ability of instruments, all of specimens were not destroyed in test, but the max. shear-strain was up to 196%,and from observation, it could be predicted that the shear-strain still had potentiality to increasing. Vertical loading was up to 1800N/cm^2. It was presented that the bearing had mid -high loading ability. So, it was concluded that the manufactured bearing in this subject had good properties to get to the design goal successfully.

3. SEISMIC RESPONSE ANALYSIS OF CONTAINMENT

In order to study the seismic response properties of containment base-isolated and investigate the characteristics of Lead - Rubber bearing, the Finite -Element Analysis was carried out, Daya Bay NPP containment was the analysis object. El centro wave was input.

3.1 Model

Analysis Model: Lumped mass model and 3-dimensional model for containment
Bi-linear model for base-isolation system (refer to Fig.4)

Analysis Method : 1) Modal Analysis
2) Time-History Response Analysis

Hypothesis : 1) The Soil-Structure Interaction was overlooked;
2) Containment was directly set on an infinite rigid body;
3) The traveling wave effect was ignored.

This analysis was completed by ANSYS4.3 on VAX780 .

3.2 Modal analysis

The results were shown on table 1.

It was concluded that the first natural frequency of containment was decreased from 5.22Hz(non-isolated) to 0.42~1Hz range (isolated), laid away from main energy frequencies range (2~10Hz) of earthquake wave.

The results came from Lumped Mass model were similar to those from 3-dimensional model.

3.3 Time-history response analysis

Input Intensity : 0.1g, 0.2g, 0.4g, and 0.8g

Wave Shape : El centro

Input Direction: Horizontal

The analysis results (refer to table 2, Fig.5 and Fig.6) showed:

1) In non-isolation case, the seismic acceleration response at the top of containment was very large(reduction ratio=Max. response acceleration / max. input acceleration=2.07), but in isolation case, the reduction ratio was decreased to 0.41~0.9 corresponding to difference input seismic intensities, and the bigger seismic intensity that was input, the more decreasing of the reduction value was.

2) In isolation case, the movement of superstructure in earthquake was gently, but its displacement was increased obviously. For instance, responding to 0.8g inputting, the horizontal displacement that Lead Rubber bearing generated was 150 millimeter. So a good shear deformation-ability was required for Base-Isolation System. In general, the design shear deformation of it was up to 400%, having enough safety for application in NPP.

4. CONCLUSION

This subject lasted two years. It was completed by cooperation with NPIC、factory and university. The results was achieved the goal that we predicted. Main achievements were showed as follow:

I) Following international development tendency, a lot of base-research works were completed, such as nationalization developing rubber material、seismic isolation theory analysis、setting up mechanical model of isolated system of NPP and so on. It was a basement for isolation technology applied in NPP.

II) The production technology of Φ440 Lead-Rubber bearing was successful had in hand. The tested characteristics were presented that the property of this kind of bearing was better than Φ250 Lead-Rubber bearing's manufactured a few years ago: hysteresis curve had more containing room; ability of absorbing energy was increased and loading ability was improved. It was the biggest one in size of China. Its characteristic parameters came up to advanced world standards at the beginning of 1990s.

III) In China, it was the first time to completed the effectiveness analysis of isolated containment of NPP. The results was showed that adopting Lead-Rubber bearing developed in the subject, acceleration peak of containment response was cut down obviously. In severe earthquake, the maximum response in isolation was 1/4~1/5 times of those in non-isolation. The Lumped Mass model could be applied in actual calculation.

From the results, it could be concluded that the achievements attained in the subject filled in the gaps in the fields of isolation technology applied in NPP of China. The analysis model of isolation system and the manufactured Lead-Rubber bearing came up to advanced world standards in the end of 1980s or the beginning of 1990s.

In future, some aspects may be improved:

a) To improve the reliability of estimation for relative long period earthquake wave.

b) To reduce the quantity of isolators by heightening the vertical pressure for cost down.

c) To develop 3-dimensional isolation device.

d) To set up design code of isolation system.

References:

1. Clough Penzien, Dynamics of Structures

2. Gu Fangyu, "About Base-Isolation Issues of NPP", 1991

3.Zhang Xiong, "The Theory and Experiment Study of Base-Isolation Technology ",1994,5

4. Argonne National Laboratory , "On the French Nuclear industry Experience in the Design of Seismic Isolation of NPP" , 1989,12
5. A.H.DADJIAN, W.S.TSENG, "Issues in Seismic Isolation of Nuclear Power Plants" , Nuclear Engineering and Design 84 (1985)

Table 1. Natural frequencies of containment

Non-isolation		
natural frequency(Hz)	lumped mass model(Hz)	3-dimensional model(Hz)
the first	5.22	5.38
the second	19.48	17.50
Isolation		
the first	1.07(0.42)	1.09(0.44)
the second	6.13	6.63
the third	20.43	18.72

Table 2. Input El Centro Wave

Non-isolation			
input intensity (g)	Max. accel response at m/s^2	the top of containment g	reduction ratio Max.res/Max.input
0.1g	2.025	0.207	2.07
0.2g	4.051	0.413	2.07
0.4g	8.102	0.827	2.07
0.8g	16.204	1.654	2.07
Isolation			
0.1g	0.915	0.09	0.90
0.2g	1.318	0.13	0.65
0.4g	1.997	0.20	0.50
0.8g	3.245	0.33	0.41

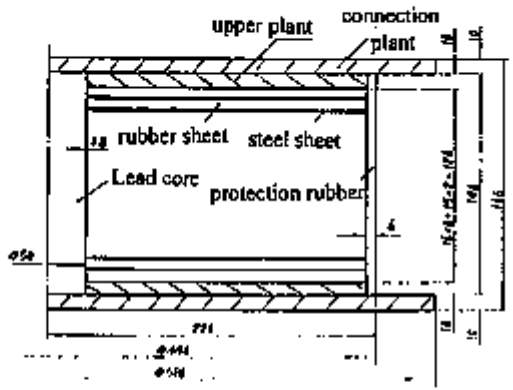

Fig.1 The Section of Φ440 Bearing

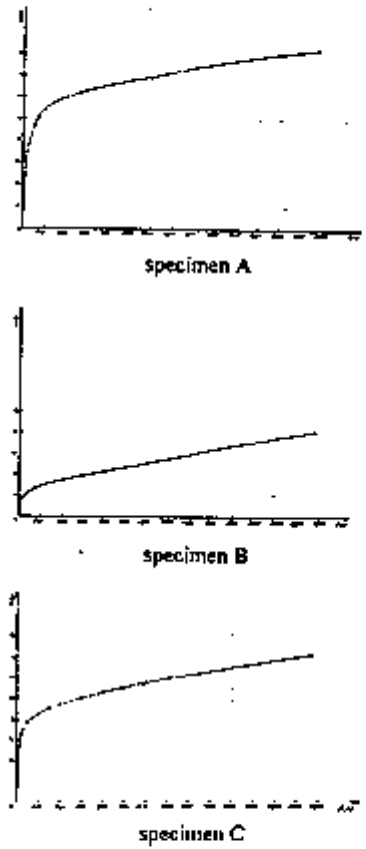

Fig.2 Vertical Loading-Deformation Curve of Φ440 Bearing

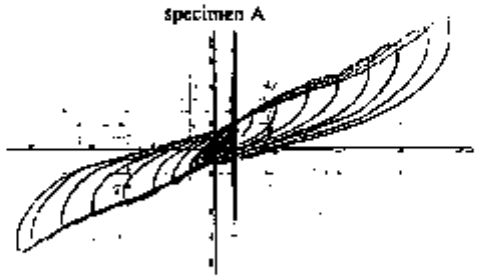

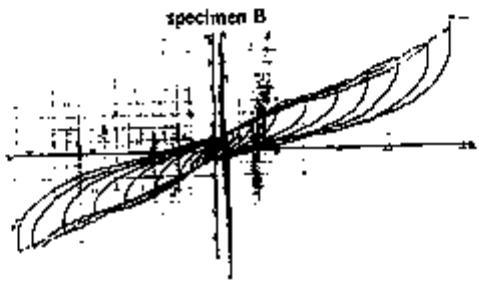

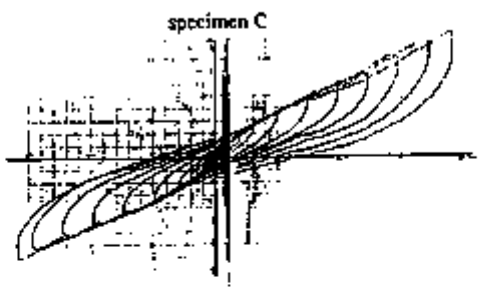

Fig.3 Hysteresis Curve of Φ440 Bearing

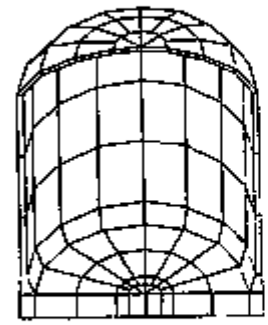

3-dimensional model for containment

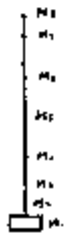

Lumped mass model for containment

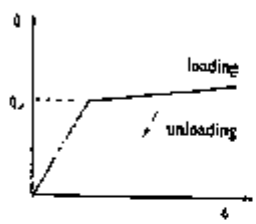

Bi- linear model for base-isolation system

Fig.4 Analysis moadel

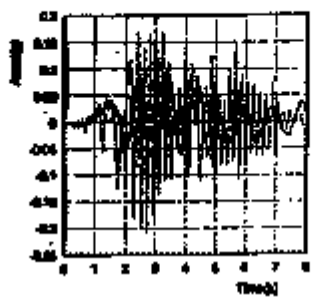

Input El centro Wave (0.1g)

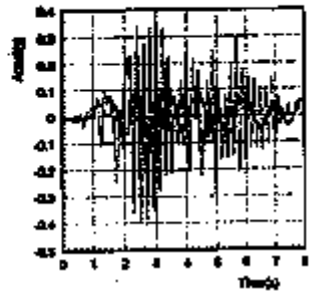

Input El centro Wave (0.2g)

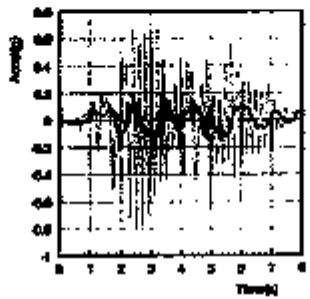

Input El centro Wave (0.4g)

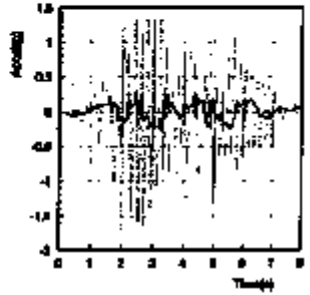

Input El centro Wave (0.8g)

Imaginary Line: Non-isolated

Real Line: Isolated

Fig.5 Acceleration Response History at the Top of Containment in Isolated and Non-isolated

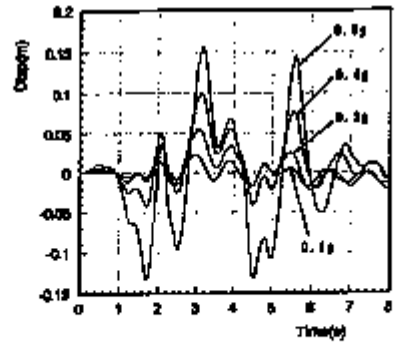

Fig.6 Relative Displacement Time-History Response Between the Upper and Bottom of Bearing (Input Intensity: 0.1g, 0.2g, 0.4g, 0.8g)

Transactions of the 15th International Conference on
Structural Mechanics in Reactor Technology (SMiRT-15)
Seoul, Korea, August 15-20, 1999

Stability of Rubber Bearings for Seismic Isolation

Jong Sch Lee and Jong Won Oh

Hanyang University, Korea

ABSTRACT

Laminated rubber bearings(LRB's) are widely used as a basic component in seismic isolation systems for structures. Increasing the number of steel shims and thickness of the elastomers can achieve large period shifts. However, the shear flexibility of these short columns can lead to relatively low buckling loads which may be further reduced when high shear strains are applied. In this paper, a nonlinear finite element study is presented with an aims at determining the effect of high shear strain on the critical load of elastomeric bearings. Both the geometric and material nonlinearities are considered in the study. From the load-displacement curve for each specified shear displacement, the buckling load is calculated using the Southwell procedures. The results obtained are then compared against the theoretical predictions in order to examine the validity and the conservatism of the theoretical formulas.

INTRODUCTION

Recent surveys of seismic isolation systems around the world indicate that the majority of these systems use elastomeric bearings as the element of flexibility. These bearings may be of natural or synthetic rubber and usually compounded to enhance their hysteretic damping. These typically consist of several layers of rubber inter-layered by steel shims. This composite structure results in a very high vertical stiffness without a considerable increase in the horizontal stiffness over the same rubber block lacking reinforcement. In a typical building, isolators are located under each column, usually in a sub-basement. In a bridge they may be placed under each girder at the abutment seats and between the column capbeam and the superstructure. The individual bearings which make up the isolation systems are frequently interconnected by a diaphram which is rigid in its own plane and enforces displacement compatibility amongst the various isolators.

Of particular interest to the design engineer is the failure modes or limit states of the isolator systems. There are three separate limit states to consider. These are the maximum shear strain in the rubber compound, the displacement at which roll-over commences, and the load at which buckling occur. This paper is concerned with the buckling limit state of laminated elastomeric bearings under the combined actions of compression and shear. Although it is recognized that the system stability

is a function of the spatial distribution of axial load and bearing stiffness, the properties of individual bearings must be well understood in order to make meaningful calculations of system response.

STABILITY THEORY OF RUBBER BEARINGS

Laminated elastomeric bearings exhibit buckling phenomena in much the same way that structural columns are susceptible to compressive loads. Despite their short length, these columns may have low critical loads due to their extreme flexibility in shear compared with steel bearings. Associated with the buckling phenomenon is the corresponding dependence of shear stiffness on axial loads. The relationship between axial load and shear stiffness at small shear deformations has been established. The theory for the buckling of isolation bearings is an outgrowth of work by Haringx[1] on the mechanical characteristics of helical steel springs and rubber rods used for vibration mountings. The Haringx theory was later applied by Gent[2,3] to the problem of the stability of multilayer rubber springs. Gent's extension forms the basis of the stability theory given below[4].

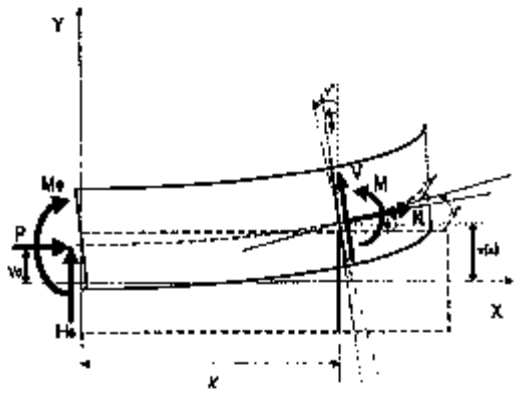

Fig. 1 Internal forces and external loads on a deformed bearing

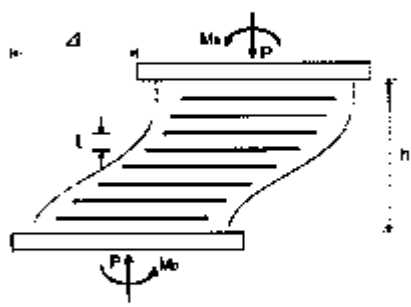

Fig. 2 Boundary conditions

Fig. 1 shows the internal and external forces on the bearing in the deformed position. The equations of equilibrium for bending moment and shear force in the deformed state are given by

$$M + P(v - v_\phi) - M_0 - H_0 x = 0 \tag{1}$$

$$V + H_0 - P\phi = 0 \tag{2}$$

where $v(x)$ is the displacement of the middle surface of the bearing and $\phi(x)$ is the rotation of the face originally normal to the undeformed axis. P, M and M_0 are the axial load, lateral reaction, and bending moments, respectively.

Upon substitution of the constitutive equations and application of the boundary conditions shown in Fig. 2, the solution for $v(x)$ and $\phi(x)$ can be given by the following:

$$v(x) = \frac{1}{2}\left(1 - \cos\frac{\pi x}{h}\right)v(h) \tag{3}$$

$$\phi(x) = \frac{1}{2}\frac{\alpha(GA)_{eff}}{(GA)_{eff} + P}\left(\sin\frac{\pi x}{h}\right)v(h) \tag{4}$$

where

$$\alpha^2 = \frac{P((GA)_{eff} + P)}{(EI)_{eff} \cdot (GA)_{eff}} = \frac{\pi^2}{h^2} \tag{5}$$

From the above equations, the buckling load P_{cr} can be determined as the followings:

$$P_{cr} = \frac{(GA)_{eff}}{2}\left[\left(1 + \frac{4P_E}{(GA)_{eff}}\right)^{\frac{1}{2}} - 1\right] \tag{6}$$

where

$$P_E = \frac{\pi^2 (EI)_{eff}}{h^2} = \text{Euler buckling load}$$

$$(EI)_{eff} = \frac{4S^2}{15} EI\left(\frac{h}{t}\right) = \text{Effective bending stiffness}$$

$$(GA)_{eff} = GA\left(\frac{h}{t}\right) = \text{Effective shear stiffness}$$

In the above, EI and GA denote the bending and shear stiffness respectively; S is the shape factor defined by b/t; b and h are the half-width and height of the bearing respectively; t is the thickness of the thickness of a single rubber layer. The buckling theory described above, however, is applicable only to the bearings at zero shear displacement. Various approximate methods have been proposed to account for the reduction in buckling load when there are non-zoro shear displacements as

shown in Fig. 3. The most common method is the area reduction formula given by Eq. (7) which implies that the critical load is zero when the shear displacement is equal to the width of the bearing[5].

$$\overline{P_{cr}} = P_{cr}\left(1 - \frac{\Delta}{B}\right) \tag{7}$$

where $\overline{P_{cr}}$ is the modified buckling load, P_{cr} the buckling load calculated by Eq. (6), B the bearing width, and Δ the shear displacement. The validity of the formula is also to be examined in this study.

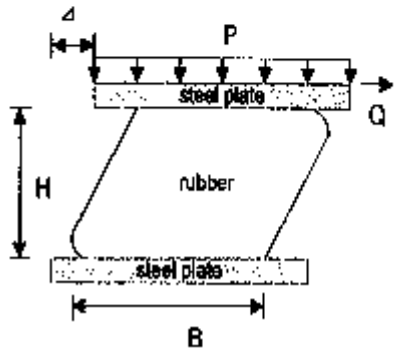

Fig. 3 Elastomeric bearing under combined compression and shear

FINITE ELEMENT ANALYSIS

The objective of the finite element analysis is to examine the buckling behavior of elastomeric bearings with high shear strains. Critical loads at imposed shear strains are determined using the Southwell Plot method[6]. As a finite element analysis program, the LUSAS[7] computer program is chosen. This program permits the geometric and material non-linearities of both compressible and almost incompressible solids. Incremental analysis is performed using a displacementbased finite element formulation. The Mooney-Rivlin material model is used to characterize the rubber at high strains, and the co-rotational formulation to address the geometric non-linearity. A hydrostatic work term was added to the energy function to permit the inclusion of compressibility in the rubber. In order to reduce the computational effort, a plane strain restriction is imposed so that 2-D analyses could be performed. This assumption is valid for strip elastomeric bearings, but care should be taken when applying these results to square or rectangular bearings.

Table 1 summarizes the three bearings analyzed. They are all 12 cm wide and 10 cm tall with the number of internal layers to be three, four or five. The shape factor ranges from 3.75 to 6.67 which is considered to be important in a comparative study of buckling loads.

Table 1. Bearing details

Unit: cm

Series No.	Width	Height	No. of Rubber Layer	Thickness of Rubber Layer	Shape Factor
LRB1	12	10	3	1.6	3.75
LRB2	12	10	4	1.15	5.22
LRB3	12	10	5	0.9	6.67

In the case of LRB2 model, the finite element mesh with 4 layers comprised of 1000 elements, 1074 nodes and 2148 displacement degrees of freedom. Fig. 4 and 5 show the dimensions of the bearing and the corresponding finite element mesh respectively.

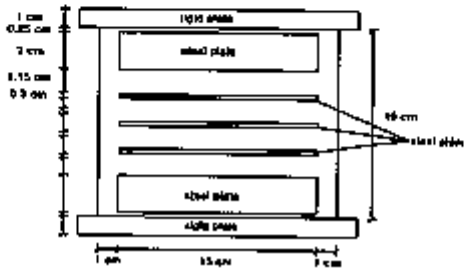

Fig. 4 Dimensions of Bearing (LRB2)

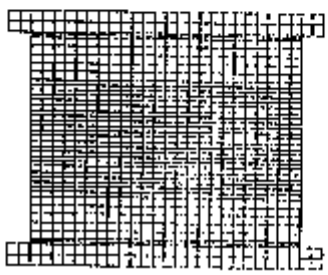

Fig. 5 FE Model (LRB2)

The bearings are first deformed in shear to a predetermined lateral displacement (Δ) and the additional lateral displacement (δ) is monitored as the axial load (P) is increased. Figs. 6(a) and (b) show the deformed finite element meshes which are first loaded in shear and then deformed in compression respectively. It can be seen in the figures that the steel reinforcements experience very little deformation compared to the rubber elements.

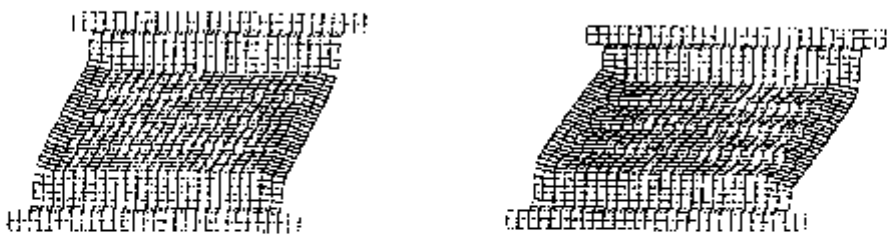

(a) Shear Only

(b) Compression After Shear

Fig. 6 Deformed Mesh (LRB2)

NUMERICAL RESULTS

Lateral displacements described above are plotted against the vertical loads for

each specified shear displacement in Fig. 7. The Southwell Plot may be applied to each P - δ curve in Fig. 7 to determine the buckling load for the specified shear displacement. In the Southwell procedure, the ratio P/Δ is plotted against P, and a straight line is then fitted to the calculate responses. The intercept of this line with the horizontal axis is an indicator of the critical load at the specified initial displacement Δ. An example is shown in Fig. 8 where the apparent critical load is determined to be 730 KN at the initial displacement of 3 cm.

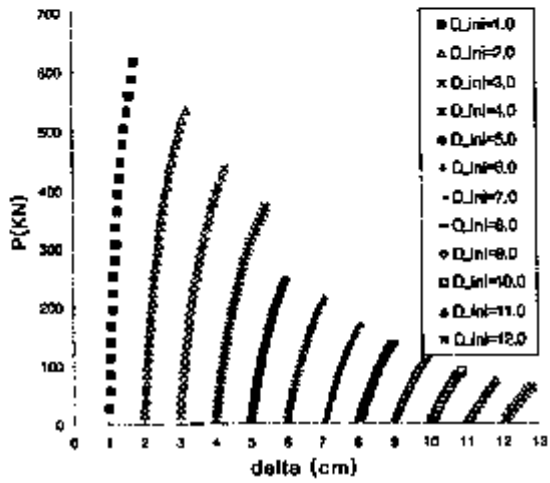

Fig. 7 P - δ Plot (LRB2)

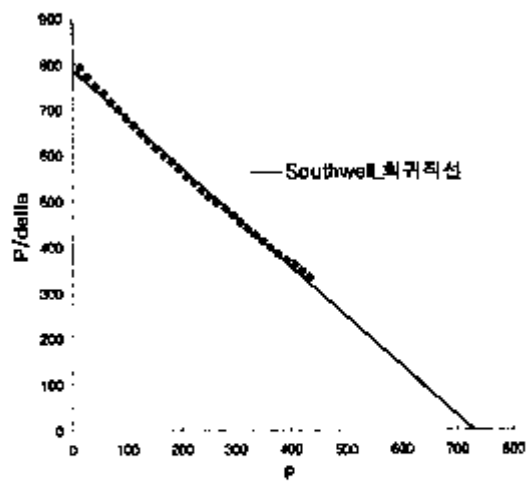

Fig. 8 Southwell Plot (Δ=3cm, LRB2)

Fig. 9 shows the bucking load as a function of the shape factor. It can be seen that the critical loads from the finite element analysis become smaller than the theoretical predictions when shape factors are greater than about 5.

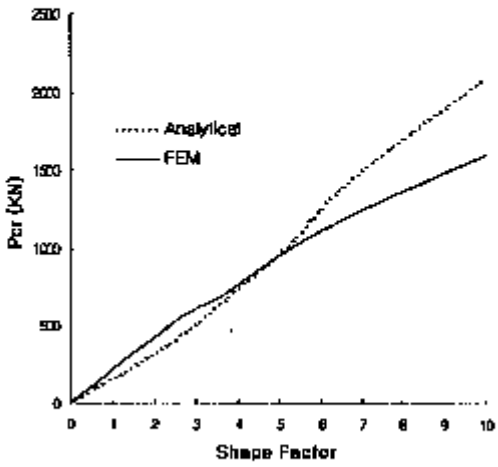

Fig. 9 Bucking loads for different shape factors

The effective buckling load ratio($\overline{P_{cr}}/P_{cr}$) is plotted against the shear displacement as a fraction of the bearing width in Fig. 10. Also shown in Fig. 10 is the relationship given by Eq. (7) for comparison. It is shown in the figure that the numerical results start to veer from the straight line when the shear displacement is about 40 percents of the bearing width. Fig. 10 indicates a substantial residual capacity at Δ = B whereas Eq. (7) implies that $\overline{P_{cr}}$ should be zero at this point.

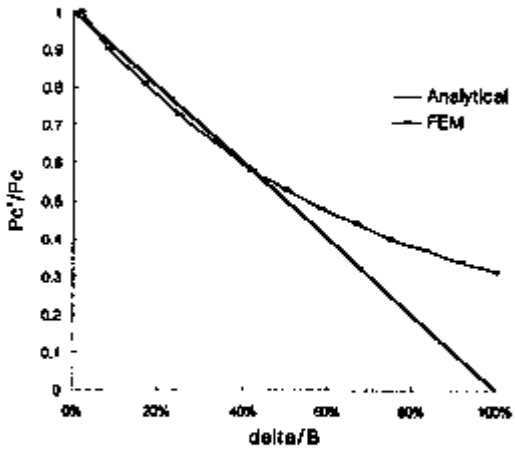

Fig. 10 Effective buckling load ratio (Δ=3cm, LRB2)

CONCLUSIONS

A finite element analytical study is carried out to determine the buckling loads of laminated rubber bearings with an aim at developing a viable numerical technique for critical load analysis of isolation bearings. From the results of the limited number of cases considered, it appears that a substantial reserve of the vertical load capacity exists even after the shear displacement reaches way about 40 percents of the bearing width. It may be calculated that the area reduction formula is a conservative estimate of the reduction in critical load due to the effective of high shear strains. Since there is some degree of restraint in most bearing isolation systems the unrestrained results may be more conservative. Additional case studies should be performed to determine if this is generally true.

ACKNOWLEDGEMENT

This work was supported in part by the Korea Science and Engineering Foundation(KOSEF) through the Korea Earthquake Engineering Research Center at Seoul National University.

REFERENCES

1. Haringx, J. A., "On Highly Compressible Helical Springs and Rubber Rods, And Their Application For Vibration-Free Mountings II," *Philips Res. Report* 4, pp.49~80, 1948

2. Gent, A. N. and Lindley, P. B., "The Compression of Bonded Rubber Blocks," *Proc. Instn. Mech. Engrs*, Vol. 173, No 3., pp.111~117, 1959

3. Gent, A. N., "Elastic Stability of Rubber Compression Springs," *Journal of Mechanical Engineering Sciences*, Vol.6, No. 4, pp. 318~326, 1964

4. Kelly, J. M., *"Earthquake-Resistant Design with Rubber,"* 2nd Ed., Springer-Verlag, London, England, 1997

5. Buckle, I. G., and Liu, He., "Finite Element Analysis of Elastomeric Isolation Bearings for different Connection Details," *Proceedings from the First U.S.-Japan Workshop on Earthquake Protective Systems for Bridges*, Technical Report NCEER-92-0004, pp.151~167, 1992

6. Koh, C. G., and Kelly, J. M., "Applicability of the Southwell Plot to Shear Deformable Columns," *Journal of Testing and Evaluation*, Vol. 17, No. 5, pp.287~291, 1989

7. FEA Ltd., *"LUSAS Element Library, User's Guide, Theory Manual,"* Ver. 12, London, England, 1997

Transactions of the 15th International Conference on
Structural Mechanics in Reactor Technology (SMiRT-15)
Seoul, Korea, August 15-20, 1999

Characteristic Tests of High Damping Rubber Shear Specimens for Seismic Isolators of KALIMER

Jae-Han Lee, Bong Yoo and Gyeong-Hoi Koo

Korea Atomic Energy Research Institute, Korea

ABSTRACT

The shear modulus and the equivalent damping of rubber shear specimens are investigated through various shear dynamic tests such as cyclical loading tests, loading rate tests, incremented shear strain tests, loading history tests, and recovery tests. The shear modulus and shear damping are decreased as the number of loading cycles increases, and increased as the loading rate increases. As the shear strain is larger than 100%, the shear modulus of rubber is increased due to the rubber hardening. Two types of loading history are applied to each rubber specimen and the affection on the rubber characteristic is estimated. From the recovery tests, it is revealed that the stabilized rubber mechanical properties are recovered after about 3 hours, and the rubber behavior approaches the initial properties after 1.5 years of relaxation.

1. INTRODUCTION

The seismic isolators fabricated for the seismic isolation design for KALIMER (Korea Advanced Liquid Metal Reactor) are shown in Fig.1. The manufacture and testing of these bearings have taken a lot of time and cost. Since rubber is the main deformable element in the bearing, the finite element analysis technique for rubber bearings based on the rubber specimen test data such as uniaxial, pure shear and compression has being developed[1,2]. Various shear dynamic tests for small specimens of rubber were performed to correlate the test results with the behaviors of the isolator, because the mechanical behavior are obtained quickly compared to full- and scale-sized bearing tests [3,4,5]. In this paper, extensive tests of small specimens of rubber used in seismic isolator for KALIMER are performed to obtain the mechanical characteristic responses of rubber compounds.

A testing facility for rubber specimens has been established in Argonne National Laboratory(ANL). High precision dynamic testing is performed on Instrons Corporation's 8500 series universal testing machine. This servo-hydraulic machine has a 55 kip load frame, a 5 kip actuator and can comfortably perform tests over the range of interest responses for rubber specimens, which is from 0.005Hz to 5Hz.

The 26 specimens made of high damping rubber used in the seismic isolators of the KALIMER, which is developed by KAERI, are 3 bar lap shear specimens of LTV type (Fig.2). The 26 specimens are sequentially named and many kinds of tests have been performed over the last 1.5 years. The test results for the several representative specimens named as SD9704A, SD9704B, K98-13, K98-17, K98-19 are presented in this paper. The dimensions of the LTV

type rubber specimens are measured in Table 1. A comparison of test results for shear strain level tests between the specimen and the isolator is also briefly introduced.

Table 1. Dimensions of Rubber Specimens

	SD9704B SD9704A	K98-13	K98-17	K98-19
Steel Bar Thickness(cm)	0.445 x 3	0.813 x 3	0.800 x 3	0.805 x 3
Rubber Area (cm^2)	2.54 x 2.54	2.54 x 2.54	2.54 x 2.54	2.54 x 2.54
Rubber Thickness(cm)	0.686	0.635	0.640	0.643

Fig. 1 Scaled Laminated Rubber Bearings

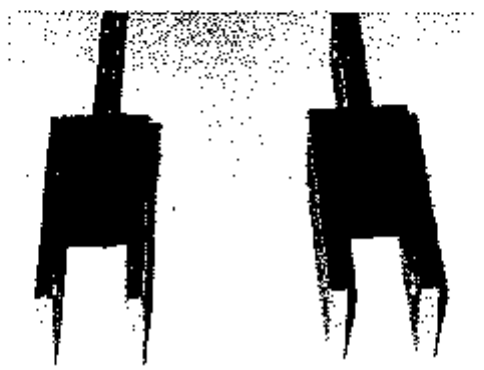

Fig. 2 Rubber Specimen for Shear Dynamic Test

2. TEST ITEMS FOR RUBBER SPECIMENS

The cyclical test, which is consecutively cycled for twenty-six fully reversed cycles at 100% strain and 0.5 Hz, is performed with the specimen SD9704B. After 3 days relaxation, loading rate tests are performed on the same specimen to find its sensitivity to the loading rate in which each loading rate has six cyclical loads at 100% shear strain. The applied loading rates are of 0.005, 0.025, 0.05, 0.10, 0.5, 1.0, 2.5 and 5.0Hz. After another 2 days relaxation, shear strain level tests of six cycles of fully reversed loading at 0.5 Hz are applied at the shear strain levels of 5, 10, 20, 50, 75, 100, 150, 200, and 250%.

For ascertaining the loading history effects of rubber specimens, two types of test sequence are defined and applied to the two specimens of K98-13 and K98-17, respectively.

Using the K98-19 specimen, recovery tests using the 26-cycles loads at 100% shear strain are performed with test intervals of 15 minutes and three hours. And the 26-cycles test for the SD9704A specimen taken at a large shear strain 1.5 years ago is performed to compare the results with those of 1.5 years ago.

3. TEST RESULTS OF RUBBER SPECIMENS

The shear modulus and the effective damping per cycle for all six kinds of tests are calculated and represented in Figures 3 to 9.

3.1 Cyclical test

A cyclical test was performed on an unscragged (virgin) specimen. The specimen was subjected to 26 cycles of sinusoidal shear strain of 100% at 0.5 Hz. Fig.3 shows the variations of shear modulus and damping with cycle numbers. The main decrease of shear modulus and damping occurs within a few cycles, and relatively small changes occur after a few cycles.

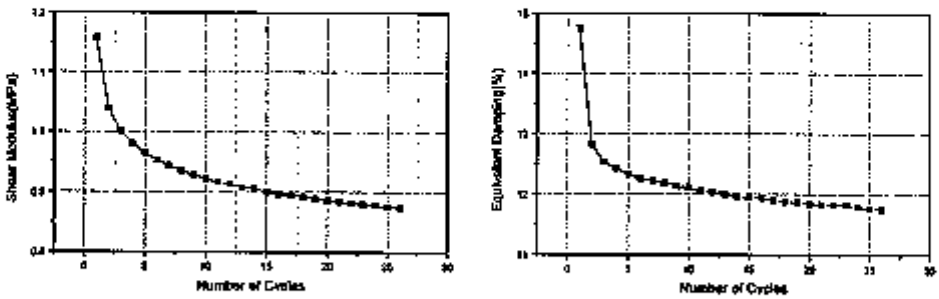

Fig. 3 Cyclical Test of 100% Shear Strain for SD9704B

3.2 Loading Rate Tests

The loading rate tests of 100% shear strain with 6 cycles and 8 different test frequencies were performed using the same specimen(SD9704B) which had taken the shear cyclical test with 100% strain 3 days ago. Fig. 4 shows the variations of shear modulus and damping with loading rate over the frequency range of 0.005 Hz to 5.0 Hz. The shear modulus and the damping values increase as the loading rate increases. The shear modulus and damping at 0.005 Hz are smaller than those at 0.5 Hz by about 30% and 15%, respectively.

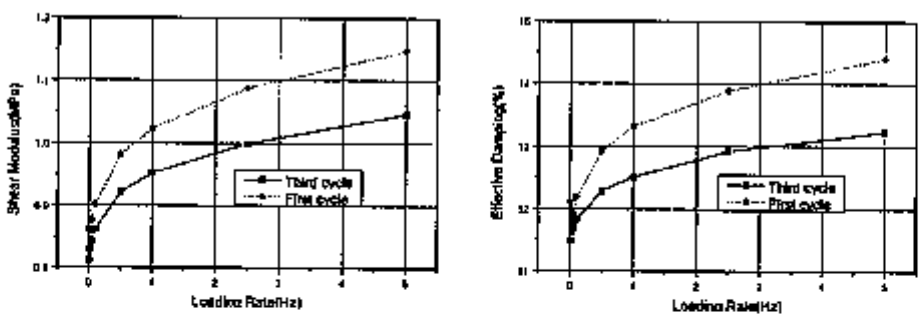

Fig. 4 Loading Rate Tests of 100% Shear Strain after 26-Cycles Test for SD9704B

3.3 Shear Strain Level Tests

The tests were performed with various shear strains of 5%, 10%, 25%, 50%, 75%, 100%, 150%, 200% and 250% at 0.5Hz. The results for the effective shear modulus and the equivalent damping for the first and the third cycles for the SD9704B specimen are given in Fig.5. As the shear strain increases, the shear modulus decreases until 100%, and after that is increased by rubber hardening. The damping monotonically decreases according to the shear strain level. The characteristic values of the third cycle are decreased compared with the first ones because of the rubber softening.

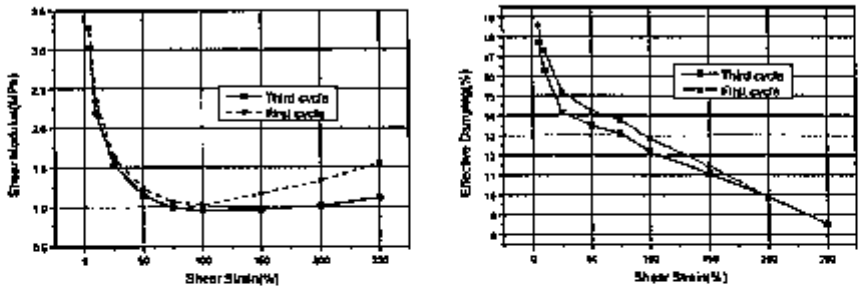

Fig. 5 Shear Strain Level Tests after 26-Cycles and Loading Rate Tests for SD9704B

3.4 Loading History Effect Tests

A characteristic test sequence (Type I), referred to as strain-buildup tests, involves the shear strains of 10/50%, 10/50/100%, 10/50/100/150%, 10/50/100/150/200%, and 10/50/100% to assess the change in modulus at lower shear strains due to cycling at higher shear strains. If these effects are great, then there can be significant implication on analytical models for bearing response, particularly for analyses of response to long-duration earthquakes where repeated cycling at a wide range of strains could occur.

As the historical shear strain taken by the rubber specimen is larger, the reduction of the shear modulus values at 10% strain is larger. The equivalent damping at 10% shear strain is not greatly affected by the shear strain magnitude experienced by the rubber specimen. The shear modulus values at 50% are slowly decreased, but the equivalent damping is slightly

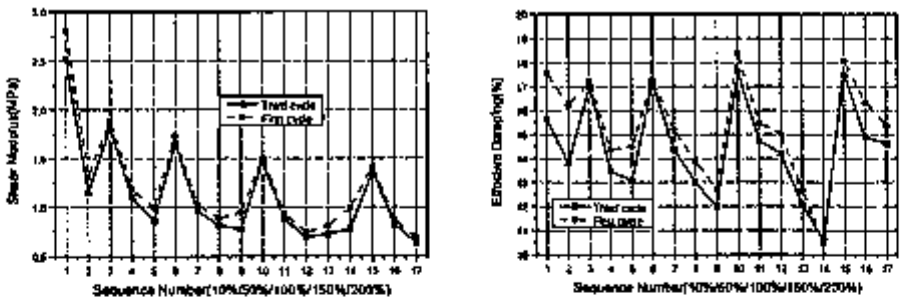

increased.

Fig. 6 Results of Loading History Effect Tests – Type I of K98-13

Similar sequence (Type II), intended to capture load-history effects in the bearings, involves alternating strains of 10% and 150% with five cycles. The objective of this group of tests is to examine the change in the effective modulus at 150% strain due to repeated cycling and recover. As shown in Fig. 7, the shear modulus and damping values remains similar values except the first cycle at the 10% and 150% both.

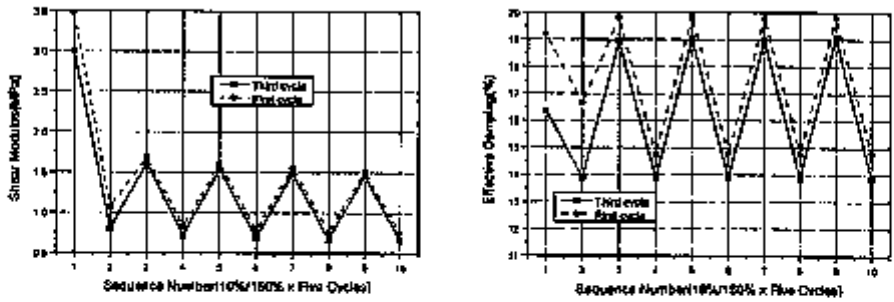

Fig. 7 Results of Loading History Effect Tests –Type II for K98-17

The shear modulus of the shear strain range of 10% to 150% varies 1.7 - 0.7 MPa for Type I and 1.6 - 0.7 MPa for Type II. The equivalent damping varies 17.5 – 12% for Type I and 19 – 14% for Type II. This means that the rubber behavior is almost independent of loading history Type.

3.5 Recovery Tests

To investigate the recovering of the mechanical performance of rubber after shear dynamic loading, two times of 26-cycles test at 100% shear strain for K98-19 specimen are carried out at 15 minutes and at 3 hours after initial 26-cycles test. Fig. 8 shows that the shear modulus and the damping have not recovered to the initial mechanical performance, but the test results of 3 hours are very close to the 15 minutes test ones. It means that the rubber mechanical characteristics are recovered after 3 hours after initial deformation.

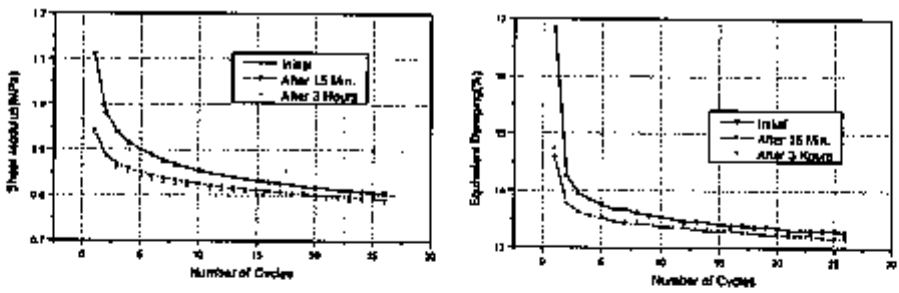

Fig. 8 Recovery Tests for K98-19

An interesting 26-cycles test was performed to check the recovering ability of rubber for the SD9704A specimen, which had taken the shear strain level tests of the strain range of 5% to 300%, loading rate tests of 100% shear strain, and shear cyclical tests 1.5 years ago. The comparison of the shear cyclical test results is represented in Fig. 9. The results show that the shear modulus of the rubber specimen taken 3 different kinds of tests 1.5 years ago can be recovered exceedingly by about 110% of those in the 1st cyclical test, but the damping by about 90% of those in the 1st cyclical test.

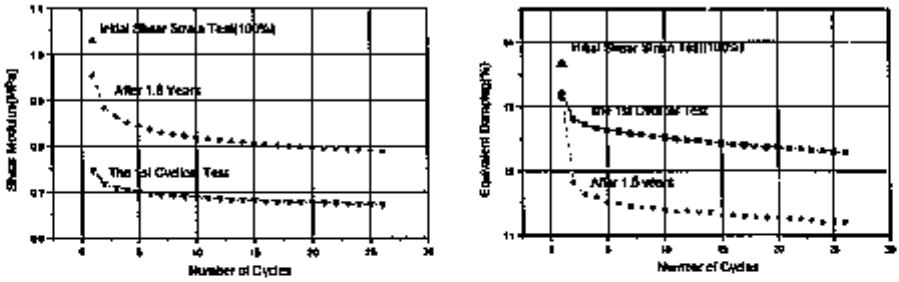

Fig. 9 Recovery Tests for SD9704A

3.6 Correlation between Specimen Tests and Bearing Tests

The characteristic test results of the rubber specimen are compared with those of the 1/8 scaled-bearing [6]. As shown in Fig.10, the shear modulus of the specimen is higher than those of the bearing by about12%, but the equivalent damping is smaller than those of the bearing by about 17%.

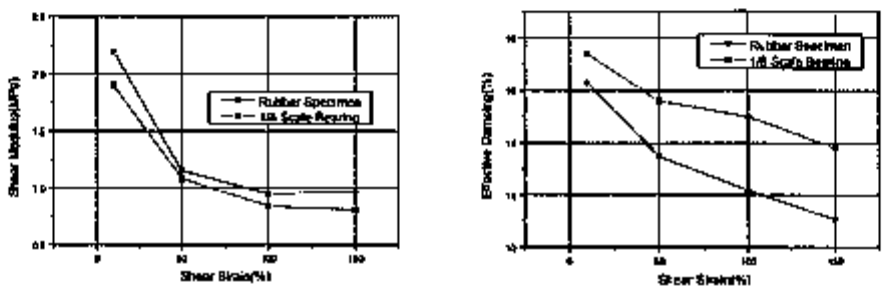

Fig. 10 Correlation between Specimen Tests and Bearing Tests

4. CONCLUSIONS

Through the various shear dynamic tests such as cyclical loading, loading rate, shear strain level, loading history effect, and recovery tests, the shear modulus and the equivalent damping decreases as the number of loading cycles increases, and increases as the loading rate increases. As the shear strain is larger than 100% shear above, the shear modulus of rubber is increased due to the rubber hardening.

From two types of loading history effect tests, the reduction magnitude of the shear modulus values at 10% strain is larger as the experienced shear strain is larger, while the equivalent damping at 10% shear strain is not affected by the shear strain magnitude experienced by rubber specimen. The shear modulus and the equivalent damping are mostly dependent on the maximum shear strain experienced by the specimen rather than the loading history types.

From the recovery tests, the stabilized mechanical properties of rubber are recovered after

about 3 hours, and after 1.5 years of relaxation, which approach the initial virgin properties.

The shear modulus of specimen test is higher than those of 1/8 scaled bearing by about12%, but the equivalent damping is smaller than those of the bearing by about 17%.

Acknowledgement

This work was performed under the long term nuclear R&D program sponsored by the Ministry of Science and Technology of Korea. We also greatly appreciate Dr. H. Chung and his colleagues for their cooperation on the tests at ANL.

REFERENCES

1. Yoo, B., Lee, J.H. and Koo,G.H., IAEA Research Co-ordination Meeting (RCM) on "Intercomparison of Analysis Methods for Seismically Isolated Nuclear Structures," Hertford, UK, May 26-27, 1998.
2. IAEA Research Co-ordination Meeting(RCM) on "Intercomparison of Analysis Methods for Seismically Isolated Nuclear Structures," St. Petersburg, Russian Federation,1996.
3. Kulak, R.F. and Hughes, T.H., "Correlation of Elastomer Material Properties from Small Specimen Tests and Scale-size Bearing Tests," Proceedings Fifth National Conference on Earthquake Eng., Chicago, IL, 1994.
4. Kulak, R.F. and Hughes, T.H., "Mechanical Behavior of a Suite of Elastomers Used for Seismic Base Isolation," PVP Vol.319,Seismic, Shock and Vibration,ASME,1995, pp211-214
5. Kulak, R.F., "Key Findings from R&D Activities at Argonne National Laboratory for Seismic Isolation Bearings," ASME PVP 96, 1996.
6. Aikan, Ian D., Clark, Peter W. and Kelly, James M., Experimental Testing of Reduced-Scale KAERI Seismic Isolation Bearings, EERC, Univ. of California at Berkeley, August 1996.

Transactions of the 15th International Conference on
Structural Mechanics in Reactor Technology (SMiRT-15)
Seoul, Korea, August 15-20, 1999

Shaking Table Test of Three-Dimensional Base Isolation System Using Laminated Thick Rubber Bearings

Kenji Kanazawa, Kazuta Hirata and Akihiro Matsuda

Central Research Institute of Electric Power Industry, Japan

ABSTRACT

In order to reduce horizontal and vertical seismic response of internal equipment in fast breeder reactor (FBR) plants, performance of three-dimensional (3-D) base isolation system using laminated thick rubber bearings as isolators is evaluated. Shaking table tests for scale models of base isolated structure are carried out. At first, horizontal and vertical shaking table tests are conducted independently for sinusoidal wave and white noise input to evaluate response characteristics of the model structures. Then an artificial earthquake and the natural earthquake motions are used for horizontal and vertical simultaneous shaking to evaluate the effect of the base isolation. Test results show that the horizontal response of the 3-D and the horizontal base isolation system is reduced similarly, and the vertical response of the 3-D base isolation system is reduced in the frequency range influential to internal equipment.

INTRODUCTION

In the case of FBR plants, reduction of the seismic loads is a matter of great concern in the design aspect, as internal pressure of the components is not a dominant load and structural design of components is strongly affected by seismic load. Three-dimensional (3-D) base isolation system, where seismic loads in both horizontal and vertical directions are to be reduced, is considered very effective, in order to reduce seismic loads for inner equipment in fast breeder reactor (FBR) plants.

In the last decade, researches on the application of horizontal (or two-dimensional, 2-D) base isolation systems to FBR have been conducted in Japan (e.g., Sawada, et al., 1989). In these studies, laminated thin rubber bearings (thin RBs) are supposed as seismic isolators. By using thin RBs, horizontal base isolation system is realized which can reduce horizontal seismic loads to superstructure and equipment, and the concept of horizontally base-isolated FBR plants using thin RBs have been widely accepted. Usually, the vertical stiffness of thin RBs used for horizontal base isolation system is far higher than the horizontal one and vertical response amplification is suppressed, but still vertical response cannot be reduced.

However, it is pointed out that the reduction of vertical seismic load as well as horizontal one can be effective to seismic design of some components of FBR (Yashiro et al, 1998), and various types of 3-D isolation systems have been proposed, which are classified into two types. One is the 3-D base isolation type where whole reactor building is three-dimensionally isolated, and the other is the partial 3-D isolation type where reactor building is

supported by horizontal isolators and primary equipment in the building are supported by vertical isolators. In the former type, 3-D isolators such as thick RBs, or series combination of horizontal and vertical isolators (in this case, thin RBs are used as horizontal isolators and dish springs (Fujita, et al, 1995) or air springs (Tokuda, et al, 1995) are used as vertical isolators) are proposed. In the latter type, the building is horizontally isolated by thin RBs and the equipment are supported and vertically isolated by coil springs (Sonoda, et al, 1987) or dish springs (Morishita, et al, 1995). In these previous studies, vertical isolation period were chosen between 0.25 and 0.5 sec, which is considered effective to reduce vertical response of primary equipment. For 3-D isolation system with this vertical isolation period, maximum vertical acceleration (or ZPA: Zero Period Acceleration) of the reactor building is still larger than that of the ground motions, however, the maximum vertical acceleration response of the primary equipment is reduced compared to that in horizontally base-isolated reactor building. The 3-D isolation system with thick RBs proposed here is also based on the same principle.

In this research, authors conducted shaking table tests for scale models of the 3-D base isolation system, for the purpose of evaluating the effectiveness of the 3-D base isolation system using thick RBs. In the study on the horizontally base-isolated FBR plant, horizontal and vertical fundamental periods of the 2-D base isolation system are chosen to be 0.5 and 0.05 sec respectively (Sawada, et al., 1989). According to the study on the 3-D base isolation system (Yashiro, et al, 1998), when the vertical isolation period is set to be 0.25 sec, the 3-D base isolation system reduces vertical seismic load for internal equipment. Hence, in the reference plant in this study, horizontal and vertical isolation period are set to be 0.5 and 0.25 sec in 3-D base isolation system, and 0.5 and 0.05 sec in 2-D base isolation system, respectively.

EXPERIMENTAL MODEL

Base Isolated Model

Shaking table tests were carried out for three types of scale models shown in Table 1 (Model-1, 2 and 3), and these models were designed according to the law of similarity shown in Table 2. Each model is constructed of a rigid mass supported by four natural rubber bearings, with dampers for horizontal and vertical directions attached. Model-1 is the 3-D base isolation system, which is the high-rise rigid mass supported by thick RBs. In Model-2, a low-rise rigid mass of the same weight as used in Model-1 is supported by thick RBs, and Model-3 is the 2-D base isolation system in which the same rigid mass as Model-1 is supported by thin RBs, with dampers attached for horizontal direction only.

Fig.1 shows the high-rise model (Model-1 and Model-3) and the row-rise model (Model-2). Ratio of the height of the center of gravity of the rigid mass to the distance between isolators

Table 1 Specification of Models

Item	Model-1 3-D Isolation	Model-2 3-D Isolation	Model-3 2-D Isolation
Superstructure	High Rise	Low Rise	High Rise
Weight(tonf)	8.86	9.00	9.00
Isolator	Thick NRB	Thick NRB	Thin NRB
Damper Hori.	Attached	Attached	Attached
Vert.	Attached	Attached	Not-Attached

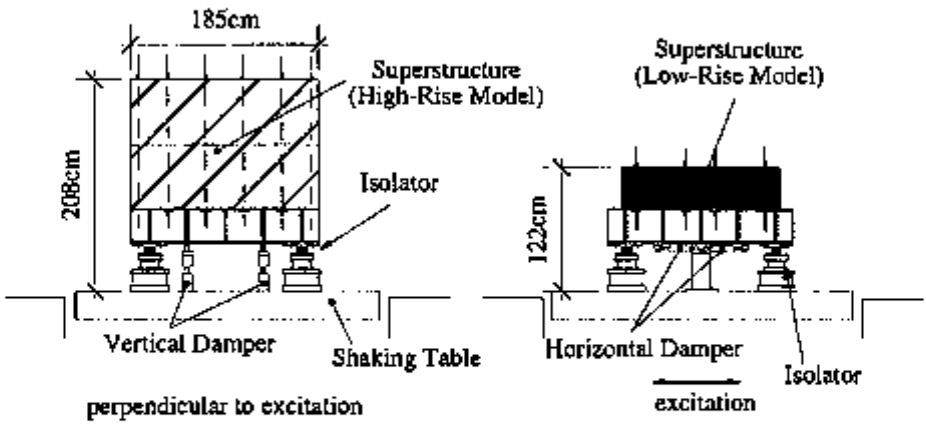

Fig.1 Experimental Models

for high and low-rise model is 0.6 and 0.3, respectively.

Table 2 Low of Similarity

Parameter	Prototype	Model
Displacement	1	1/9.4
Acceleration	1	1
Force	1	9.4
Vertical Pressure	1	1
Time	1	$1/\sqrt{9.4}$

Isolator

The prototype thick RB is natural rubber bearing and its dimensions are; diameter = 101cm, total thickness of rubber = 24.6cm, number of rubber sheets = 3, design vertical load = 190 tonf, primary shape factor (= loaded area / force-free area) S1 = 3.1 and secondary shape factor (= diameter / total thickness of rubber) S2 = 4.1, respectively. Scale models of thick RB were made according to the law of similarity depicted in Table 2.

Table 3 shows dimensions of thick and thin RBs. In this table, horizontal period and vertical frequency are evaluated from the loading test results of RBs. Transforming from the

Table 3 Dimensions of Isolators

Item		Thick NRB	Thin NRB
Loading Weight	(tonf)	2.25	2.25
Hori. Spring Const.	(tonf/cm)	0.201	0.244
Hori. Natural Period	(sec)	0.672	0.609
Vert. Spring Const.	(tonf/cm)	24.9	129.4
Vert. Natural Freq.	(Hz)	16.57	37.78
Rubber Layers	(cm x num)	6.5 x 4	2.6 x 10
Diamater	(cm)	10.7	10.7
Shear Modulus of Rubber	(kg/cm2)	6	6

scale model to real plant, the horizontal isolation period and the vertical isolation frequency of thick RBs became 2.1 sec and 5.4 Hz, and those of thin RBs became 1.9 sec and 12.3Hz, respectively. Vertical natural frequency of thick RBs were slightly higher, and that of thin RBs were lower, than specified values.

Damper

Cylindrical oil dampers were used as damping device in horizontal and vertical directions, and attached to the basement of the rigid mass and to the shaking table with hinges. The damping force which is proportional to the axial velocity was selected so that the modal damping factors of the scale models would become 20% for the 1st natural frequency of both horizontal and vertical directions.

TEST METHOD

Input Motion

A shaking table was used, which could generate horizontal (one direction) and vertical motions simultaneously.

At first, in order to evaluate fundamental dynamic characteristics of the base-isolated models, horizontal and vertical shaking were given independently to the models using sinusoidal wave (1-30Hz, table acceleration 50gal) and white noise (1-50Hz, table acceleration 200gal).

Then, in order to confirm the performance of the models under earthquake motions, an artificial earthquake and the natural earthquake motions such as El Centro (1940) and JMA Kobe (1995) were used for horizontal and vertical simultaneous shaking. Fig.2 shows target response spectra (Sv, h=5%) of the artificial earthquake, which takes into account slightly long period contents (Ishida, et al., 1989). The artificial earthquake are synthesized to fit the target response spectra with phase components of earthquake records at La Union (1985 Mexico Earthquake), and the ratio of the vertical target response spectrum to the horizontal one is assumed to be 0.6. Fig.3 shows response spectra calculated from the original records of El Centro and JMA Kobe. The acceleration amplitude for El Centro and JMA Kobe was set to be 1.0 and 0.5 times the original records respectively. For the input motion of the shaking table, time scale of these waves were reduced by 1/3.1 according to the law of similarity.

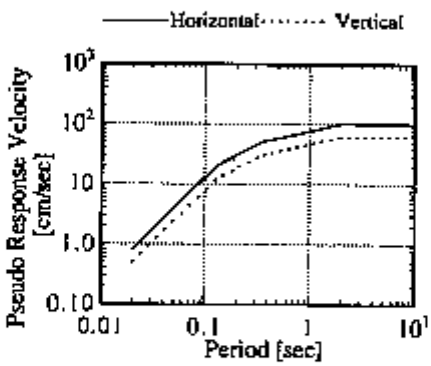

Fig.2 Design Response Spectra for Artificial Earthquake Motion

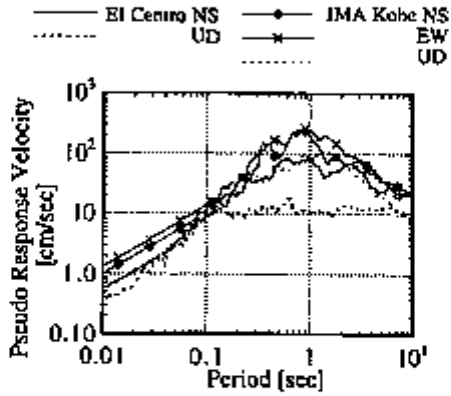

Fig.3 Response Spectra of Natural Earthquake Records

Response Reduction

Maximum acceleration of the shaking table and the models at the center of gravity, and their ratios are shown in Table 4. As for horizontal response, maximum acceleration response of the scale models (Model-1, 2, 3) is reduced compared to that of shaking table. On the other hand, as for vertical response, in Model-1, Model-2 and Model-3, maximum acceleration response is amplified compared to that of shaking table, except for the case of Model-1 and Model-2 of El Centro wave input. This result indicates that 3-D base isolation system with the thick RBs cannot necessarily reduce vertical maximum acceleration response in term of peak value. Exceptions in the case of El Centro wave input can be explained because the dominant frequency components of this wave lie in the frequency range over 25Hz where response reduction effect appears.

Table 4 Maximum Acceleration of Input Motions and Responses of Model Structures

	Model-1			Model-2			Model-3		
	Inp.	Resp.	Resp./Inp.	Inp.	Resp.	Resp./Inp.	Inp.	Resp.	Resp./Inp.
Horizontal Responses									
Artificial Earthquake	332	225	0.68	320	214	0.67	304	227	0.75
El Centro(NS-UD)	311	134	0.43	312	129	0.41	298	169	0.57
JMA Kobe(NS-UD)	319	90	0.28	328	88	0.27	303	117	0.38
JMA Kobe(EW-UD)	395	161	0.41	402	137	0.34	405	218	0.54
Vertical Responses									
Artificial Earthquake	210	327	1.56	197	358	1.81	182	221	1.21
El Centro(NS-UD)	192	141	0.73	209	146	0.70	168	431	2.56
JMA Kobe(NS-UD)	117	208	1.78	157	243	1.55	183	230	1.25
JMA Kobe(EW-UD)	158	249	1.58	166	231	1.39	182	221	1.21

Horizontal floor response spectra (FRS) at the center of gravity (CG) and the bottom are shown in Figs.7 and 8 respectively. As shown in Fig.7, three FRS curves for scale models at CG are almost the same. On the other hand, as shown in Fig.8, three FRS curves for the models at the bottom show slightly difference in the period range less than 0.1 sec. FRS curves for Model-1 and Model-3 have peaks between 0.04 and 0.1 sec and between 0.02 and 0.03 sec respectively. These peaks seem to be affected by the rocking mode, and the FRS curve for Model-2 which is the low-rise model dose not have a significant peak by the rocking mode.

Vertical FRS for Model-1 and Model-3 are shown in Figs.9 and 10, and the vertical natural frequencies of the primary equipment exist in the period range shorter than 0.04 sec (in real plant; more than 8 Hz). It is noted that vertical components of the input waves in these cases are not in good agreement with each other, because the shaking table was affected by the response of the model structure. As shown in Fig.9, FRS of the three-dimensionally base-isolated Model-1 is larger than that of the shaking table in the period range between 0.04 and 0.1 sec, however, in the period range less than 0.04 sec it dose not hold true. On the other hand, as shown in Fig.10, FRS of the horizontally base-isolated Model-3 agree with the response spectrum of the input motion in the period range longer than 1.0 sec, however, in the period range between 0.01 and 0.02 sec FRS of the model is larger than the response spectrum of the input motion.

Measurement

Fig.4 shows arrangement of measuring instruments on the models. Displacement transducers were set to measure relative displacement between shaking table and the bottom of the superstructure (rigid mass), and force transducers were installed between the shaking table and the isolators, to measure shear and axial forces acting on each isolator.

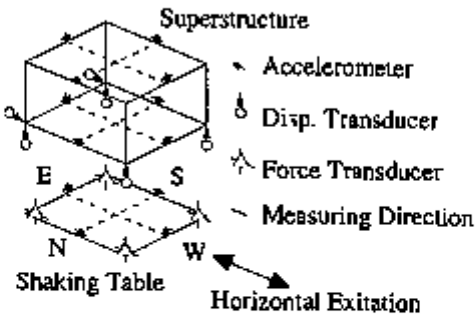

Fig.4 Arrangement of Instruments

TEST RESULTS

Dynamic Characteristics of Scale Models

Fig.5 shows horizontal resonance curves at the top of the models obtained from the simusoidal shaking test. The 1st horizontal resonance frequencies of Model-1 and Model-2 are 1.4-1.5Hz, and that of Model-3 is 1.7 Hz. From theoretical transfer functions fitting these experimental curves, the horizontal damping factors for the 1st mode of the models are estimated 20-22%. The 2nd horizontal resonance frequencies of Model-1 and Model-2 estimated from phase curves in this figure are 17Hz and 26 Hz respectively, which agree well with the theoretical rocking frequencies (17.6 Hz and 25.9 Hz) using the design parameters. By the same calculation, the theoretical rocking frequency of Model-3 is estimated 42.6 Hz.

Fig.6 shows vertical resonance curves at the top of the scale models obtained from the white noise excitation. The 1st vertical resonance frequencies of Model-1 and Model-2 are 16-17 Hz, and that of Model-3 is 37 Hz. The 1st vertical damping factors of Model-1 and Model-2 are 11-13%, and that of Model-3 is 6%, which are estimated in the same way as the horizontal damping factors. In the case of Model-1 and Model-2, where vertical dampers were attached, vertical damping factors by the experiment prove smaller than the designed one (20%), which is because the vertical relative displacement of the models was so small that enough damping force of the damper could not be obtained.

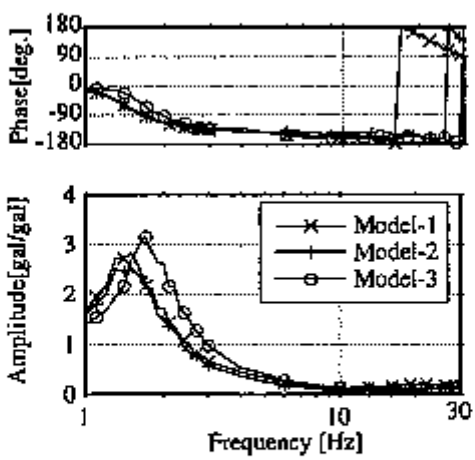

Fig.5 Horizontal Frequency Respose

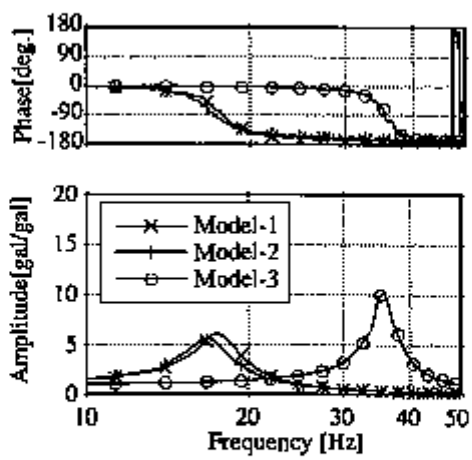

Fig.6 Vertical Frequency Response

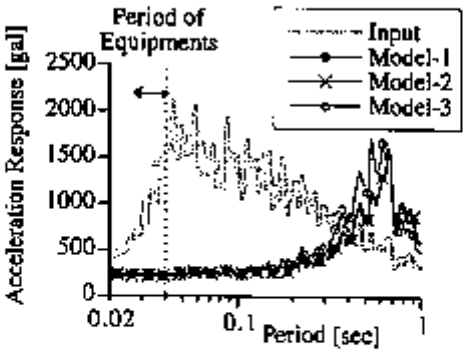

Fig.7 Horizontal Response Spectra at the Center of Gravity of Models

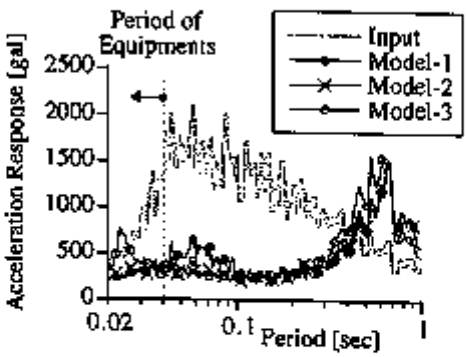

Fig.8 Horizontal Response Spectra at the Bottom of Models

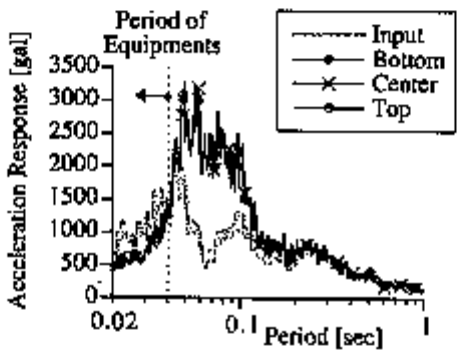

Fig.9 Vertical Response Spectra of Model-1

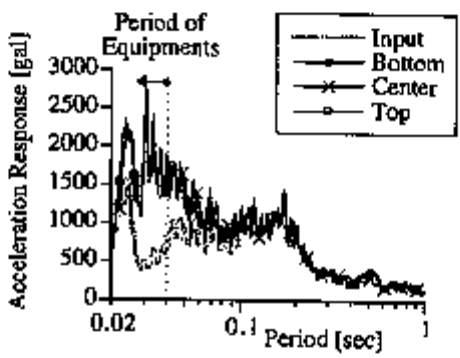

Fig.10 Vertical Response Spectra of Model-3

Above results indicate that the vertical seismic load for the equipment can be reduced, by setting the vertical isolation frequency appropriately considering the vertical dominant frequency of the equipment or ground conditions. Thus the vertical isolation frequency is selected between the maximum and minimum limit specified from several factors (e.g., stability, manufacturability). For example, if the dominant vertical frequencies of the primary equipment exist over 8 Hz, the vertical acceleration response of these equipment can be reduced by 3-D isolation system with the thick RBs whose specifications for the reference plant were presented in this paper.

Rocking Motion of Isolated Models

Rocking ratios of the the models under the earthquake excitations are shown in Table 5, where the rocking ratio r is defined as the follows.

$$r = Xr / Xmax \times 100\ [\%] \qquad (1)$$

where Xr is the horizontal displacement at the top of the model due to rotational motion when the maximum horizontal displacement occurs, Xmax is the maximum horizontal displacement at the top of the models.

The rocking ratios of Model-1 (3-D) is about three times as large as those of Model-3 (2-D), however, the rotational angle is assessed at 3.48×10^{-4} rad in the case of the artificial earthquake input, and the rotational motion is considered quite small.

Table 5 Ratios of Rocking Motion

	Mode-1	Model-2	Model-3
Artificial Earthquake	3.28	1.63	1.09
El Centro (NS-UD)	3.21	1.63	1.06
JMA Kobe (NS-UD)	3.12	1.88	1.16
JMA Kobe (EW-UD)	3.02	1.52	1.08

CONCLUDING REMARKS

The results of this research are summarized as follows.
(1) As for the horizontal response, 3-D base isolation system using thick rubber bearings shows similar performance to that of 2-D system using thin rubber bearings, and for both systems rocking response is very small.
(2) It is shown that the vertical response of the 3-D base isolation system can be reduced in term of floor response spectrum in the specific frequency range where the vertical response of the internal components are affected. And the effectiveness of the 3-D base isolation system using the thick rubber bearings is proved from the experiment.

ACKNOWLEDGMENT

The authors are grateful to Dr. T. Matsuda of Kyusyu University, Dr. S. Yabana of CRIEPI and Dr. Y. Fukushima of Kajima Corporation for their useful discussions.

REFERENCES

1.Sawada, Y. et al., "Seismic isolation test program," *Trans. of the 10th SMiRT*, pp.K.691-696, 1989.
2.Yashiro, T, et al., "A Study on the Simplification for FBR Nuclear Components by 3-D Base Isolated System," *Proc. of the 6th International Conference on Nuclear Engineering*, pp.305-314, 1998.
3.Fujita, T. et al., "Fundamental study of three-dimensional seismic isolation system for nuclear power plants," *Proc. of the 11th World Conference on Earthquake Engineering*, Paper No. 1440, 1996
4.Tokuda, N. et al., "Three-dimensional base isolation system for assumed FBR reactor building," *Trans. of the 13th SMiRT*, pp.K.513-518, 1995.
5.Sonoda, Y. et al., "A study of the seismic isolation of fast breeder reactor plant 3-D seismic isolation of reactor structure," *Trans. of the 9th SMiRT*, pp.K.673-678, 1987.
6.Morishita, M., "A conceptual study on vertical seismic isolation for fast reactor components", *Trans. of the 13th SMiRT*, pp.K.529-534, 1995.
7. Ishida, K, et al., "Tentative design response spectrum for seismically isolated FBR," *Trans. of the 10th SMiRT*, pp.K.685-690, 1989.

Transactions of the 15th International Conference on
Structural Mechanics in Reactor Technology (SMiRT-15)
Seoul, Korea, August 15-20, 1999

Seismic Isolation Effects on Core Seismic Response of KALIMER

Gyeong Hoi Koo, Hyeong Yeon Lee and Bong Yoo

Korea Atomic Energy Research Institute, Korea

ABSTRACT

The seismic response characteristics for conceptually designed KALIMER(Korea Advanced Liquid MEtal Reactor) with a seismic isolation technology are investigated using the single row model for SSE load conditions by SAC-CORE code. To study the seismic isolation effects on core seismic responses, the input motions of seismic isolation and non-isolation cases are generated from the seismic time history analysis of reactor system. From the results of analyses, it is verified that an efficient seismic isolation design of reactor system gives significantly reduced core seismic responses and can make to easily satisfy the structural design requirements.

1. INTRODUCTION

In general, seismically isolated system gives a great reduction of seismic acceleration responses. Many researchers are studying to apply this concept to nuclear power plant for enhancing the safety and economy of the structural design[1,2].

The advantages of seismic isolation of reactor system are both on reductions of absolute acceleration response and relative displacement of internal structures. These become more apparent for the LMR core assemblies which have no intermediate core support plates and thus more vulnerable to seismic loads[3].

The analysis modeling of core structure is very complex due to the collision of adjacent assemblies. In this paper, a single row model of conceptually designed KALIMER core is used for seismic time history analysis. This modeling method has been studied to produce more accurate results than the clustering method for RAPSODIE core mock-up[4].

To investigate the seismic isolation effects on core seismic responses, the input motions at the lower diagrid are obtained from the seismic analysis of KALIMER reactor system for 0.5 Hz seismic isolation case and non-isolation case.

2. CORE SEISMIC ANALYSIS

2.1 Core Layout

The conceptually designed KALIMER reactor core is shown in Fig.1, consisting of 379 identical assemblies; 66 drive fuel, 30 internal blanket, 42 radial blanket, 6 control rod, 1 self-actuated shutdown system, 6 gas expansion module, 48 reflector, 54 B_4C shield, 54 in-vessel

storage space, 72 shield. The duct material is HT9 and the duct wall thickness, the outer flat to flat, and the gap between ducts are 4 mm, 157 mm and 4 mm respectively. The assemblies, 4546.7 mm in length with 384.3 mm nosepiece, are locked at the lower diagrid. To prevent the direct contact between adjacent ducts, the load pads are provided at the locations of above active core top and the top of ducts. At the top locations of the outer shield assemblies, a former ring is designed to restrain core free-flowering behavior.

2.2 Seismic Analysis Model

For the core seismic analysis model of very complex core layout, a single row model of a diametral row of the core is used as shown in Fig.1. A single row model used in this paper consists of 21 assemblies including shield, reflector, blanket, GEM, drive fuel, control rod, and USS assembly. Table I shows the sectional properties of assembly used in analysis model. In this table, the equivalent density is obtained using the assumed total mass of each assembly.

Table 1. Input Properties for KALIMER Core Seismic Model

Assembly Type		Elastic Modulus (GPa)	Moment of Inertia (10^{-6} m^4)	Sectional Area (10^{-3} m^2)	Equi-Density (kg/m^3)	Poisson's Ratio	Damping Ratio (%)
Shield	Nosepiece	174.8	1.39	1.206	47619.0	0.3	3.0
	Duct	159.9	6.90	2.120	47619.0	0.3	3.0
Reflector	Nosepiece	174.8	1.39	1.206	50523.9	0.3	3.0
	Duct	159.9	6.90	2.120	50523.9	0.3	3.0
Blanket	Nosepiece	174.8	1.39	1.206	50938.0	0.3	3.0
	Duct	159.9	6.90	2.120	50938.0	0.3	3.0
GEM	Nosepiece	174.8	1.39	1.206	41498.1	0.3	3.0
	Duct	159.9	6.90	2.120	41498.1	0.3	3.0
Drive Fuel	Nosepiece	174.8	1.39	1.206	43676.7	0.3	3.0
	Duct	159.9	6.90	2.120	43676.3	0.3	3.0
Control Rod	Nosepiece	174.8	1.39	1.206	42743.0	0.3	3.0
	Duct	159.9	6.90	2.120	42743.0	0.3	3.0
USS	Nosepiece	174.8	1.39	1.206	42743.0	0.3	3.0
	Duct	159.9	6.90	2.120	42743.0	0.3	3.0

Fig.2 shows the core seismic model used in analysis, consisting of 168-beam elements and 42-impact gap elements. The locations of gap elements are the top load pad (TLP), above-core load pad (ALP), and the top of the outer shield assemblies.

The elastic modulus of the duct using HT9 is calculated using the equation as[5]

$$E = 212.0(1.144 - 4.856\times10^{-4}T),\ GPa,$$

where T is absolute temperature, $^{\circ}K$.

The calculated elastic modulus of duct and nosepiece is 159.86 *GPa* (530°C) and 174.79 *GPa* (380°C) respectively.

The gap properties used in analyses are as follows:

Gaps at ACLP and TLP;

K_g = 10.0 *MN/m*, C_g = 2.44 *kN.s/m*, gap=3.0 *mm*

Gaps between former ring and outer shields;

K_g = 10.0 *MN/m*, C_g = 2.44 *kN.s/m*, gap=4.0 *mm*

The shock damping, C_g during impact is calculated as follows[6];

$$C_g = K_g \frac{(1-\varepsilon^2)T_s}{\pi},$$

where K_g, ε and T_s are the gap stiffness, the contact coefficient of restitution, and the shock duration respectively. In this analysis, ε=0.55, which is for the steel-steel contact, is used and the shock duration is assumed 2.0 ms.

The sectional properties of the duct are calculated as

Area; $A_D = 2\sqrt{3}(DT - T^2) = 2\sqrt{3}\,(0.157\text{x}0.004 - 0.004^2) = 2.12\text{x}10^{-3}\ m^2$

Moment of Inertia;

$$I_D = \frac{5}{48\sqrt{3}}\left[D^4 - (D-2T)^4\right] = \frac{5}{48\sqrt{3}}\left[0.157^4 - (0.157 - 2\text{x}0.004)^4\right] = 6.9\text{x}10^{-6}\ m^4$$

The sectional properties of the nosepiece are calculated as

Area; $A_N = \frac{\pi}{4}(D_o^2 - D_i^2) = \frac{\pi}{4}(0.1^2 - 0.092^2) = 1.206\text{x}10^{-3}\ m^2$

Moment of Inertia; $I_N = \frac{\pi}{64}(D_o^4 - D_i^4) = \frac{\pi}{64}(0.1^4 - 0.092^4) = 1.392\text{x}10^{-6}\ m^4$

The structural damping is assumed as 3% critical damping uniformly. This damping is converted to the proportional damping considering the natural frequencies of each assembly as follows;

$$[C] = \alpha[M] + \beta[K],$$

where α and β are calculated using the relationships

$$\alpha + \beta\omega_i^2 = 2\omega_i\zeta_i.$$

The general assumptions used in modeling are as follows;

- All ducts have uniform sectional properties.
- Ducts are supported as a cantilever at the lower diagrid.
- Core shroud attached to the lower diagrid has a rigid body motion, i.e. there is no relative motion between the core shroud and the lower diagrid.
- Sodium damping and squeeze film damping are ignored.
- No information concerning assembly bowing due to thermal and neutron flux gradients is available so all assemblies are assumed as a straight beam.

2.3 Modal Analysis

The natural frequencies of each assembly are shown in Table 2. From this table, the fundamental frequencies of core assemblies are in range of 1.9Hz to 2.1Hz. This result is used to generate the core stick model included in full seismic analysis model of KALIMER reactor structure. Fig.3 shows the mode shapes of core assemblies obtained from SAC-CORE code.

Table 2. Natural frequencies of Each Assembly Type

Assembly Type	1st frequency (Hz)	2nd frequency (Hz)
Shield	1.96	15.15
Reflector	1.91	14.71
Blanket	1.90	14.65
GEM	2.10	16.23
Drive Fuel	2.05	15.82
Control Rod	2.07	15.99
USS	2.07	15.99

2.4 Seismic Loads

The input motions for the core seismic analysis are generated from the full seismic analysis model of KALIMER reactor system as shown in Fig.4. From the seismic analysis for SSE 0.3g load in cases of the seismic isolation (0.5Hz) and the non-isolation design, the acceleration time history responses at the lower diagrid, which will be used as the input motions of the core seismic analysis, are obtained as shown in Fig.5. From the Fig.5, it is evident that the seismic isolation design gives a significant reduction of the seismic responses in KALIMER design compared with the non-isolation design. This can be showed in the floor response spectra of Fig.6. The maximum peak acceleration of the core input motion is about 0.14g for the seismic isolation case and 0.95g for the non-isolation case.

For the input motions obtained from the seismic analyses of KALIMER reactor structures, the non-linear time history analyses are carried out using the SAC-CORE code. The time interval used in analyses is 2.0ms and the total analysis time is 21 seconds.

3. ANALYSIS RESULTS AND DISCUSSIONS

Fig.7 and Fig.8 show the time history displacement responses of the top locations of the control rod assembly (node 72) and the USS assembly (node 99). In these results, the maximum displacement response of the seismic isolation case is about 2 times lower than that of the non-isolation case. Actually the maximum relative displacement of the core may be so increased in case of the non-isolation design when considering the deflection of the core shroud. The displacement responses at top locations of the control rod assembly and the USS assembly is very important in functional design of the upper internal structure (UIS). The significantly reduced core seismic displacement response affords to easily satisfy the requirements of the relative deflection limits between UIS and core for SSE load condition. Therefore, the seismic isolation design of KALIMER reactor structures gives a great benefit in seismic design of the core and main structures.

Fig.9 shows the maximum peak displacements at top locations of core assemblies. In these results, the displacement responses of the outer shield assemblies are smaller than other ducts because the former ring attached to the core shroud structures restrains severe deflection of outer duct assemblies. The seismic isolation case gives significantly reduced responses in all assemblies than the non-isolation case.

Fig.10 shows the maximum impact forces at the top load pads. The impact responses are smaller in case of the seismic isolation at most load pads than the case of the non-isolation. The small impact force at load pads can ensure the structural integrity of the core in seismic events.

4. CONCLUSIONS

This paper investigates the seismic isolation effects on the core seismic responses of a conceptually designed KALIMER reactor system. From the seismic analyses using 21- single row model of core assemblies by SAC-CORE code, we can see that the seismic isolation design provides significantly reduced core seismic responses compared with the non-isolation design. It is expected that the significantly reduced core seismic displacement response can make to easily satisfy the requirements of the UIS/core relative deflection limits and the core compaction and reactivity insertions for SSE load condition.

ACKNOWLEDGMENT

This paper has carried out under the Nuclear R&D Program by MOST.

REFERENCES

1. T. Yashiro, H.Ikeuchi, and et al.,"A Study on the Simplification for FBR Nclear Components by 3-D Base Isolated System," *ICONE-6*, pp.305-314,1998.
2. G.H. Koo, J.H. Lee, and B. Yoo, "Seismic Response Analyses of Seismically Isolated Structures Using the Laminated Rubber Bearings," *Journal of the Korean Nuclear Society*, Vol.30, No.5, pp.387-395,1998.
3. G.H. Koo, J.H. Lee, and B. Yoo,"Core Seismic Analysis for a Seismically Isolated LMR,"*ASME PVP-Vol. 379, Seismic, Shock, and Vibration Isolation*, pp.221-227, 1998.
4. M. Morishita,"Seismic Response Analysis of RAPSODIE Core Mock-Up in Water Experiment," *IAEA-TECDOC-882*, Vol. 3, pp.39-60, 1995.
5. R.I.DiMelfi et al.,"Microstructural Evolution in a Ferritic-Martensitic Stainless Steel and Its Relation to High-Temperature Deformation and Rupture Models," *The Minerals, Metals & Materials Society*, 1991.
6. K. Itoh, T.Sato, and I.Aizawa,"PEC Core Mock-Up Seismic Analyses by the FINDS Code," *IAEA-TECDOC-789*, Vol.I, pp.79-98,1995.

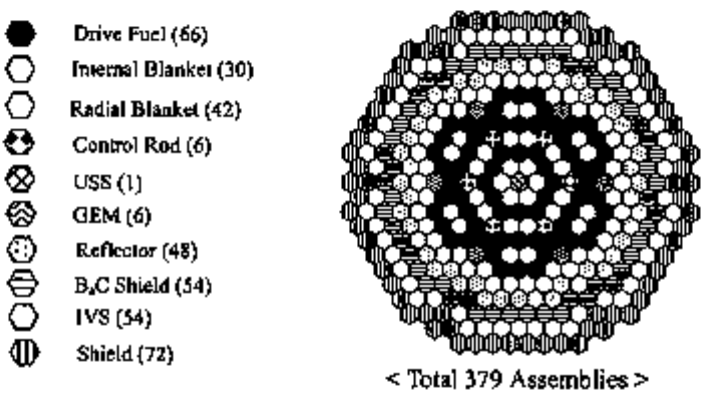

Fig. 1 KALIMER Core Assembly Layout

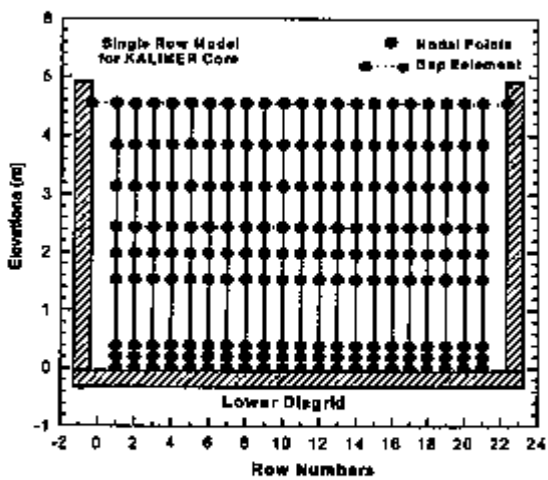

Fig. 2 KALIMER Reactor Core Seismic Analysis Model

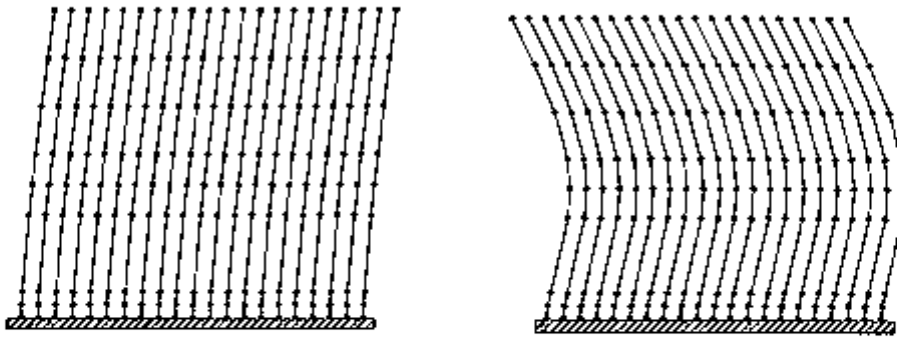

(a) 1st Mode (b) 2nd Mode

Fig. 3 Mode Shapes of Duct Assemblies

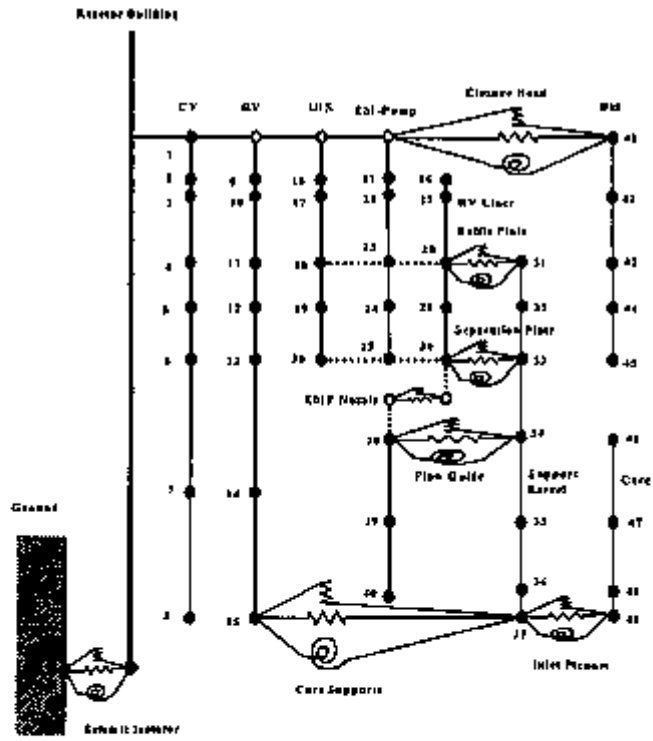

Fig. 4 Seismic Analysis Model for KALIMER Reactor Structures

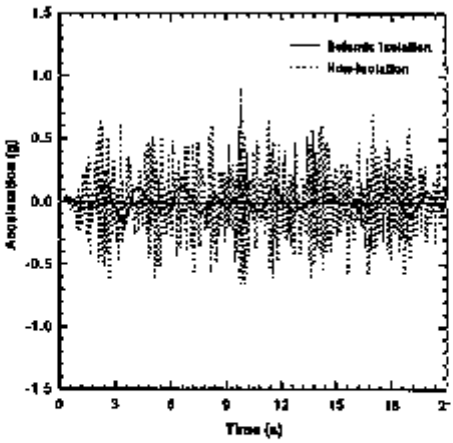

Fig. 5 Input Motions

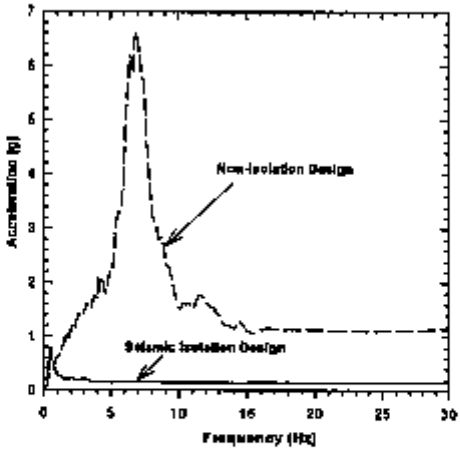

Fig. 6 Spectra for Input Motions

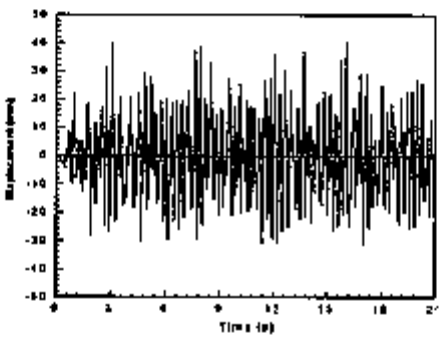

(a) Non-Isolation Case

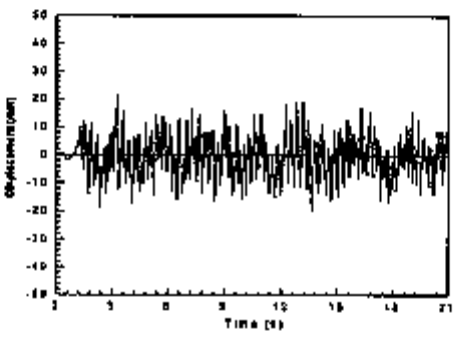

(b) Seismic Isolation Case

Fig. 7 Displacement Responses at Top of Control Rod Assembly (Node 72)

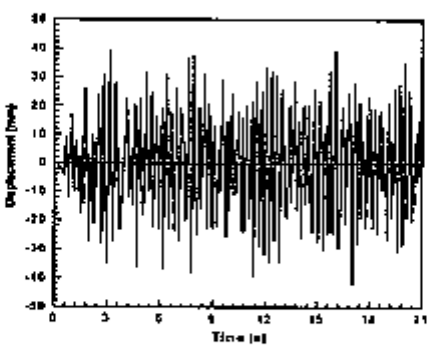

(a) Non-Isolation Case

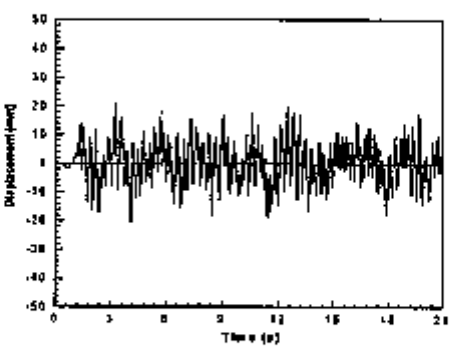

(b) Seismic Isolation Case

Fig. 8 Displacement Responses at Top of USS Assembly (Node 99)

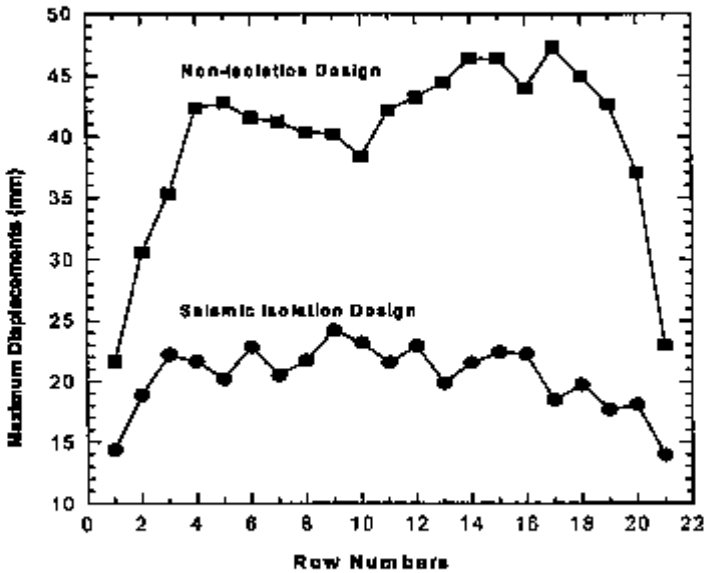

Fig. 9 Maximum Peak Displacements at Core Top Nodes (SSE Load)

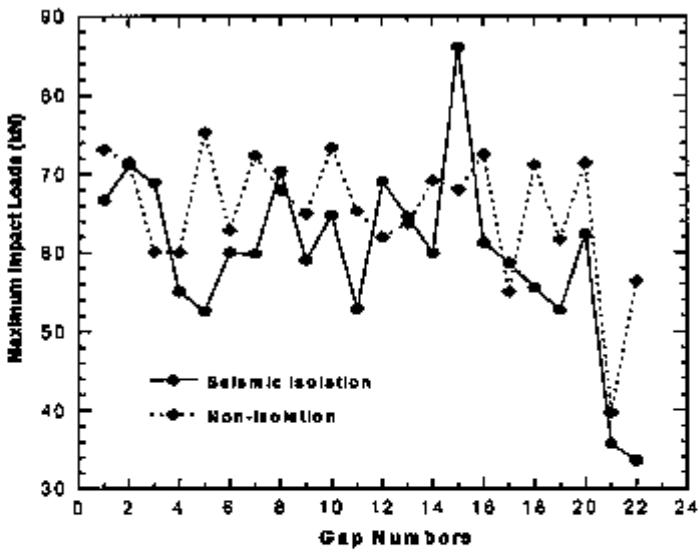

Fig. 10 Maximum Impact Loads at Load Pads (SSE Load)

Transactions of the 15th International Conference on
Structural Mechanics in Reactor Technology (SMiRT-15)
Seoul, Korea, August 15-20, 1999

Seismic Base Isolation Technologies for KALIMER

Bong Yoo, Jae-Han Lee, Gyeong-Hoi Koo, Hyeong-Yeon Lee and Jong-Bum Kim

Korea Atomic Energy Research Institute, Korea

ABSTRACT

This paper describes the status and prospects of the seismic base isolation technologies for the Korea Advanced Liquid Metal Reactor (KALIMER). The research and development program on the seismic base isolation was begun in 1993 by KAERI under the national long-term R&D program. The objective of this program is to enhance the seismic safety, to accomplish the economic design, and to standardize the plant design through the establishment of technologies on seismic base isolation for liquid metal reactors. In this paper, tests and analyses performed in the program are presented.

1. INTRODUCTION

Recently, many countries have been trying to apply seismic base isolation technology to their nuclear power plants, especially liquid metal reactors such as EFR in Europe, DFBR in Japan and PRISM in USA[1-3]. Seismic base isolation can give a significant reduction in seismic response and provide an economic benefit[4]. For seismic base isolation, it is essential to develop the isolation devices, which are to be installed between the superstructure and the basemat. For the seismic isolation device, the laminated rubber bearing (LRB) is adapted, which can support the heavy weight of the superstructure and dissipate the horizontal seismic input energy.

The contents of the R&D program are listed in Tables 1 and 2. The characteristic tests were performed for the rubber specimen, the high damping LRB(Fig.1), the lead inserted LRB[5], and the 3D-LRB. To investigate the seismic isolation capability and produce the test data for verification of the seismic analysis methodology, shaking table tests are carried out with the test model, simulating the KALIMER building and structures. The numerical methodology was developed to simulate the LRB behavior and the seismic responses of the KALIMER building and reactor structures[6-9]. Seismic analyses are performed to obtain the seismic isolation performance and the seismic margins of reactor structures.

2. TESTS FOR SEISMIC ISOLATION

2.1 Rubber Specimen Tests

The test results of rubber specimens can be obtained quickly and economically when compared to the tests of full- and reduced- scale LRBs. The type of rubber specimen tested at ANL is the 3 bar lap shear specimen, which is an LTV type as shown in Fig.2. The shear

modulus and the effective damping are calculated. The shear strain level tests for six cycles of fully reversed loading at 0.5 Hz are applied to the three specimens at the strain levels of 5, 10, 20, 50, 100, 150, 200, 250, and 300% respectively. The effective stiffness and the equivalent damping for the sixth cycle of the three specimens are represented in Fig. 3. As the shear strain increases, the shear stiffness is continuously decreased to near 150% and then increased by rubber hardening; the damping is continuously decreased as the shear strain increases.

After several hours following the shear strain tests, loading rate tests are performed on a each specimen to find its sensitivity to the loading rates of 0.005, 0.05, 0.5, 1.0, and 5.0Hz, respectively, at which the six cycles at a 100% shear strain level are applied to the three specimens. Fig. 4 shows the variations of shear stiffness and damping between 0.005 Hz and 0.5 Hz.

2.2 Laminated Rubber Bearing Tests

The three types of LRB developed in the program are HLRB (High Damping Laminated Rubber Bearing), LLRB (Lead Laminated Rubber Bearing) and 3D-LRB. Two kinds of scaled HLRB and LLRB, which are to 1/4 and 1/8 scale, as shown in Fig.1, are designed, fabricated and tested, and 3D-LRB is to 1/8 scale. The 1/8-scaled LRB contains 29 rubber layers of 1.2mm thickness and 28 steel shims of 1.6mm thickness. The diameter is 150 mm. The end plate has a thickness of 25 mm and a diameter of 150mm. The total height of the LRB is 129.6 mm, and the total rubber thickness is 34.8 mm.

All tests for the reduced scale LRB are carried out at KAIST[5] and EERC (Earthquake Engineering Research Center of the University of California at Berkeley)[10]. The specific characteristic behaviors of HLRB are investigated as below.

2.2.1 Shear Strain Level Tests

The characteristic hysteretic behavior of the 1/8-scaled LRB is shown in Fig. 5. The first and the third cycle loops are plotted for shear strains of 50, 100, and 150 %, the axial stress is 2.55 MPa, and the loading frequency is 0.7 Hz. These results are for the tests up to 150 % shear strain of the respective LRB. The LRB shows less than a 10% reduction in stiffness between the first and third cycles. The effective shear modulus for LRB 1/8-04 is 1.18 MPa in the first cycle and 1.07 MPa in the third cycle. The equivalent damping is 14.2 % for the third cycle.

2.2.2 Loading Rate Effects

For evaluating the effect of loading frequency, a single test signal consisting of five cycles at strain amplitudes of 10 to 150 % is first run on a bearing at a given frequency. Thus, the LRB has then been strained to 150 %. The next test is done using another signal with strain amplitudes of 10 to 150 %, but at a different frequency. These tests are then repeated at the frequencies of 0.7Hz and 2.0 Hz (1/8-scale). Constant-velocity (saw tooth) tests at velocities of 2.12 mm/s (0.083in/s) and 4.24mm/s (0.167in/s) are also run with the axial stress of 2.55 MPa. An increase in the rate of loading leads to an increase in both the effective modulus and the equivalent viscous damping, as shown in Fig. 6. For the 1/8-scale LRB, the shear modulus increases by 12 % and the equivalent damping by about 15 % from the slow test (2.12 mm/s) to the fast test (2 Hz).

2.2.3 Axial Load Effects

For investigating the effect of axial loads for the 1/8 scaled LRB, shear cycle tests are performed at each constant strain of 25, 50, 75, 100, 125, 150, 175, and 200 %. The sequence of applied axial stresses at each strain is 2.55, 0.26, 6.37, and -0.69 MPa. The loading

frequency of the test is 0.7Hz.

Fig. 7 illustrates the influence of axial stress on the third-cycle properties of 1/8-scaled LRB; however, the conclusion that can be drawn from them is related more to load history than to axial stress. The modulus is nearly constant with axial stress. In fact, while it appears that there is a reduction in modulus as the axial stress goes from 2.55 to 0.26, then to 6.37, and then to -0.69 MPa, this is due to repeated cycling at a constant strain. These results have significant implications for the interpretation of tests and the need for the careful consideration of load history in developing test programs.

2.2.4 Shear Failure Tests

The final tests performed on the 1/8-scale LRBs are shear failure tests. Three of the four LRBs are subjected to a monotonic displacement for failure at a constant shear strain rate of 10 % per second. The applied axial stress is different for each of these tests: 2.55MPa, 6.37MPa, and 0.69MPa in tension. The fourth failure test is performed at a loading rate of 200 % strain per second, and consists of one fully-reversed cycle to 50 % strain and then a monotonic displacement for failure. This test is designed to show the influence of loading rate on the bearing failure mechanism.

The results of the shear failure tests of four 1/8-scale LRBs are presented in Fig. 8. The lowest failure occurs at 91.2mm (262% strain) for the fast failure test, with a loading rate of 200 % strain/second. There is no discernible trend based on axial load: for the three slow failure tests, the ultimate strains reached are 104.4, 101.6, 100.9mm (300, 292, and 290% strain) for axial stresses of 2.55 MPa, 6.37 MPa, and 0.69 MPa in tension, respectively.

2.3 Tests of Seismically Isolated Structures

The purposes of tests are to verify the seismic isolation performance and to produce actual test data for the practical application of LRB to the KALIMER seismic isolation design.

2.3.1 Test Model and Shaking Tables System

The test model is shown in Fig. 9, which is designed to represent the dynamic characteristics of the KALIMER. This model is composed of the rectangular basemat (16.5 tons, size of 4.3m x 4.3m x 0.6m) and four columns (0.5 ton each) supporting the slab (6.0 tons). To increase the horizontal stiffness and the safety feature of the column structure, X-type crossbars are attached to the superstructure. The seismic isolators are 1/8-scaled LRB shown in Fig. 1, and four isolators are installed under the four corners of the basemat. The hysteretic characteristics of the adopted LRB are shown in Fig. 5.

The size of the shaking table system used in the test, which can control 6 degrees of freedom motions, is 4m x 4m and the shaking capacity is 30 tons.

2.3.2 Input Motions Used in Tests

The excitation frequency band of the input random waves is from 0.5 Hz to 40 Hz and the maximum table acceleration range is from 0.1g to 0.9g.

For the shaking table tests, the three types of input motions used are the 1940 El-Centro NS, the artificial time history, and the 1985 Mexico earthquakes. All input motions are reconstructed through the band limited filtering of original data from 0.07Hz to 25Hz. With consideration of the similarity of the 1/8 scaled down system, the time interval of input motions is re-scaled from 0.02 second to 7.07 ms.

2.3.3 Test Results and Discussions

Fig. 10 shows the variations of the seismic isolation frequencies corresponding to the

maximum peak input accelerations obtained from random tests. In the results, as the excitation levels increase, the seismic isolation frequencies of a seismically isolated structure decrease. This result indicates that the horizontal stiffness of LRB is evidently changed with the shear strains. The fundamental frequencies of X and Y directions are about 7 Hz and 6 Hz for the case of the seismic isolation, and 6 Hz and 5 Hz for the fixed base case respectively.

Fig. 11 shows the results of the floor response spectrum at the slab. For cases using the 1940 El-Centro NS and the artificial time history earthquakes, the seismic responses are significantly reduced. However, the 1985 Mexico earthquake, in which the dominant excitation frequency is 1.3Hz, produces severe resonant responses in structures. In reality, it is not expected that a type of earthquake similar to the 1985 Mexico earthquake containing very long period components tuning the seismic isolation frequency will occur at a hard rock nuclear power plant site. Therefore, the 1985 Mexico earthquake may be treated as a hypothetical or the worst loading case in seismic isolation design.

In the cases of the 1940 El-Centro and the artificial time history earthquakes, the maximum shear deflections of LRB in tests are both lower than 50%(17.5mm) shear strain for a 0.3g and 200%(70.0mm) for a 0.9g. When considering a SSE (Safe Shutdown Earthquake) load of 0.3g in the KALIMER seismic design, the safety margin of LRB is enough to cover the design requirements of the minimum failure shear strain of LRB, 300%[11]. For the 1985 Mexico earthquake, resonant responses occur and LRB shows large shear deflection responses.

Fig. 12 shows the test results of the maximum peak acceleration responses at the slab for various magnitudes of each input motion. For the cases of the 1940 El-Centro and the artificial time history earthquakes, the seismic responses are significantly reduced by about 8 and 6 times respectively for a 0.3g input magnitude compared with those of the non-isolated system. However, as previously mentioned for the 1985 Mexico earthquake, a counter result of the seismic isolation effects occurs in seismic responses.

3. NUMERICAL SIMULATION OF A SEISMICALLY ISOLATED KALIMER

Analysis methodologies using finite element methods are developed to predict the behaviors of LRB used for KALIMER isolation. The numerical simulations verified have been applied to the response analyses of the reactor building, reactor structures and components.

3.1 Shear Deformation Analysis for Laminated Rubber Bearings

The finite element analyses for shear deformation of the KAERI HLRB made of MRPRA rubber compounds are performed. In those, the hyperelastic material option of ABAQUS for the strain energy functions is used for modeling rubber layers. The 2D harmonic elements and 3D solid elements are used in finite element analyses, and three kinds of strain energy density functions calculated with four kinds of rubber compound test data are used in modeling the rubber layers [9].

For a 2D model, the element types for steel shims and rubber layers are the CAXA41 and CAXA8H1, respectively, which have an axisymmetric geometry with a non-axisymmetric load. For the 3D model, the 3D solid element of C3D8H is used. The boundaries are fixed at the bottom of the bearing, vertically coupled and horizontally freed at the top of the bearing. The Young's modulus and Poisson ratio of the steel shims are chosen as 200 GPa and 0.3 respectively. The horizontal displacements are applied from 0% to 300% of the total rubber height under the vertical pressure of 2.55 MPa.

In 2D model, the number of elements for a rubber layer is three in the thickness direction. According to the material models for rubber, there are some different results, as shown in

Fig.13(a). The analyses with the Mooney-Rivlin and Polynomial (N=2) models gives quite a discrepancy with the test results, but the analysis with the Ogden (N=3) method results in a relatively good agreement with the test results up to a shear displacement of 63 mm(equivalent to 180% shear strain).

In 3D solid model, one element in the thickness direction is used for a rubber layer. Force and displacement relations are represented in Fig.13(b). The results using the Ogden model are closer to the test data, as in case of the 2D model.

3.2 Seismic Analysis for Reactor Building

For obtaining the time history of the seismic responses of reactor building as shown in Fig. 14, a lumped-mass beam model is developed as shown in Fig.15. The model is composed of two sticks; the one is for the reactor building and the other is for the reactor support structure. The time history responses for the non-isolated and isolated reactor buildings are calculated for an artificial time history earthquake, which is generated by using the seismic design spectrum curve of US NRC RG1.60.

The isolation frequency of the reactor building is 0.5 Hz and the equivalent damping of LRB is 12%. The horizontal stiffness of the total isolator is 5.77×10^8 N/m and the damping coefficient is 4.356×10^7 N.sec/m. The total weight is about 68,000 tons. The first frequencies for x, y, z directions of the isolated reactor building are 10.1Hz, 8.73Hz, 12.8Hz, respectively.

For the artificial time history (ATH), the maximum acceleration responses of the non-isolated and isolated reactor buildings for the horizontal and vertical earthquake data are shown in Table 3. The displacement responses of x-direction are presented in Fig. 16. The response spectra at major locations are represented in Fig.17. For the horizontal seismic input of 0.3g ZPA, the maximum acceleration is reduced to 0.177g for an isolated condition, while one is 1.46g for a non-isolated condition. The maximum displacement is larger to 15.0cm for the isolated condition. The maximum acceleration for the vertical earthquake of 0.208g ZPA is amplified to 0.848g for the isolated condition, while the one is amplified to 0.557g for the non-isolated condition. This agrees with the general trend that the horizontal isolation of a structure can amplify the vertical responses [1-3].

3.3 Seismic Analysis for Reactor Structures and Components

For the preliminary investigation of the seismic isolation effects on KALIMER reactor internals as shown in Fig.18, the seismic analyses are carried out with a lumped-mass model. Using the 3-dimensional finite element model, detail local stiffness analyses are performed to construct the lumped-mass seismic analysis model shown in Fig.19. The hydrodynamic mass of primary sodium is implemented to the model. The seismic analysis and evaluation are presented through the modal analysis, the seismic time history analysis, and the equivalent seismic stress analysis.

Table 4 shows the natural frequencies of the reactor structures. For the non-isolated system, the dominant fundamental coupled mode of whole reactor internal structures including reactor vessel is 8.1Hz. This fundamental frequency is increased to 11.5Hz when the seismic isolation is applied to the fixed basemat system. Therefore, when considering the assumed seismic isolation frequency of 0.7Hz, the significant horizontal response reductions are expected. The first and second natural frequencies are 1.9Hz and 8.1Hz in vertical direction.

The seismic design loads used in this analyses are OBE(0.15g) and SSE(0.3g). The same seismic input motions are used in both the horizontal and vertical directions. To investigate the seismic responses for beyond the design basis(BDB), the postulated 1.0g seismic event is used. The synthetic acceleration time history contains enough number of peaks enveloping the

NRC Reg.1.60 seismic design spectrum.

The seismic responses of reactor structures of the seismically isolated KALIMER are significantly reduced for accelerations and relative displacements in the horizontal direction as shown in Tables 5 &6. For the isolation case, the maximum peak accelerations in the horizontal direction for the all structures and components is 0.11g for OBE and 0.22g for SSE. The responses are reduced about 14 times in IHX, 9 times in EMP and 8 times in the reactor vessel liner, support barrel, and core compared with those in the non-isolated case. However, for the vertical direction, significant response amplifications occur in whole structures. This is due to the vertical structural frequency of 8.1Hz located in the dominant excitation frequency band of the input motion.

Essentially, single-frequency response of the isolated system permits the reactor seismic stresses to be based on equivalent static analysis using the inertia loads obtained by applying the amplification factors calculated in system dynamic analyses. The results of the seismic analysis for seismically isolated KALIMER show that there are no seismic response amplifications in horizontal responses of the reactor structures and components.

The equivalent seismic loads are OBE of 0.11g and SSE of 0.22g for the horizontal direction and OBE of 1.97g and SSE of 2.94g, which are including the gravity effects of 1.0g, for the vertical direction. Not like the horizontal responses, the vertical responses are different in each structure but the maximum peak acceleration is selected as conservative. The horizontal and vertical loads are simultaneously applied in stress analysis.

The seismic margin evaluations are performed using the stress limit conditions of ASME Code, Section III, Appendix F, Rules for Evaluation of Service Loadings with Level D Service Limits. Table 7 shows the results of the seismic margin evaluations and the seismic capacity. From the results, the containment vessel, reactor vessel, inlet plenum, and core support have large seismic stress margins but the reactor vessel liner, support barrel, separation plate, and baffle plate have small margins. The maximum stress occurs in reactor vessel liner parts connected with the separation plate due to the vertical seismic loads.

The maximum seismic resistance in the reactor internal structures is evaluated as 0.354g by the index of seismic capability(SC) defined in Table 7.

4. CONCLUSIONS

The R&D program on seismic base isolation technologies for the KALIMER established in 1993 has made important progress in validating the isolation technologies essential to enhancing the seismic safety, and the economic structural design.

The various tests for rubber specimens, LRBs, and isolated structural model, and the numerical simulations for the evaluation of LRBs and seismically isolated KALIMER structures have been done in this program to verify the performance and the effectiveness of the seismic base isolation.

Further R&D on seismic isolation techniques will produce fruitful results to enhance the structural safety of the KALIMER subjected to design basis earthquakes as follows;

- Development of 3D isolator that can reduce both horizontal and vertical seismic responses, while the horizontal base isolation only has a benefit on the horizontal direction.
- Development of seismic isolation design guidelines for the KALIMER from the future R&D program and collaboration with foreign countries.
- Large scale structural tests for the KALIMER including reactor vessel, reactor core, piping systems, etc to verify the seismic isolation design.

Acknowledgement

This work was performed under the long term nuclear R&D program sponsored by the Ministry of Science and Technology of Korea.

References

1. Proc. of the First International Seminar, "Seismic Base Isolation for Nuclear Facilities," San Francisco, Cal., USA, A Post Conf. Seminar of the 10th Int'l. Conf. on SMIRT-10, USA, 1989.
2. Proc. of 11th SMIRT Post Conf. Seminar, "Seismic Isolation of Nuclear and Non-nuclear Structures," Nara, Japan,1991.
3. Proc. of Int'l Post-SMIRT(13th) Conf. Seminar, "Seismic isolation, passive energy dissipation and active control of vibrations of structures," Santiago, Chile,1995.
4. Yoo, B., Lee, J.H., Koo, G.H. and Y.-H. Kim, "Effects of High Damping Rubber Bearing on Seismic Response of Superstructure in Base Isolated System," 13-th SMiRT, Brazil, 1995.
5. Yoo, B., Lee,J.H. and Koo,G.H.,"Study of Reduced-Scale Model Test Results of High Dampmg and Lead Laminated Rubber Bearing for Liquid Metal Reactor," KAERI/TR-809/97, 1995 (in Korean).
6. Yoo, B., Lee, J.H., Koo, G.H. and Lee, D.G., "Seismic Isolation for Nuclear Reactors in Korea," Int. Post-SMiRT Conf. Seminar on Seismic Isolation, Passive Energy Dissipation and Control of Vibrations of Structures, Santiago, Chile, 1995.
7. Yoo, B et al, "Analytical Modeling and Seismic Response Analyses of KALIMER Reactor Building," KNS, Proceedings of 98 Spring Conference, 1998, pp.903-908(in Korean)
8. Yoo, B., Koo, G.H. and Lee, J.H, "Conceptual Design by Analysis of KALIMER Seismic Isolation," KAERI/TR-697/96, 1998.
9. Yoo, B. and Lee J.H., and Koo, G.H., 3rd IAEA Research Co-ordination Meeting on "Intercomparison of Analysis Methods for Seismically Isolated Nuclear Structures," UK,1998.
10. Kelly, J.M., Aiken, I.D. and Clark, P.W., "Experimental Testing of Reduced-Scale Seismic Isolation Bearings for Nuclear Application," Proc. of the Int. Post-SMiRT Conference Seminar, Taormina, Sicily, Italy, 1997.
11. Yoo, B., Koo, G.H. and Lee, J.H, "Development of Guidelines for Seismic Isolation Design of LMR," Proceedings of Earthquake Engineering Society of Korea, 1998, pp.147-154 (in Korean).

Table 1. Test Programs on Seismic Isolation Technology for KALIMER

Items	Years							Joint Work on Test & Fab.	Remarks
	93	94	95	96	97	98	99		
Rubber Specimens								UNISON(Fab.)	
-Shear Dynamic Test								ANL & ENEL	ANL Instron 8500 (5Klps)
-Uniaxial Tensile Test								ENEL	
-Equibiaxial Tensile Test								ENEL	
-Planar(pure shear) Test								ENEL	
-Volumetric Test								ENEL	
Rubber Bearings								UNISON(Fab.)	
-HLRB(1/4 &1/8 scales)								GE/EERC(*)	EERC (V240Kips x H
-LLRB(1/4 &1/8 scales)								& KAIST	75Kips,Max. Disp. ±6in)
-3DLRB(1/8 scale)								KAIST	V50ton x H18ton(±11cm)
Isolated Model Structure								UNISON(Fab.)	
-Fixed								KIMM	30ton, 6DOF (4m x 4m)
-2D isolation(1/8scale)								KIMM	"
-3D Isolation(1/8scale)								KIMM	"

Table 2. Numerical Evaluation Models for Rubber Bearings and Isolated Structures

Items		Numerical Models	Computer Code	Remarks
LRB& LLRB	Rubber	• Strain Energy Functions -Mooney Rivlin/ -Polynomial -Ogden/ -Seki	ABAQUS	IAEA CRP Program (1996 ~ 1999)
	Steel Shim	• Linear Elastic		
	Lead	• Elastic-Plasticity Constitutive Law		
LRB Structure behaviors for Isolated Structures		• Linear Model • Bilinear / Modified Bilinear Model • Rate Model	ABAQUS User Subroutine	SMiRT 13&14
Reactor Core		• Nonlinear Model	SAC-CORE	ASME PVP '98

Table 3. Acceleration Responses of KALIMER Building for ATH Earthquake

Location	X-Direction(g)		Y-Direction(g)		Z-Vertical (g)	
	Isolated	Non-isolated	Isolated	Non-isolated	Isolated	Non-isolated
Base	0.175	0.30	0.177	0.30	0.321	0.205
Top	0.177	1.461	0.179	1.609	0.848	0.577
RV support	0.173	0.583	0.175	0.676	0.558	0.362

Table 4. Natural Frequencies of KALIMER Reactor Structures

Mode	Horizontal (Hz)		Vertical (Hz)	
	Isolation	Non-isolation	Isolation	Non-isolation
1	0.70	8.11	1.87	1.87
2	11.51	11.88	8.09	8.25
3	13.69	18.81	17.77	17.94
4	21.04	27.85	23.08	34.26
5	27.90	27.97	34.85	36.59

Table 5. Results of Zero Period Accelerations for Isolated System

Items	Horizontal ZPA (g)			Vertical ZPA (g)		
	OBE (0.15g)	SSE (0.3g)	BDB (1.0g)	OBE (0.15g)	SSE (0.3g)	BDB (1.0g)
CV	0.11(0.17)	0.22(0.34)	0.73(1.13)	0.15(0.14)	0.30(0.28)	1.00(0.93)
RV	0.11(0.64)	0.22(1.28)	0.73(4.27)	0.17 (0.16)	0.34(0.32)	1.13(1.07)
IHX	0.11(1.56)	0.22(3.12)	0.73(10.4)	0.16(0.14)	0.32(0.28)	1.07(0.93)
EMP	0.11(0.98)	0.22(1.96)	0.73(6.53)	0.16(0.14)	0.32(0.28)	1.07(0.93)
RV Liner	0.11(0.95)	0.22(1.90)	0.73(6.33)	0.97(0.97)	1.94(1.94)	6.47(6.47)
SB	0.11(0.92)	0.22(1.84)	0.73(6.13)	0.67(0.66)	1.34(1.32)	4.47(4.40)
UIS	0.11(0.15)	0.22(0.30)	0.73(1.00)	0.16(0.14)	0.32(0.28)	1.07(0.93)
Core	0.11(0.88)	0.22(1.76)	0.73(5.87)	0.94(0.91)	1.88(1.83)	6.27(6.07)

( ) : for non-isolation system

Table 6. Results of Displacement Responses

Loads	Isolator Deflections (cm)		Rel-Disp. Between UIS and Core (cm)	
	Horizontal	Vertical	Horizontal	Vertical
OBE (0.15g)	5.266	0.018	0.045(0.379)*	0.485(0.456)*
SSE (0.3g)	10.531	0.035	0.089(0.758)*	0.970(0.913)*
SC (0.354g)	12.428	0.043	0.106(0.894)*	1.145(1.076)*

SC : Seismic Capacity, ( )* indicates the results of non-isolated system.

Table 7. Seismic Margin and Seismic Capacity of KALIMER Reactor Structures

Items	σ_{SSE} (MPa)	P_{L+b} (MPa)	Margins	Min. Seismic Capacity
Containment Vessel	21.4	401.9	17.78	
Reactor Vessel	39.6	401.9	9.15	
RV Liner	340.0	401.9	*0.18*	0.354g
Support Barrel	113.0	382.4	*2.38*	
Inlet Plenum	20.8	401.9	18.32	
Separation Plate	188.0	401.9	*1.14*	
Baffle Plate	193.0	382.4	*0.98*	
Core Supports	72.1	401.9	4.57	

* σ_{SSE} = Total stress intensity for horizontal and vertical SSE loads
* P_{L+b} = 1.5 x Min [2.4 S_m , 0.7 S_u], ASME Code Sec.III App.F.
* Margin = (P_{L+b} / σ_{SSE}) - 1
* Seismic Capacity = Min[Seismic Stress Margin +1] x SSE

Fig. 1 Scaled Laminated Rubber Bearings

Fig. 2 Rubber Specimen for Shear Dynamic Test

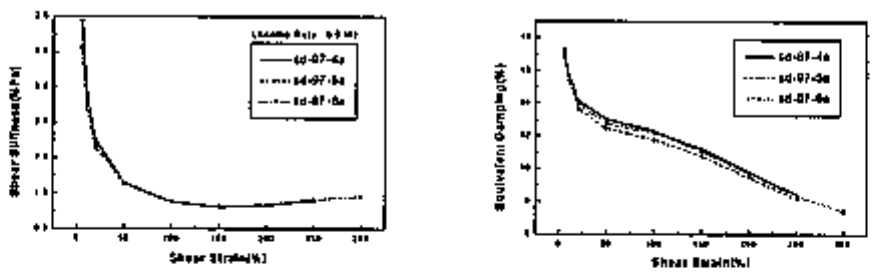

Fig. 3 Equivalent Shear Stress and Damping vs. Shear Strain for Rubber Specimen

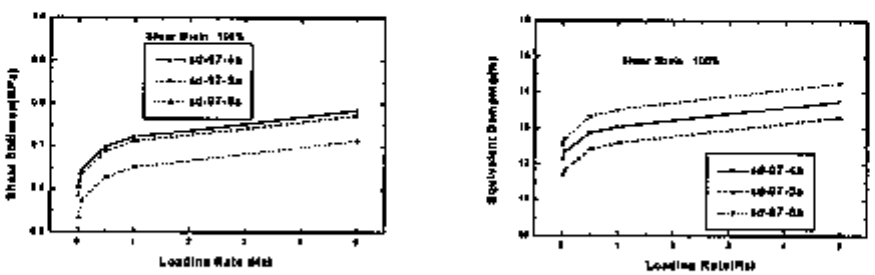

Fig. 4 Equivalent Shear Stress and Damping vs. Loading Rate for Rubber Specimen

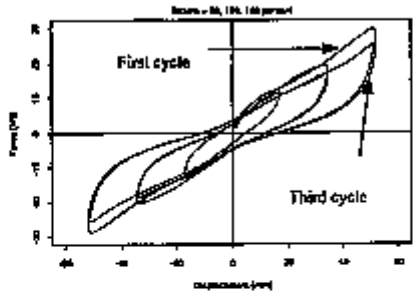

Fig. 5 Hysteretic Behavior of HLRB 1/8-04

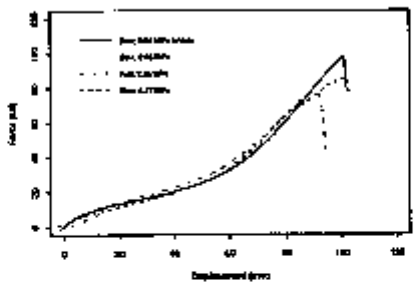

Fig.8 Shear Failure Tests of 1/8 Scale Bearings

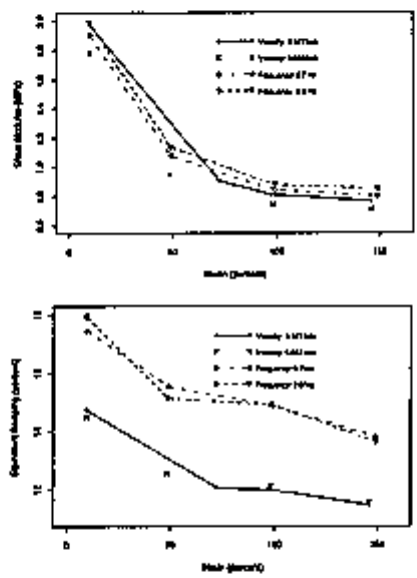

Fig. 6 Dependence on Loading Rate, HLRB 1/8-04

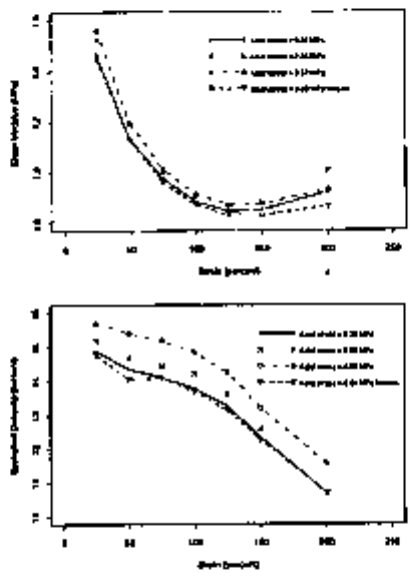

Fig.7 Dependence on Axial Stress, HLRB 1/8-03

Fig. 9 Seismically Isolated Test Model

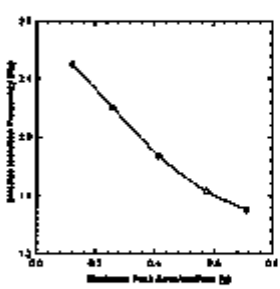

Fig. 10 Isolation Frequencies vs. Base Exciting Acc.

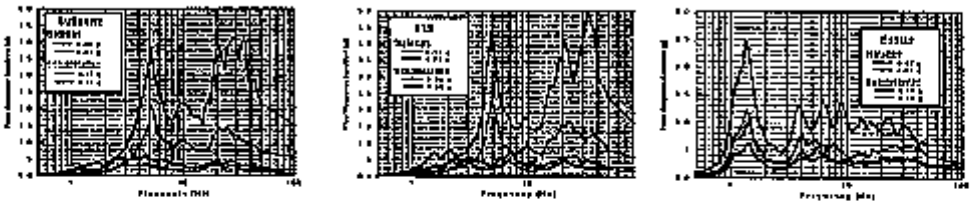

(a) 1940 El-Centro NS (b) Artificial Time History (c) 1985 Mexico

Fig. 11 Floor Response Spectrum at Slab

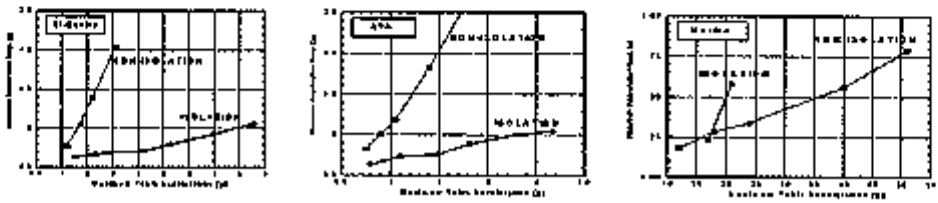

(a) 1940 El-Centro NS (b) Artificial Time History (c) 1985 Mexico

Fig. 12 Test Results of Seismic Isolation Frequencies

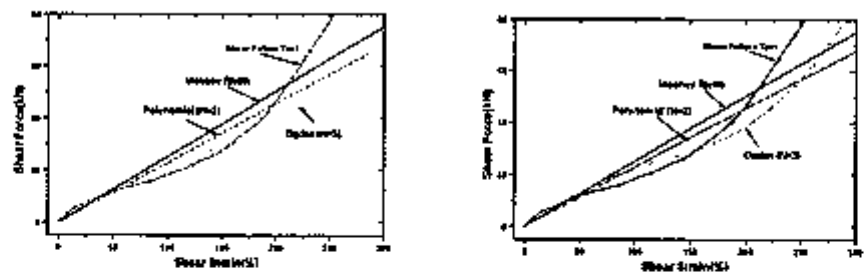

(a) 2D, No. of Elements for a Rubber Layer : 3 (b) 3D, No. of Elements for a Rubber Layer : 1

Fig. 13 Shear Forces vs. Shear Strain of Rubber Bearing

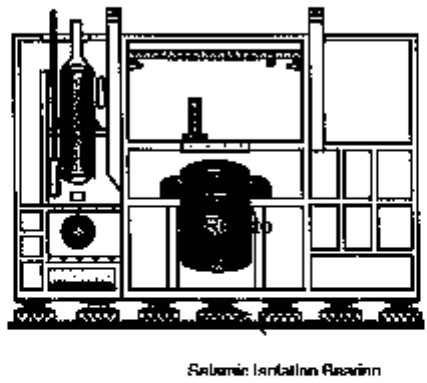

Fig. 14 KALIMER Reactor Building

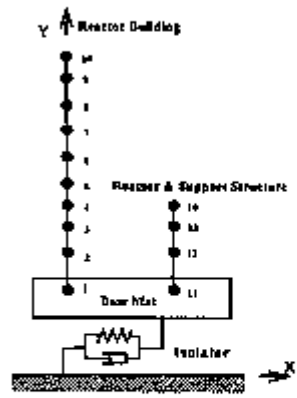

Fig. 15 Lumped Mass-Beam Models of KALIMER Building

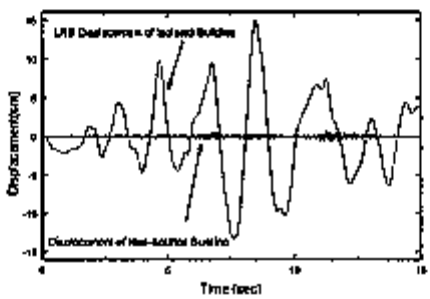

Fig. 16 Displ. Responses of Reactor Building (Artificial Time History Input)

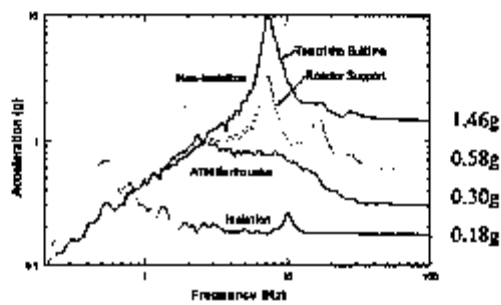

Fig. 17 Accel. Resp. Spectra of Reactor Building (ATIL, X-dir. 0.3g)

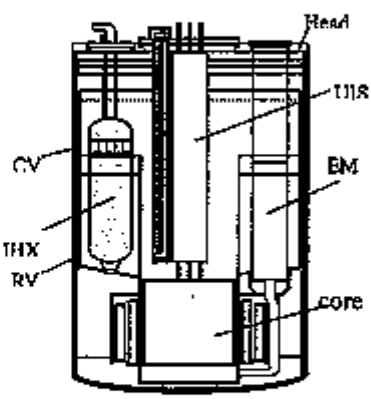

Fig. 18 KALIMER Reactor Structure and Components

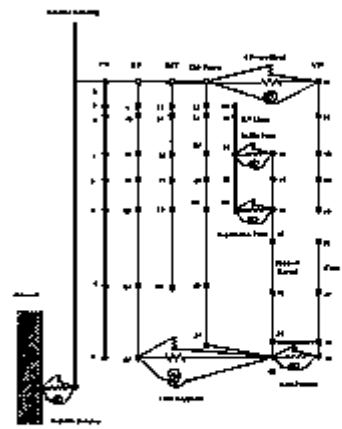

Fig. 19 Seismic Analysis Model of KALIMER Reactor Structure and Components

Transactions of the 15th International Conference on
Structural Mechanics in Reactor Technology (SMiRT-15)
Seoul, Korea, August 15-20, 1999

Optimal Seismic Design Method for Base-Isolated Pool Structure by Minimizing Life Cycle Cost

Hyun Moo Koh, Kwan Soon Park and Junho Song

Seoul National University, Korea

ABSTRACT

An optimal seismic design method for base-isolated and fluid-filled pool structures subjected to random ground excitation is studied. The criterion selected for the optimization is minimum life-cycle cost. The damage cost is estimated based on the structural failure probability calculated by the stochastic response analysis. Prescribed values of the isolator displacement and the wall base shear force are predetermined to constitute the limit-state levels. Added mass matrix derived by FEM modeling is able to consider fluid-structure interaction effects between the flexible walls and contained fluid. Design variables for optimization are the wall thickness and isolator stiffness. Flexible isolator allows us to choose relatively thinner lateral wall with similar failure probability. The more flexible isolator is, the smaller failure probability and total life-cycle cost are. This optimal design case is insensitive to assumed damage cost scale.

1. INTRODUCTION

Civil structures should be designed to maximize their profit to the society by minimizing life-cycle cost, which consists of initial construction cost and expected damage cost under natural hazards such as earthquake. Numerous researches and applications on optimal seismic design and economical efficiency evaluation method have been performed based on the life-cycle cost concept for various structural systems, e.g. buildings, bridges, active and passive control systems (Ang and Leon, 1996; Koh and Song 1998; Wen, 1991).

But there are few researches on optimal seismic design method for seismic-isolated pool structure. To define and evaluate the life-cycle cost function, the method should consider the properties of input ground motions, limit states of pool structure, properties of seismic isolation, and failure probabilities. In this study, we aim to develop an optimal seismic design method for base-isolated fluid-filled pool structures that can take the aforementioned features into account.

2. INPUT GROUND MOTION MODELING

To consider conveniently acceleration and site conditions in optimal design and cost effectiveness evaluation, we model input ground motion as spectral density function compatible with response spectra. Acceleration coefficient A and site coefficient S in

response spectrum reflect on acceleration and site condition of the construction site, respectively. We can obtain the compatible spectral density by upgrading spectral density repeatedly while comparing the target response spectrum with the response spectrum simulated from the upgraded spectral density (Deodatis, 1996). The results are as follows (Figs.1, 2). The acceleration coefficient describes the scale of the input ground motion, and the site coefficient reflects on frequency properties of ground motion and amplification of displacement by soil effect.

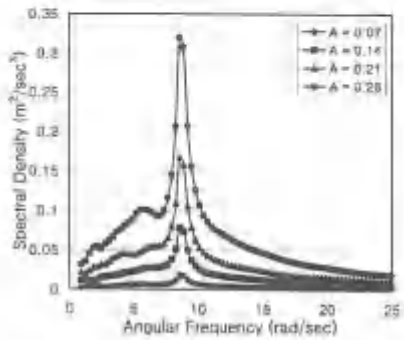

Figure 1. Variation of Spectral Density with Acceleration Coefficient

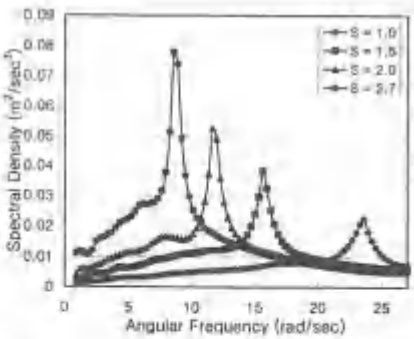

Figure 2. Variation of Spectral Density with Site Coefficient

3. FLUID-STRUCTURE INTERACTION MODELING

To describe the interaction between the flexible wall and fluid motion, fluid dynamic pressure at the wall is considered in the form of added matrix. The added mass matrix is derived by FEM of fluid motion. Irrotational flow of incompressible and inviscid ideal fluid can be described with velocity potential $\phi(z,t)$, which satisfies the following equations (Fig. 3).

$$\hat{u}_i = \frac{\partial \phi}{\partial z_i}, \quad \nabla^2 \phi = \left(\frac{\partial^2}{\partial z_1^2} + \frac{\partial^2}{\partial z_2^2} \right) \phi(\mathbf{z}, t) = 0 \tag{1)-(2)}$$

$$\frac{\partial \phi}{\partial t} + \frac{p}{\rho} = 0 \ \text{ in } \Omega, \quad \frac{\partial \phi}{\partial t} + g\eta = 0 \ \text{ on } S_f, \quad \frac{\partial \phi}{\partial n} = \hat{\eta} \ \text{ on } S_f \tag{3)-(5)}$$

where $\mathbf{z} = (z_1, z_2)$ is the location vector in inertia reference frame, $\hat{u}_i = \hat{u}_i(\mathbf{z})$ is an i-direction component of fluid velocity vector in inertial reference frame, $p = p(\mathbf{z})$ is the pressure of fluid, $\eta = \eta(\mathbf{z}, t)$ is the height of free surface, $\mathbf{n} = \mathbf{n}(\mathbf{z})$ is the outward normal vector, ρ is the fluid density, g is the acceleration of gravity. Ω is the fluid domain, and S_f is the free surface.

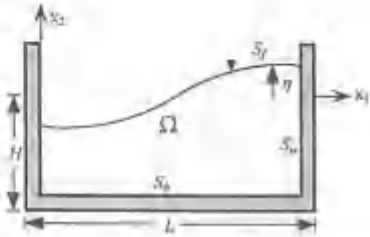

Figure 3. Domain and Boundary of Fluid

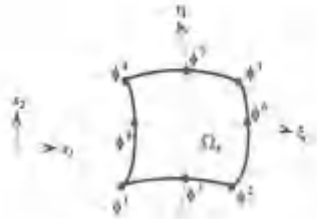

Figure 4. Nodal Velocity Potential

Velocity potential ϕ in each element is represented by nodal velocity potential ϕ_e^j.

$$\phi = \sum_{j=1}^{8} N^j \phi_e^j \tag{6}$$

where N^j is the shape function of 8-node isoparametric element. When Galerkin method is applied to Eq. 2 with vector identity and Eq. 6, weighted residuals of each shape function are

$$\begin{aligned} R_i &= \int_{\Omega_e} N^i \nabla^2 \phi dV = \int_{\Omega_e} \left(-\nabla N^i \nabla \phi \right) dV + \int_{\Omega_e} \nabla \left(N^i \nabla \phi \right) dV \\ &= -\sum_{j=1}^{8} \phi_e^j \int_{\Omega_e} \left(N_k^i N_k^j \right) dV + \sum_{j=1}^{4} \int_{\Omega_e} N^i q dS = 0 \end{aligned} \tag{7}$$

where $q = \nabla \phi \cdot \mathbf{n} = \phi_n$, Ω_e is the element domain, and S_e^j is the element boundary.

Normal derivative of potential, q is also discretized using the same shape function, and then Eq. 7 is transformed into the following matrix equation at each element.

$$\mathbf{A}_e \boldsymbol{\phi}_e = \mathbf{H}_e \mathbf{q}_e \tag{8}$$

where $\boldsymbol{\phi}_e$ is the nodal velocity potential vector of element, $\mathbf{q}_e$ is the normal derivative of potential at the nodes, and $\mathbf{A}_e, \mathbf{H}_e$ are coefficient matrices about potential and flux. We can obtain the governing equation of the entire fluid domain by assembling Eq.8 using direct

stiffness method. The equation describing the relation between nodal potential vector and nodal velocity vector is derived by static condensation. If we differentiate the equation by time and apply the conditions of Eqs. 1, 4, and 5, equation about the relation between nodal pressure vector and nodal acceleration vector comes out. Using virtual work principle, the equation can be transformed into the following equation (Koh et al, 1994).

$$\mathbf{M}^f\ddot{\mathbf{u}} = -\mathbf{f}^f \tag{9}$$

where $\mathbf{f}^f$, $\ddot{\mathbf{u}}$, $\mathbf{M}^f$ are respectively the nodal force vector acting on one side of the wall, the nodal acceleration vector, and the added mass matrix. We can consider the interaction between fluid and structure by adding this mass matrix to the corresponding DOFs of structure.

4. ISOLATED POOL STRUCTURE MODELING

Isolated pool structure can be simplified as Fig. 5, and its equation may be condensed into Eq. 10 by neglecting the slight effect of rotational inertia.

$$\mathbf{M}^w\ddot{\mathbf{x}} + \mathbf{C}^w\dot{\mathbf{x}} + \mathbf{K}^w\mathbf{x} = -\mathbf{M}^w\mathbf{1}\left(\ddot{x}_b + \ddot{x}_g\right) + \mathbf{f}^w \tag{10}$$

where $\mathbf{M}^w, \mathbf{C}^w, \mathbf{K}^w$ are respectively the condensed mass, damping, stiffness matrix of wall, and $\mathbf{f}^w$ is the external force vector acting on the nodes.

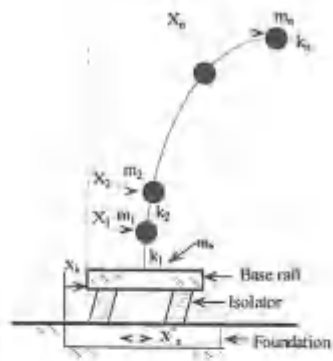

Figure 5. Lumped Parameter Model of Structure

If DOFs of nodes at the base raft are separated, added mass matrix, nodal acceleration vector, and nodal force vector in Eq. 9 can be expressed as follows.

$$\mathbf{M}^f = \begin{bmatrix} m_{11} & \cdots & m_{1n} & m_{1b} \\ \vdots & \ddots & \vdots & \vdots \\ m_{n1} & \cdots & m_{nn} & m_{nb} \\ m_{b1} & \cdots & m_{nb} & m_{bb} \end{bmatrix} = \begin{bmatrix} \mathbf{M}^f_{ww} & \mathbf{m}^f_{wb} \\ \mathbf{m}^f_{bw} & M^f_{bb} \end{bmatrix} \tag{11}$$

$$\mathbf{f}^t = \begin{pmatrix} \mathbf{f}_w^t \\ f_b^t \end{pmatrix}, \quad \ddot{\mathbf{u}}^t = \begin{pmatrix} \ddot{\mathbf{x}} + \mathbf{1}\left(\ddot{x}_b + \ddot{x}_g\right) \\ \ddot{x}_b + \ddot{x}_g \end{pmatrix} \tag{12)-(13}$$

Arranged equations of motion considering interaction between pool structure and base isolator are as follows (Koh et al., 1994).

$$\begin{cases} \mathbf{M}_s\ddot{\mathbf{x}} + \mathbf{C}_s\dot{\mathbf{x}} + \mathbf{K}_s\mathbf{x} + \mathbf{q}_s\ddot{x}_b = -\mathbf{q}_s\ddot{x}_g \\ M_b\ddot{x}_b + c_b\dot{x}_b + k_b x_b + \mathbf{q}_b\ddot{\mathbf{x}} = -M_b\ddot{x}_g \end{cases} \tag{14}$$

where $\mathbf{M}_s = \mathbf{M}^w + \mathbf{M}^l_{ww}$, $\mathbf{C}_s = \mathbf{C}^w$, $\mathbf{K}_s = \mathbf{K}^w$, $\mathbf{q}_s = \mathbf{M}_s\mathbf{1} + \mathbf{m}^l_{wb}$,
$M_b = m_b + M^l_{bb} + \mathbf{m}^l_{bw}\mathbf{1} + \mathbf{1}\mathbf{q}_s$, $\mathbf{q}_b = \mathbf{1}\left(\mathbf{M}^w + \mathbf{M}^l_{ww}\right) + \mathbf{m}^l_{bw}$.

5. FAILURE PROBABILITY ESTIMATION

Two equations in Eq. 14 can be merged into the following unique equation.

$$\mathbf{M}_e\ddot{\mathbf{x}}^t + \mathbf{C}_e\dot{\mathbf{x}}^t + \mathbf{K}_e\mathbf{x}^t = -\mathbf{m}_g\ddot{x}_g \tag{15}$$

where $\mathbf{M}_e = \begin{bmatrix} \mathbf{M}_s & \mathbf{q}_s \\ \mathbf{q}_b & M_b \end{bmatrix}$, $\mathbf{C}_e = \begin{bmatrix} \mathbf{C}_s & \mathbf{0} \\ \mathbf{0} & c_b \end{bmatrix}$, $\mathbf{K}_e = \begin{bmatrix} \mathbf{K}_s & \mathbf{0} \\ \mathbf{0} & k_b \end{bmatrix}$, $\mathbf{m}_g = \begin{pmatrix} \mathbf{q}_s \\ M_b \end{pmatrix}$,
$\ddot{\mathbf{x}}^t = \begin{pmatrix} \ddot{\mathbf{x}} \\ \ddot{x}_b \end{pmatrix}$, $\dot{\mathbf{x}}^t = \begin{pmatrix} \dot{\mathbf{x}} \\ \dot{x}_b \end{pmatrix}$, and $\mathbf{x}^t = \begin{pmatrix} \mathbf{x} \\ x_b \end{pmatrix}$.

From this equation, we can derive the transfer function vector.

$$\mathbf{h}(\omega) = \left(\omega^2\mathbf{M}_e - i\omega\mathbf{C}_e - \mathbf{K}_e\right)^{-1}\mathbf{m}_g \tag{16}$$

Spectral density function of the wall base shear is calculated by the transfer function vector, lateral stiffness vector, and input spectral density function.

$$S_V(\omega) = \left|\mathbf{k}_w\mathbf{h}_w(\omega)\right|^2 S_g(\omega) \tag{17}$$

where $\mathbf{k}_w$ is the row vector of lateral stiffness of wall, $\mathbf{h}_w(\omega)$ is the reduced vector from Eq. 16 only for wall lateral direction DOFs, and $S_g(\omega)$ is the spectral density function of input ground motion.

Standard deviations of shear force and its time rate are calculated assuming that the system is narrow-banded.

$$\sigma_V^2 = \int_{-\infty}^{\infty} S_V(\omega)d\omega, \quad \sigma_{\dot{V}}^2 = \int_{-\infty}^{\infty} \omega^2 S_V(\omega)d\omega \tag{18)-(19}$$

The crossing rate is estimated on the assumption that the input ground motion is subjected to the normal distribution (Newland, 1993).

$$\nu_a = 2\nu_a^+ = \frac{1}{\pi}\frac{\sigma_{\dot{V}}}{\sigma_V}\exp\left(-a^2/2\sigma_V^2\right) \tag{20}$$

where a is the limit state level of wall base shear force.

Supposing the number of crossing events is subjected to Poisson distribution, the failure probability during life-cycle is

$$P_f = P_{f/eq}\cdot P_{eq} = P_{eq}\left\{1-\exp\left(-\nu_a\cdot T_d^s\right)\right\} \tag{21}$$

where $P_{f/eq}$ is the conditional probability of failure given the earthquake occurrence, P_{eq} is the probability of earthquake occurrence, and T_d^s is the duration time of strong excitation.

6. OPTIMAL SEISMIC DESIGN

The total cost function of base-isolated pool structure is defined for optimal seismic design. Wall thickness t_w and isolator stiffness k_b are chosen as design variables for optimization (Song, 1999).

$$C_t(t_w,k_b) = C_i + E[C_d] = C_{uc}\cdot\{2t_w w_w h_w\} + C_d^s\sum_k r_k P_{f_k}(t_w,k_b) \tag{22}$$

where C_t is the total life-cycle cost, C_i is the initial construction cost, $E[C_d]$ is the expected value of damage cost during life-cycle, C_{uc} is the initial cost per unit volume of wall, C_d^s is the assumed damage scale, r_k is the weight of k^{th} limit state, P_{f_k} is the failure probability of k^{th} limit state, t_w is the wall thickness, w_w is the width of wall, and h_w is the height of wall.

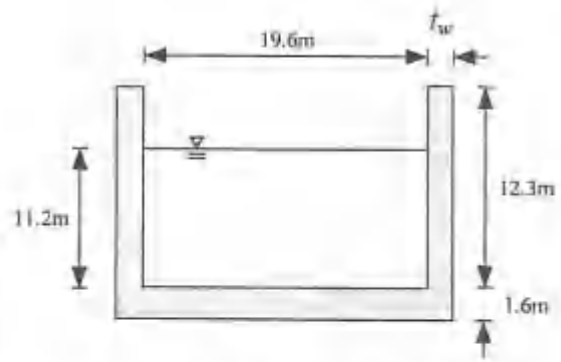

Figure 6. Fluid-Filled Pool Structure Model for Optimal Seismic Design

We applied our optimization method to fluid-filled pool structure shown in Figure 6. Its modulus of elasticity is $20.79\times10^9\,N/m^2$, density is $2300kg/m^3$, and Poisson ratio is 0.17. Spectral density with $A=0.14$ and $S=1.0$ is used for input ground motion model. Two LRB (Laminated Rubber Bearing) isolators are installed on one side, whose stiffness varies from 6.28×10^4 to $3.14\times10^5\,N/m$.

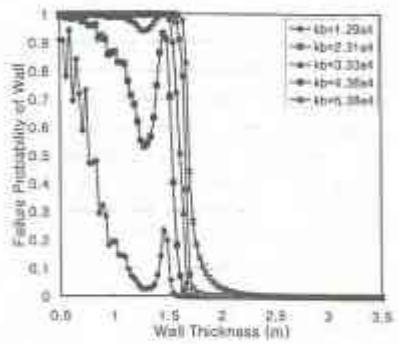

Figure 7. Failure Probability of Lateral Wall

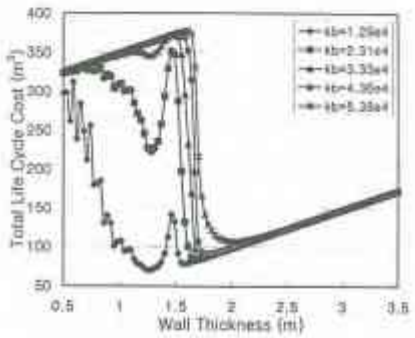

Figure 8. Total Life-Cycle Cost

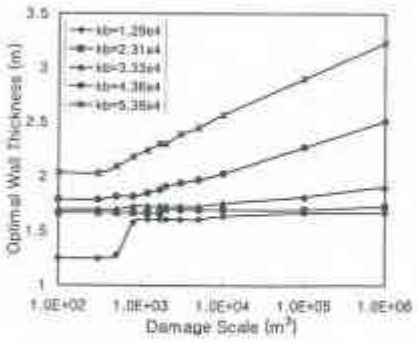

Figure 9. Sensitivity of Optimal Wall Thickness

Fig.7 shows failure probability of wall about wall thickness and isolator stiffness. Flexible isolator reduces significantly probability of failure even at very thin wall, but this effect of isolation decreases suddenly as the isolator gets stiffer. Therefore we should choose isolator stiffness properly while considering excessive displacement of isolator.

Isolator stiffness affects also the total life-cycle cost (Fig.8). Flexible isolator reduces total cost for identical wall thickness and this effect disappears when using thick wall.

Pool structure used as a container for radioactive material will lead to huge social cost if failure occurs. Therefore, the sensitivity of the resulting optimized design to any assumed damage scale should be verified (Fig. 9). Values obtained for pool structure with flexible isolator are nearly insensitive to variations of damage scale.

7. CONCLUSIONS

We developed a seismic design optimization method for fluid-filled and base-isolated pool structures based on minimum life-cycle cost concept. Fluid-structure interaction, base isolation effect, site condition of input ground motion are taken into account.

Results show that flexible isolator makes it possible to reduce wall thickness and total life-cycle cost significantly. The more flexible base isolator is, the smaller failure probability and total life-cycle cost are. Moreover, the case of optimal seismic design with flexible isolator is considerably insensitive to the assumed damage scale. This constitutes a very appreciable property because pool structures will be utilized to contain radioactive material and their failure will lead to immeasurable damage.

This method relies on linearity of system and stationarity of input ground motion. Therefore it presents some limit in considering nonlinear behavior of isolator and fluid and their effects.

If we compare minimum life-cycle cost of base-isolated pool structure with that of non-isolated and utilize the developed spectral density models, the economical efficiency evaluation of base isolation according to various conditions can be performed hereafter.

REFERENCES

1. Ang, A.H-S. and Leon, D.D., "Target Reliability for Structural Design Based on Minimum Expected Life-Cycle Cost," *Proc. of 7th IFIP WG7.5 Working Conference on Reliability and Optimization of Structural System*, pp. 71-84, 1996.
2. Wen, Y.K. and Ang, A.H-S., "Reliability and Cost-Effectiveness of Structures with Active Control," *Proc. of the International Workshop on Intelligent Systems*, pp. 63-76, 1991.
3. Koh, H.M. and Song, J., "Optimal Seismic Design Method for Base-Isolated Bridges by Minimizing Life-cycle Cost," *Proc. of the Korean Society of Civil Engineers*, Vol. I, pp. 499-502, Seoul Korea, October 1998.
4. Deodatis, G., "Non-Stationary Stochastic Vector Processes: Seismic Ground Motion Applications," *Probabilistic Engineering Mechanics*, Vol. 11, pp. 149-168, 1996.
5. Koh, H.M., Kim, J.K., Park, K.S., and Ha, D.H., "Stochastic Analysis of Base-Isolated Pool Structure Considering Fluid-Structure Interaction Effects," Journal of the Korean Society of Civil Engineers, Vol. 14, pp. 463-472, Seoul Korea, May 1994.
6. Newland, D.E., *An Introduction to Random Vibrations, Spectral and Wavelet Analysis*, John Wiley and Sons Inc., N.Y., 1993.
7. Song, J., *Economical Efficiency Evaluation of Seismic-Isolated Bridges by Minimum Life-Cycle Cost Seismic Design*, M.S. Thesis, Seoul National University, Seoul Korea, February 1999.

Transactions of the 15th International Conference on
Structural Mechanics in Reactor Technology (SMiRT-15)
Seoul, Korea, August 15-20, 1999

Seismic Risk Reduction in Italy through Innovative Techniques: 1 - Progress of R & D on Seismic Isolation

Alessandro Martelli[1], Massimo Forni[1], Alberto Dusi[2], Giuseppe Bonacina[3] and Tito Sano[4]

1) ENEA & GLIS, Italy
2) ENEL-Ricerca & GLIS, Italy
3) ISMES & GLIS, Italy
4) ANPA & GLIS, Italy

ABSTRACT: Summarised in this paper are the some of the most recent studies performed in Italy on seismic isolation (SI), partly funded by the European Commission (EC) or sponsored by the International Atomic Energy Agency (IAEA): (1) detailed numerical analyses of elastomeric isolators, performed in the framework of a IAEA Co-ordination Research Programme; (2) development of design guidelines for isolated nuclear plants applicable in the EC countries and Russian Federation; (3) analysis of the benefits of floor SI of strategic civil buildings with modular steel-frame structure; (4) records of an aftershock of the 1997 Marche & Umbria earthquake on a seismically isolated building; (5) promotion of demonstration applications of innovative anti-seismic techniques to both new constructions and existing buildings; (6) evaluation of the benefits of applying SI to chemical plant components. A separate paper deals with R&D in progress in Italy on passive energy dissipation (ED) systems.

INTRODUCTION

Large efforts are in progress in Italy on the development, validation and application of seismic isolation (SI) and passive energy dissipation (ED) for civil and industrial structures, including high risk plants such as nuclear reactors and chemical equipment [1, 2]. Such innovative anti-seismic techniques have already been adopted for over 150 Italian bridges and viaducts and over 30 Italian buildings [3]. The ongoing R&D activities are being performed in framework of both national collaborations among the members of the Italian Working Group on Seismic Isolation (GLIS), and international co-operative projects between GLIS members and other European and non-European partners.

Studies relevant to SI began in Italy in 1988, and concern experiments and numerical modelling of isolators and isolated structures, as well as development of design guidelines. In particular, a research project, funded by the European Commission (EC) and completed in 1996, allowed for the development of optimised High Damping Rubber Bearings (HDRBs) [1, 2, 4, 5]. In addition, wide-ranging numerical analyses and tests were carried out by ENEL for the enhancement of seismic protection of electric equipment using HDRBs, helical springs in parallel with viscous dampers and wire ropes [5, 6]. Based on the results of these studies, further R&D work has been carried out in Italy on both SI and ED systems [5-11].

This paper briefly summarises the main features and results of the most recent activities on SI which have been so far performed by the authors on the aforesaid items. A separate paper [12] deals with R&D in progress on ED systems.

CRP OF IAEA ON SEISMICALLY ISOLATED NUCLEAR STRUCTURES

Due to the complexity of dynamic behaviour of SI devices, high cost of their tests and non-negligible number of devices having excellent potential for nuclear applications, several countries judged of great interest to extend validation of their numerical models of such devices to the analysis of experimental data obtained by others [6]. Thus, a four-years Co-ordinated Research Program (CRP), proposed by ENEA, was endorsed by the International Atomic Energy Agency (IAEA) in 1996. There, Italy is jointly represented by ENEA, ENEL and ISMES, which supplied test results of project [4], concerning both HDRBs and the MISS (Model of Isolated Steel Structure) mock-up isolated using such bearings.

The first data, among those provided by other countries, which were jointly analysed by ENEL and ENEA, concerned U.S. scaled HDRBs that had been manufactured in Italy [5]; then, Japanese Natural Rubber Bearings (NRBs) and Lead Rubber Bearings (LRBs) and Korean HDRBs were analysed (Fig. 1) [5, 7]. Both three-dimensional (3D) and axisymmetric finite-element models (FEMs) of the isolators were developed and implemented in ABAQUS computer program, based on previous experience for the Italian HDRBs [1, 2, 5]. Hyperelastic models of the rubber, defined according to the results of suitable tests on both scragged and unscragged rubber specimens, were also implemented in ABAQUS. Extensive numerical work was performed by considering meshes with different refinements and different element types. The numerical analyses, aimed at investigating the effects of the numerous variables of the problem, allowed for optimising the type of material model, discretisation and elements to be adopted, up to large strains.

For the Japanese NRBs and especially U.S. HDRBs, good agreement between numerical and experimental results was found for horizontal stiffness; however, the agreement for compression tests was satisfactory only when compressibility was taken into account [5-7]. This confirmed the importance of volumetric tests on rubber specimens to correctly evaluate bearing vertical stiffness, especially in the case of large shape factors. Analysis also stressed that planar tests on specimens shall be performed to very large deformation, in order to allow for the definition of adequate hyperelastic models of the rubber [5-7]. Moreover, it was found that the unscragged rubber model should be used for reproducing bearing behaviour to 50% - 100% shear strain, while the scragged model should be used for larger deformations. Only slight differences were found between the results of 3D and axysimmetric models to 200% - 300% shear strain, while 3D models shall be used for larger deformations.

Also for the Korean HDRBs and Japanese LRBs (Fig. 1) [6, 7], numerical analysis was found to be adequate for horizontal stiffness, to 300% shear strain; however, at larger strains the numerical results showed hardening, contrary to test data. In addition, large discrepancy was found between the numerical results and test data for LRBs under compression with different offset strains: this must be attributed again to modelling rubber as incompressible in constitutive equations. Similar to the NRBs, for LRBs the need was stressed for an improvement of the analyses, based on more precise data concerning the characterisation of materials (natural rubber and lead), including effects of rubber compressibility. In addition, an attempt should be made to consider temperature effects on lead behaviour.

In any case, the already achieved results confirmed the conclusions of previous studies [1, 2, 5] that FEMs are useful tools for both the detailed design of elastomeric bearings and their qualification; for the latter, they allow for a considerable reduction of the number of tests to be performed (e.g. those concerning effects of parameters like temperature, ageing, vertical load on horizontal stiffness, initial or arisen defects, etc.).

With regard to the analysis of isolated structures [8], a new non-linear simplified isolator model was developed by ENEL, with an exponential constitutive law for describing rubber

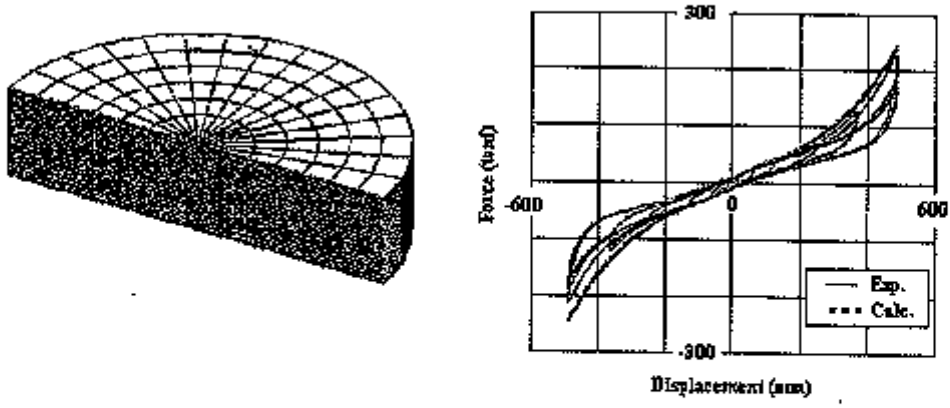

Figure 1: Finite element model of a lead rubber bearing and numerical - experimental comparison (combined vertical and horizontal cyclic tests up to 400% shear strain)

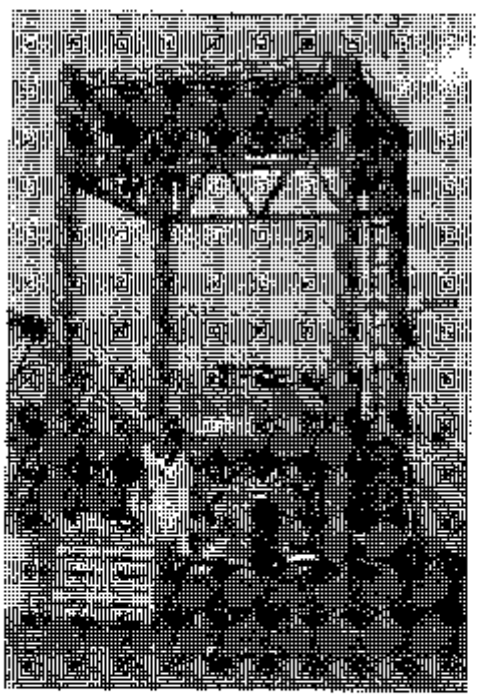

Figure 2: Model of a steel-frame (INSO hospital) with floor isolation during shaking table tests at ENEA laboratories at Casaccia (Rome)

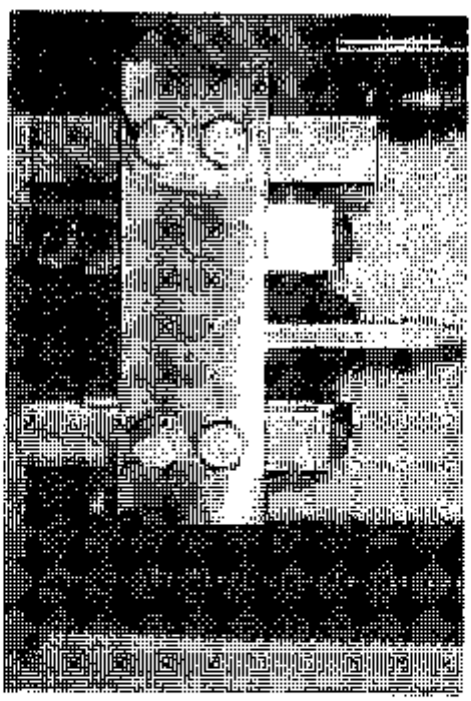

Figure 3: Floor isolation devices with innovative high-friction attachment system during qualification test (ALGA) at 400% shear strain

behaviour [9]. It was implemented in ABAQUS as a "User Subroutine". It is based on three rubber parameters and allows for a very accurate evaluation of the response of seismically isolated structures, as shown by comparison with the results of shake table tests carried out on MISS [8, 9]. Although it was developed for elastomeric bearings, it may be also applied to other kinds of SI devices having a continuously decreasing stiffness with increasing displacement (e.g. rubber or helical springs coupled with metallic yielding elements, wire rope friction isolators, etc.).

DESIGN GUIDELINES FOR ISOLATED NUCLEAR PLANTS AND CIVIL BUILDINGS

The development of design guidelines for isolated structures was initiated in Italy by ENEA in 1989, making reference to the nuclear plants. The most recent activities were performed, with the co-operation of ENEL, ISMES and other partners, in the framework of EC-funded projects and concerned harmonisation of such guidelines between the EC countries and Russian Federation and their extension to Russian 3D SI systems and innovative rolling systems, developed in a further ongoing EC-funded project (REEDS) [10, 11].

In addition, ANPA, ENEA, ENEL and ISMES co-operated on the development of national rules for civil buildings, by supporting the Italian National Survey on the assessment of a proposal for guidelines which was submitted to the Ministry of Constructions in 1993, by collaborating with the National Standard Authority (UNI) and European Code Committee (CEN) on the development of national and European rules for the isolation devices and in 1998, by collaborating with other GLIS members on the preparation of comments to guidelines drafted by the Italian Ministry of Constructions [11].

FLOOR ISOLATION OF CIVIL BUILDINGS WITH MODULAR STRUCTURE

In the framework of a study contract of "Studio Antonucci" [11], numerical analyses and shake table tests (Fig. 2) were performed by ENEA in 1998 for a full scale portion of a steel structure building of the Company INSO, which has the patent for the construction method ("Oxford Method"). It is a modular structure, which is being used for the construction of public buildings (in the our case, a hospital). The purpose was the evaluation of feasibility and technical and economic benefits of floor SI. This is a very innovative technology, for which no applications exist yet (to the knowledge of the authors), in Europe at least.

In addition to the above-mentioned analyses and tests, ENEA also designed the isolators (HDRB type); in particular, it designed a new, very innovative and low cost isolator restraint system, consisting of shagreened plates (Fig. 3) and designed and supervised the isolators' qualification tests. Such tests stressed the great efficiency of the new restraint system, which allows for isolator lateral deformation to about 400% shear strain, i.e. very close to those typical of more complicated and expensive systems, such as bolting [1, 2, 4, 5]. Numerical analyses of the isolated structure and the related tests also provided excellent results [11].

RECORDS OF AN AFTERSHOCK OF 1997 MARCHE - UMBRIA EARTHQUAKE

Some interesting records of an aftershock (March 1998) of the earthquake which struck Central Italy (Marche and Umbria Regions) on September 26, 1997, became available for one of the five isolated buildings of the National Telephone Company ("TELECOM Italia") Centre at Ancona (Fig. 4). This building had been subjected to both forced and free-vibration excitation tests in 1990, just after completion of structure construction [2, 5]. The first,

Figure 4: Telecom building (Ancona) subjected to on-site tests and provided with monitoring system.

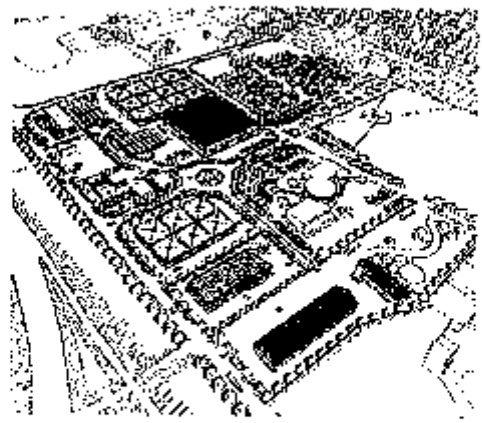

Figure 6: Plan of the new Emergency Management Centre of Central Italy, Foligno, Umbria.

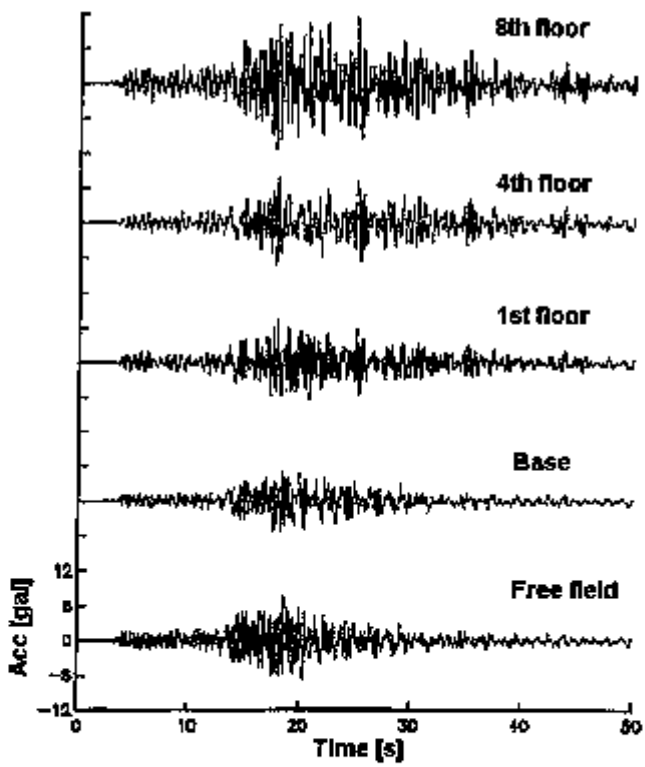

Figure 5: Telecom building: aftershock records (March 1998) of the 1997 Umbria & Marche earthquake

carried out by means of an eccentric mass mechanical vibrator located on the roof, had allowed for the dynamic characterisation of the superstructure and evaluation of the behaviour of the SI system at low excitation level (lateral displacement being only a few millimeters). The second, on the contrary, had enabled the characterisation of SI system at high excitation: they had been conducted by laterally displacing the building (to a maximum of about 110 mm) by means of hydraulic jacks, then replacing them with collapsible devices provided with explosive bolts and finally, exploding bolts.

After full construction completion, the building had been provided by ENEL and ISMES with an innovative monitoring system, capable of recording both seismic and wind vibrations. However, during the first two main shocks of September 26, 1997, of Marche and Umbria earthquake, the system did not record any signal, because its threshold level (0.01 g) was too high (Ancona is located at about 100 km from the epicentre). Thus, such a threshold was lowered to 0.005 g. This enabled for the aforesaid recording in March 1998 (Fig. 5). Data processing [11] showed results which are fully consistent with those of 1990 forced vibration tests (the structure displacement was about 3 mm, similar to that reached in those tests). They also showed that life effects of the SI system are negligible, in agreement with the results of natural ageing tests which are being periodically performed by ISMES, on behalf of the owner SEAT and with the co-operation of ENEA, on spare isolators stored on-site, under the vertical design load (through a suitable equipment), close to those supporting the building.

PILOT APPLICATIONS OF THE INNOVATIVE ANTI-SEISMIC TECHNIQUES

Although the innovative anti-seismic techniques are fully mature for an extensive use and excellent experience and knowledge are available for this in Italy [5], in our country the recent applications of these techniques are less numerous than in others that are characterised by high seismic risk. This is due to both the continuing absence, in Italy, of suitable design rules or guidelines, and construction costs which are usually larger than those related to conventional constructions (although only by about 10% and only if basing on the present law requirements, which are insufficient for strategic structures, at least) [11]. Thus, there is the need for stimulating new applications, with the collaboration, even from the financial point of view, of Regional Governments and through promotion actions towards Local Institutions, designers and public opinion.

For these reasons, in 1997, ENEA started actions to promote pilot applications of innovative anti-seismic techniques to both new constructions and existing buildings in Italian Regions. Such actions, which later became part of those foreseen by the 1998 National Conference on Energy and Environment [11], include formal agreements among ENEA, local Universities, Regional Governments, Local Institutions and other partners. The latter may comprise: (a) identification of the pilot applications, in co-operation all partners; (b) funding of Regional Governments of possible extra-costs due to the use of the innovative systems; (c) technical support of ENEA, local Universities and other technical partners, for the design phase (selection of the anti-seismic system, numerical analyses, assistance for qualification tests, verification of compatibility with design rules) and / or construction (verification of consistency with design requirements, assistance for the acceptance of anti-seismic devices and installation of seismic monitoring system), and /or certification of the building; and (d) technical support of ENEA for the adoption (where possible) of design solutions which are also capable of improving building energetic efficiency.

The aforesaid agreements have already been formally proposed to Marche, Tuscany and Umbria Regions, and in a preliminary way, to Sicilian Region. Umbria has already accepted the ENEA proposal and the agreement document has already been drafted. To develop the

aforesaid proposals, numerous Local Institutions have also been contacted, by also organising or participating in various Seminars or Conferences for both engineers an the public.

In both Marche and Umbria Regions some pilot applications have already been identified. The most important is to the new Emergency Management Centre of Central Italy of Foligno, which is already partly under design (Fig. 6). Other already identified applications should be at Città di Castello, Camerino (the new Department of Biology and a building owned by the municipality) and Nocera Umbra (reconstruction of a village, strongly damaged by the 1997 earthquake, using original masonry materials and SI, possibly within an EC-funded project).

Finally, Regional and Local Institutions of Marche and Umbria ensured their collaboration to a national project concerning the "development and application of integrated innovative technologies and assessment of comparison methodologies to optimise interventions of seismic protection of cultural heritage by respecting safety and preservation requirements", which was proposed to the Italian Ministry of University and Scientific Research [11].

SEISMIC ISOLATION OF INDUSTRIAL PLANTS

A study, proposed by ENEA, ANPA and University of Rome "La Sapienza", was funded by the Italian National Research Council (CNR) in 1998 to evaluate the benefits of applying SI to the protection of industrial plant components [11]. The ongoing first step on the study concerns the identification of a reference typical component. The aim is also to make a real SI application possible, at the conclusion of the study. A chemical plant component was chosen, according to the particular seismic vulnerability of some of such plants. Contacts have been established with important national chemical companies, which anticipated their interest in collaborating to the project. The partners proposed a tank as the reference component. The final decision will be taken as soon as answers to such a proposal are received from contacted companies.

CONCLUSIONS

Activities on SI of the Institutions to which the authors belong have been shortly described. It has been shown that such activities cover numerous important fields, including R&D and design for civil and industrial structures, development of design rules and promotion of new applications. Work performed for energy dissipation systems is reported in a separate paper.

ACKNOWLEDGMENTS

Particular thanks are due to Mr. F. Bettinali of ENEL, Mrs. G. Bergamo of ISMES, Mr. A. Pugliese of ANPA and Mr. M. Indirli and Mr. G. De Canio of ENEA: their names were not included among those of co-authors only due to the limit to five co-authors which was allowed for this paper.

REFERENCES

1. Forni, M. et al., "Development and Validation of FEMs for the Design and Qualification of HDRBs," *Trans. of the 14th International Conference on Structural Mechanics in Reactor Technology*, Vol. 7, pp. 491-498, Lyon, France, August 1997.

2. Dusi, A. et al., "Experimental and Numerical Evaluation of Benefits of Optimized HDRBs for Seismic Isolation," *Trans. of the 14th International Conference on Structural Mechanics in Reactor Technology*, Vol. 7, pp. 507-514, Lyon, France, August 1997.

3. Martelli, A. and Forni, M., "Seismic isolation of civil buildings in Europe," *Progress in Structural Engineering and Materials*, Construction Research Communications Ltd., London, Vol. 1 (3), 1998, pp. 286-294.

4. Enel, Alga, Dywidag, Enea, Mrpra, Shw, Stin, *Optimization of Design and Performance of High Damping Rubber Bearings for Seismic and Vibration Isolation*, EC Contract BR2 CT93 0524, Project BE7010, Bruxelles, Belgium, 1993.

5. Martelli, A. and Forni, M. (eds.), *Seismic Isolation, Passive Energy Dissipation and Active Control of Seismic Vibrations of Structures - Proceedings of the International Post-SMiRT Conference Seminar, Taormina, Italy, August 25 to 27, 1997*, GLIS, Bologna, Italy, 1998.

6. Forni, M. et al., "Progress of Activities Performed in Italy by ENEA and ENEL on Seismic Isolation and Passive Energy Dissipation," *Proc. of the 1998 ASME-Pressure Vessel and Piping Conference*, PVP-Vol. 379 (Seismic, Shock and Vibration Isolation – 1998), pp. 19-41, San Diego, CA, USA, July 1998.

7. Dusi, A. et al., "Contribution of Italy to the Activities on Intercomparison of Analysis Methods for Seismically Isolated Nuclear Structures: Finite Element Analysis of Lead Rubber Bearings," *Proc. of the Third Research Co-ordination Meeting of IAEA CRP on "Intercomparison of Analysis Methods for Seismically Isolated Nuclear Structures", IAEA-RC-624.3 (IWGFR/95)*, pp. 50-63, Hertford, UK, May 1998.

8. Forni, M. et al., "Contribution of Italy to the Activities on Intercomparison of Analysis Methods for Seismically Isolated Nuclear Structures: Shake Table Tests on a Steel Structure Mock-up," *Proc. of the Third Research Co-ordination Meeting of IAEA CRP on "Intercomparison of Analysis Methods for Seismically Isolated Nuclear Structures", IAEA-RC-624.3 (IWGFR/95)*, pp. 63-100, Hertford, UK, May 1998.

9. Dusi, A. and Rebecchi, V., "Contribution of Italy to the Activities on Intercomparison of Analysis Methods for Seismically Isolated Nuclear Structures: a Parallel Elastic-Plastic Model for Non-Linear Analysis of Base Isolated Structures," *Proc. of the Third Research Co-ordination Meeting of IAEA CRP on "Intercomparison of Analysis Methods for Seismically Isolated Nuclear Structures", IAEA-RC-624.3 (IWGFR/95)*, pp. 42-49, Hertford, UK, May 1998.

10. Forni, M. et al., *Extension of the Available Design Guidelines for Seismically Isolated Nuclear Plants to 3D Systems Developed in the Russian Federation and Rolling-Ball Rubber-Layer Systems*, Final Report, EC Contract EC B7-6340/95/001169/MAR/C2, ENEA, Bologna, Italy, 1998.

11. Martelli, A. et al., "New Activities Performed in Italy on Innovative Anti-Seismic Techniques for Civil and Industrial Structures," *Proc. of the 1999 ASME-PVP Conf., Boston, USA*, Boston, USA, July 1999.

12. Dusi, A. et al., "Seismic Risk Reduction in Italy through Innovative Techniques: 2 – R&D on Passive Energy Dissipation Systems," *Trans. of the 15th International Conference on Structural Mechanics in Reactor Technology*, Seoul, Korea, August 1999.

Transactions of the 15th International Conference on
Structural Mechanics in Reactor Technology (SMiRT-15)
Seoul, Korea, August 15-20, 1999

Shaking Table Tests on Failure Characteristics of Base Isolation System

Yukio Watanabe[1], Asao Katoh[1], Masaaki Ohba[1], Yasuaki Fukushima[2], Nobuhisa Satoh[2] and Masao Iizuka[2]

1) The Japan Atomic Power Company, Japan
2) Kajima Corporation, Japan

ABSTRACT

A series of shaking table tests were conducted for reduced scaled model of a base isolated demonstration Fast Breeder Reactor (FBR) plant in Japan for the purpose of verifying the seismic safety of systems. Three types of base isolation systems: natural rubber bearing with steel damper (NRB+SD), lead rubber bearing (LRB), and high damping rubber bearing (HRB) were concerned. As a result of these tests, NRB+SD, LRB and HRB were within stable domain (not hardening) at S2 input, and were nearly hardening at 2×S2 input. All types of the rubber bearings did not break at 3×S2 input which was the level of design limit. And these bearings broke at over 4×S2 input.

Introduction

A demonstration FBR plant in Japan is to be planned as a base isolated building in the horizontal direction. The authors have already presented the results of the three breaking tests consisting of four, nine and twenty-five NRBs using a shaking table at 12th SMiRT Conference. In this paper seismic safety and dynamic characteristics of the rubber bearing breaks of three types of reference design base isolation system, NRB+SD, LRB and HRB for the demonstration FBR plant in Japan were confirmed by conducting shaking table tests.

1. Test Methods

a. Input condition

The test cases are shown in table.1. Four excitation levels were set up in these tests. Those were on the design level, the hardening level, the level of the design limit, and the target breaking level of the laminated rubber bearing. The time scale were reduced one-fourth by the Similarity Law where the reduced scale of acceleration and stress of the isolation system was the same as full scale.

b. Test model

Test model and its size ,about 2500(wide)*2000(deep) *3500mm(high), was about one-sixteenth, the scale of the base isolated FBR building model. The model consisted of an upper structure and a base isolation system. The outline of the model is shown in fig.1.

(a) the upper structure

The upper structure had three floors and was made of steel. Its total weight was about 17 tonf. The second floor of the upper structure was modeled as the reactor support floor of DFBR. And the first-story column was made of high strength steel so as to remain elastic through the experience, because shaking table tests were conducted to evaluate failure characteristics three times.

(b) the isolation system

The vertical stress of the rubber bearing was 50 kgf/cm^2. The period corresponding to initial stiffness of the isolation system was equal to 1.0 second for full scale building, the period corresponding to second stiffness was equal to 2.0 seconds, and the ratio of yield shear stress to design vertical stress of the rubber bearing was 0.05, which is a standard design for DFBR in Japan. The total thickness of the rubber sheet of the three types of the rubber bearings, NRB, LRB and HRB, was 7mm (NRB and LRB), and 8mm (HRB). The outline of these rubber bearings were shown in fig.2. Four rubber bearings were placed under the upper structure columns in each test.

The property of the steel damper that was used for NRB+SD is also shown in fig.2. Two steel dampers were placed in the isolated layer so as not to be twisted. The spherical bearing was placed over the joint of the steel damper of the upper structure to make the steel damper be a cantilever type. The steel dampers were replaced every test.

(c) The safety frame

The safety frame, shown in fig.1, was set so that the upper structure would not be damaged when the rubber broke because the breaking tests were conducted using the same upper structure three times. The frame was designed based on the result of the preliminary analysis, considering safety during the tests.

c. The shaking table

The six degree-of-freedom shaking table was used.

2. Measurements

Horizontal accelerations were measured at each floor and the top of the shaking table. Horizontal relative displacement and shear force of the isolated layer were also measured. As a result of these tests measurements, dynamic characteristics of the upper structure and the isolation system can be evaluated. Vertical relative displacement and vertical force of the rubber bearing were measured especially for analyzing the failure mode of the rubber bearing. Moreover, instruments were chosen for their durability throughout the tests, meaning being strong enough to receive the vibration whenever the rubber bearing breaks.

3. Static tests of the laminated rubber bearing

1) The quality of the rubber bearings were confirmed from the results of static tests for every specimen in a factory before the shaking table test. The outline of the static tests were as follows:

parameter	: shear strain	= 100,150,200%
	: the vertical stress= 50kgf/cm^2 (design value)	
loading	: 4 times cyclic loading under a design vertical load.	

measurements : Mean shear modulus and mean force at 0 displacement for the third cycle are shear stiffness (KH) and characteristic dissipator shear strength (Qd) of the rubber bearing respectively.

The results were shown in fig.3. The variation between data was approximately within ± 10% of the design value.

2) Static breaking tests by a monotonic load under a design vertical stress were conducted. Using the result of the tests, the shear strain linear limit of each type of the laminated rubber bearing could be calculated[1]. When the linear limits were calculated, the characteristic dissipator shear strength were used for the results of the former tests (shear strain 200%). The calculated shear strain linear limit of NRB was about 290%, about 310% for LRB, and about 260% for HRB. The test results were also compared with the shaking table tests.

3) Static failure limit tests using two directional loads for calculating breakage bound were conducted. The outline of the static tests were as follows:

number : five test pieces for each type of the rubber bearings

test cases : i.shear breaking test in the compression zone (vertical stress : 250kg/cm^2)
ii.shear breaking test under non vertical loading
iii.shear breaking test in the tension zone (vertical strain : 25%)
iv.shear breaking test in the tension zone (vertical strain : 50%)
v. tensional breaking test

method : static monotonic loading

As a result of static break tests using a monotonic load under a design vertical stress and static failure tests using two directional loads, static breakage bound of each type of the laminated rubber bearing was confirmed. And the breakage bound is compared with the shaking table tests. Test results and the breakage bound were shown later.

4. Test results

a. Input motion of the shaking table

Acceleration response spectra of the shaking table for example in case of 1S2 and 4S2 inputs were shown in fig.4. This figure shows that response spectra of NRB was almost the same as that of other rubber bearings. In the case of other level inputs the floor response spectra was also almost the same as in the case of 1S2 input. The result means that input motions of the shaking table of the three types of isolation systems were almost the same. There was a slight difference in the short period of response spectra at more than 4S2, but acceleration response spectra were almost the same as other bearings in the period of 0.25 to 0.5 seconds, where the period corresponding to the second stiffness of each rubber bearing was within the period region.

b. Shear force - Horizontal displacement hysteresis curve of isolation layer

The hysteresis behavior of shear force - horizontal displacement at 1S2 ,2S2, and 4S2 inputs in case of NRB+SD, at 5S2 input in the case of LRB and HRB is shown in fig.5. The hysteresis in the three quadrant areas were rotated at 180 degree. This figure also shows the breaking point of the rubber bearing and the results which were four times as much as the stress of the static breaking tests under a monotonic load.

1) NRB+SD

Max. horizontal shear strain of the isolator at 1S2 input was about 130%. This strain was under the linear limit which could be calculated from the static breaking

tests by a monotonic load. Max. horizontal shear strain of the isolated layer at 2S2 input was about 340% which was more than the linear limit. Horizontal shear strain of the isolated layer at 3S2 input was about 490%, but all the NRBs did not break. One of the NRBs (C3 in fig.1) broke at about the maximum strain which was 600% at 4S2 input, but the steel dampers did not break then.

When the hysteresis was compared with the static breaking tests, the slip phenomena could be seen from the hysteresis at 4S2 input, so the breaking strain of the shaking table test was larger than the static breaking tests.

That means the NRB was within the stable domain (not hardening) at 1S2 input, reached hardening at 2S2 input, was sound at 3S2 input which was the level of the design limit, and the rubber bearing broke at 4S2 input.

2)LRB

Max. horizontal shear strain of the isolator at 1S2 input was about 80%. This strain was under the linear limit. The maximum strain was less than other isolation systems. That was because characteristic dissipator shear strength and first stiffness of LRB were larger than other isolation systems. Max. horizontal shear strain of the isolated layer at 2S2 input was about 310% which was almost the linear limit. Max. horizontal shear strain of the isolated layer at 3S2 input was about 490%, but all the LRBs did not break. One of the LRBs (A3 in fig.1) broke at about the maximum strain which was about 640% at 5S2 input. Immediately after that the rest of the rubber bearings broke on the opposite side.

When the hysteresis was compared with the static breaking tests, the slip phenomena could be seen from the hysteresis at 4S2 input, the breaking strain of the shaking table test was larger than the static breaking tests as well as NRB+SD.

3)HRB

Max. horizontal shear strain of the isolator at S2 input was about 110%. This strain was under the linear limit. Max. horizontal shear strain of the isolated layer at 2S2 input was about 280% which was more than the linear limit. Max. horizontal shear strain of the isolated layer at 3S2 input was about 420%, but all the HRBs did not break. One of the HRBs (A1 in fig.1) broke at about maximum strain which was about 630% at 5S2 input. Immediately after that the rest of the rubber bearings broke on the opposite side.

When the hysteresis was compared with the static breaking tests, the shear strain of the shaking table tests were larger than the static breaking tests at 1S2 to 3S2 input. That was because of the shear strain velocity rate dependency of HRB which Dr. K.Ishida etc. pointed out[2]. The shear strain of the shaking table tests was less than the static breaking tests at the same stress input level of 4S2 and 5S2, so the slip phenomena could be seen from the hysteresis. But HRB were more gentle than other bearings and the maximum response was almost the same as the static breaking tests. That was because the slip phenomena and the shear strain velocity rate dependency of this HRB occurred simultaneously.

c. Failure mode

The failure mode for the rubber bearings were shown in fig.6. In the vertical stress - horizontal shear strain relation and the vertical strain - horizontal shear strain relation, the breakage bound which was calculated by the static breaking tests was included.

The vertical stress at the breakage of the rubber bearing which broke first among the four elements was 30 - 40 kgf/cm^2 on the tension side, the vertical strain was 10 - 15% for the three types of rubber bearings as shown in fig.6. That is to say all types of

the rubber bearings broke in the tension-shear zone. The breaking strain of all the rubber bearings which broke at the shaking table tests was larger than that of static breaking tests and the strain was also beyond the breakage bound.

d. Maximum response at 1S2 input

The maximum response acceleration of each floor for the three isolation systems was shown in fig.7. All the maximum response accelerations at 1S2 input of the upper structure were less than 500 gal which was the design target level of the isolation system for three types of isolation systems. The maximum response shear force and the shear coefficient of each floor is also shown in fig.7. This figure shows that the response acceleration and the shear force of third floor for LRB were a little greater than for other bearings. That was because yield stress and initial stiffness of LRB was greater than for the others, as mentioned above

5. Conclusions

The results of the shaking table tests were summarized as follows.

1) The maximum response acceleration of the upper structure for the three types of the isolation system was less than the design target level of the isolation at 1S2 input.

2) The three types of isolation system were within the stable domain (not hardening) at 1S2 input, and were nearly hardening at 2S2 input. All types of laminated rubber bearings did not break at 3S2 input which was the design limit.

3) All types of the laminated rubber bearing broke at more than 4S2 input, and the failure mode of the bearing which broke first of the four elements was tension-shear mode.

These results demonstrate that the safety requirement of each type of laminated rubber bearing was satisfied.

6. Acknowledgements

This study was carried out as a part of the FBR common research of the electronic power companies in Japan, entitled "Conceptual Design of DFBR". And this study was based on the support of Professor T.Fujita of Institute of Industrial Science, University of Tokyo, Japan, which the authors gratefully acknowledgement.

7. References

[1] S.YABANA, Y.OHTORI, K.HIRATA, K.YASUI and T.MAZDA, "Study on Linear Limits of Rubber Bearings", AIJ annual report (1996) in Japanese

[2] K.ISHIDA, H.SHIOJIRI, M.IIZUKA, K.MIZUKOSHI and K.TAKABAYASHI, "Failure Tests of Laminated Rubber Bearings " 11th SMiRT (1991) K25/5

[3] M.KATO, Y.WATANABE, A.KATO, H.KOSHIDA, K.MIZUKOSHI, Y.FUKUSHIMA, O.NOJIMA, G.YONEDA and S.ONIMARU " Dynamic Breaking Tests on Base-Isolated FBR Plant" 12th SMiRT (1993) K22/1

table.1 Input condition

TEST NAME	INPUT LEVEL	MAX. ACC. (gal)
DESIGN	1S2	380
HARDENING	2S2	760
DESIGN LIMIT	3S2	1140
BREAKING	4S2	1520
	5S2	1900

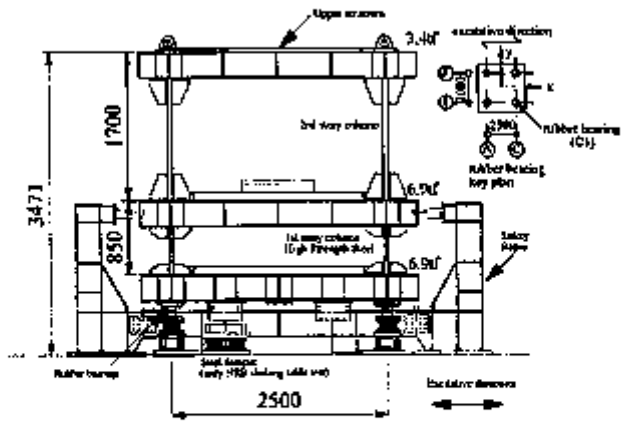

fig.1 The test model

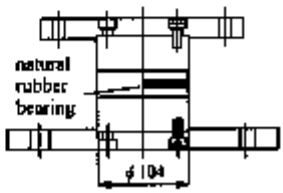

TOTAL THICKNESS OF RUBBER	7mm
A COEFFICIENT OF FIRST FORM	26
A COEFFICIENT OF SECOND FORM	15

ITEM	STEEL DAMPER
NUMBER	2
MATERIAL	STEEL
YEILD STRENGTH	235 N/mm²
DIAMATER	φ 17
HIGHT	66mm

(a) NRB+SD

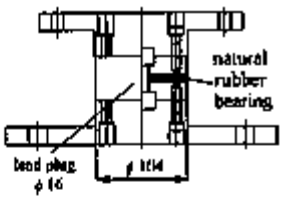

TOTAL THICKNESS OF RUBBER	7mm
A COEFFICIENT OF FIRST FORM	26
A COEFFICIENT OF SECOND FORM	15

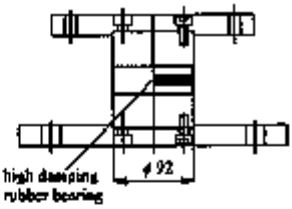

TOTAL THICKNESS OF RUBBER	8mm
A COEFFICIENT OF FIRST FORM	23
A COEFFICIENT OF SECOND FORM	12

(b) LRB **(c) HRB**

fig. 2 The outline of the rubber bearing

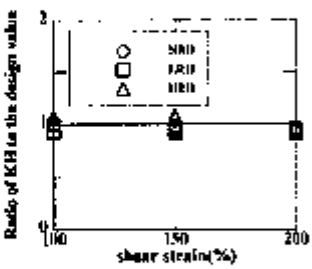

(a) the shear stiffness (KH)

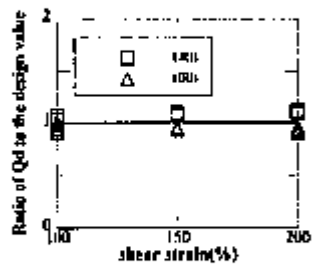

(b) characteristic dissipator shear strength (Qd)

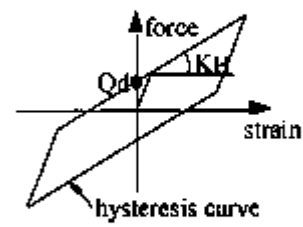

characteristics of the isolation system

fig. 3 Results of static element tests

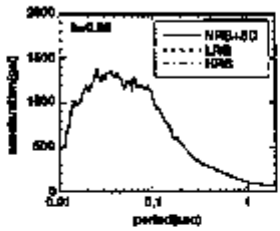

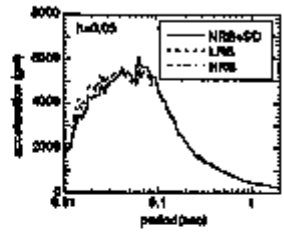

(a) 1S2 input (b) 4S2 input

fig.4 The response spectra of the shaking input motion

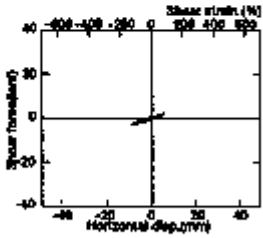

(a) 1S2 input

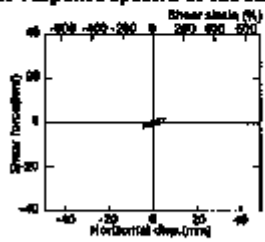

(a) 1S2 input

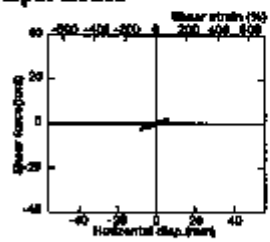

(a) 1S2 input

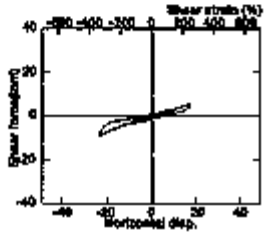

(b) 2S2 input

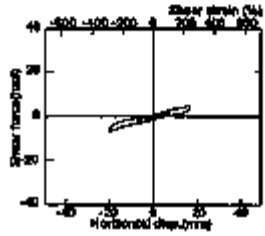

(b) 2S2 input

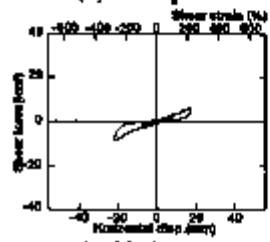

(b) 2S2 input

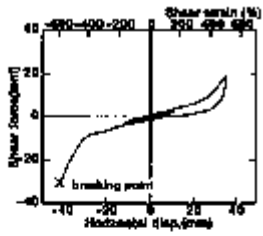

(c) 4S2 input

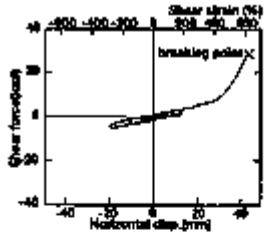

(c) 5S2 input

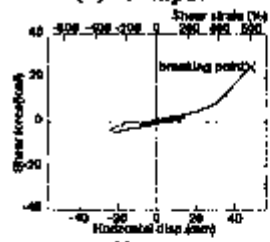

(c) 5S2 input

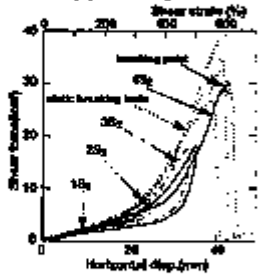

(d) static breakings test and shaking table test (NRB)

fig.5(1) hysteresis behavior (NRB+SD)

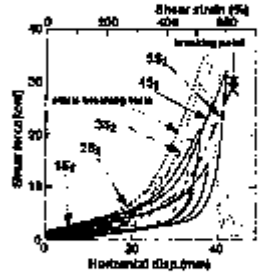

(d) static breakings test and shaking table test (LRB)

fig.5(2) hysteresis behavior (LRB)

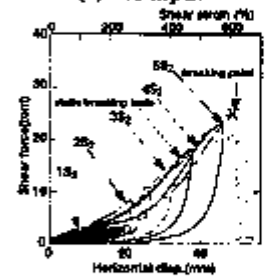

(d) static breakings test and shaking table test (HRB)

fig.5(3) hysteresis behavior (HRB)

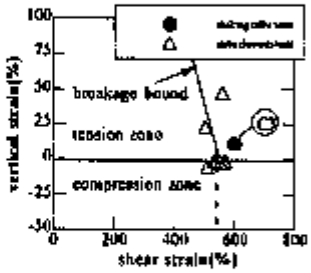

(a) vertical strain-shear strain relation

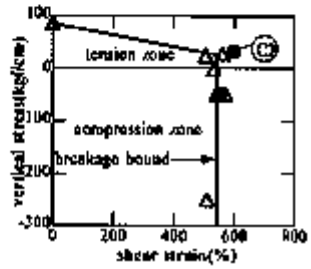

(b) vertical stress-shear strain relation

fig.6(1) failure limits (NRB+SD)

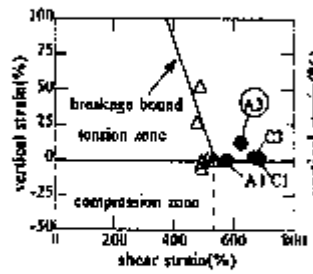

(a) vertical strain-shear strain relation

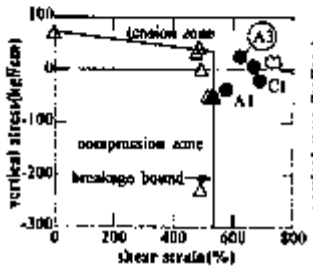

(b) vertical stress-shear strain relation

fig.6(2) failure limits (LRB)

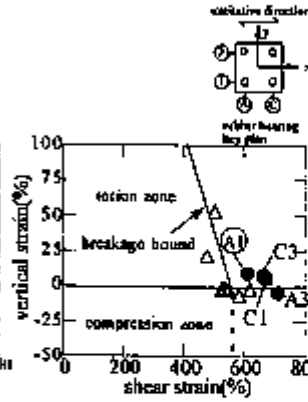

(a) vertical strain-shear strain relation

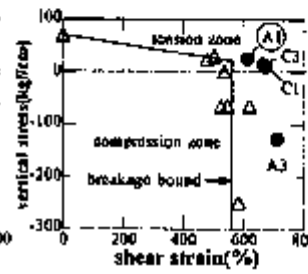

(b) vertical stress-shear strain relation

fig.6(3) failure limits (HRB)

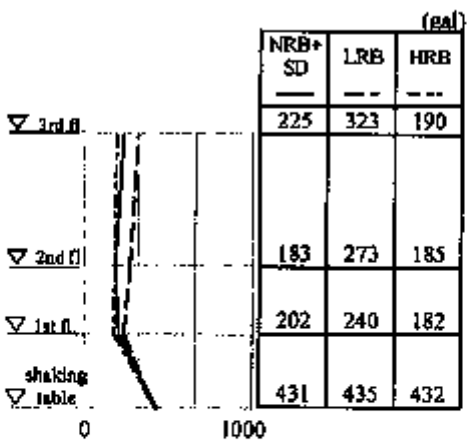

(a) maximum response accelaration

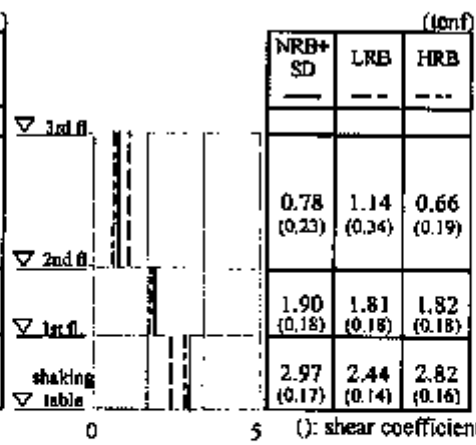

(b) maximum response shear force and shear coefficient

fig.7 maximum response of the test model